TWO-DIMENSIONAL MODELING OF *IN SITU* BIOREMEDIATION USING SEQUENTIAL ELECTRON ACCEPTORS

by

J. Steven Brauner

Thesis submitted to the Faculty of the

Virginia Polytechnic Institute and State University

in partial fulfillment of the requirements for the degree of

Master of Science

in

Civil Engineering

APPROVED:

Dr. M.A. Widdowson, Chair

Dr. P. Diplas

Dr. D. Gallagher

September, 1995

Blacksburg, Virginia 24061

2-DIMENSIONAL MODELING OF *IN SITU* BIOREMEDIATION USING SEQUENTIAL ELECTRON ACCEPTORS

by

J. Steven Brauner

Dr. Mark A. Widdowson, Chair

The Charles E. Via Department of Civil Engineering

(ABSTRACT)

One of the most promising technologies in groundwater contaminant remediation is the active use of natural microbial activity to reduce aromatic hydrocarbons and other contaminants to simpler, non-toxic compounds. Biological treatment technologies which clean an aquifer without removing aquifer material fall into the broad category of *in situ* bioremediation, and have the potential to provide cost-effective remediation plans.

Mathematical models used to simulate *in situ* bioremediation must deal with spatial variation in contaminant and electron acceptor concentration, microbial population, and media properties. Research has shown that the use of sequential electron acceptors significantly impacts biodegradation results. Aquifer conditions may switch between primary and secondary electron accepting conditions, further complicating the modeling process. This research examines the two-dimensional, sequential electron acceptor computer model SEAM2D, developed by Widdowson (1992), and extends the SEAM2D model by developing the equations and coding for the newly recognized solid phase, iron(III)-based contaminant reduction.

Both a sensitivity investigation and field simulations are provided. The sensitivity investigation identifies which input parameters most significantly impact model results (i.e. changes in contaminant mass and concentration). The modeling simulations provide an illustration of model capabilities and documents procedures used in applying SEAM2D to a USGS study site in Laurel Bay, South Carolina. The Laurel Bay site and subsequent model simulations are unique in that the natural, sequential electron acceptor process of oxygen-iron(III) reduction is specifically monitored and modeled.

Acknowledgements

First and foremost, the author wishes to thank his advisor, Dr. Mark A. Widdowson for the opportunity to work on this research project. I deeply appreciate the guidance Dr. Widdowson has provided me, both in this research and in my search to define a career. It has truly been a joy to work with him. I would also like to thank Dr. Daniel Gallagher for critiquing my work and Dr. Panayiotis Diplas for inspiring me to pursue excellence in education. I could not have hoped for a better committee.

The author also wishes to thank Dr. Richard Weisman who, as an undergraduate advisor and a mentor, inspired me to pursue continued education and a career in academia.

I also wish to thank the other graduate students in the Hydrosystems division for their support. Their advice and encouragement helped make my time here much more enjoyable while also helping me improve the quality of my work. Special thanks go out to Michael Latham and Marc Killingstad for their friendship and advice.

I also thank my best friend, Aaron Conrad, for the support he has given me over the years. Reuniting with him here at Virginia Tech has been a dream come true and I will never forget the friendship he has given me throughout my life and the writing of this thesis. Thanks also to William 'Kenny' Schmidt. During our lunchtime meetings, Kenny was always ready to listen when I was feeling discouraged, and his suggestions, encouragement, and friendship are deeply appreciated.

I also give deep appreciation to my friends on the ultimate frisbee team. All of you make me feel at home here in Blacksburg. The competition provided on the field and the friendship provided both on and off the field helped pull me through the times when research or other parts of my life did not progress as I was hoping.

Finally, I wish to thank my family, especially my parents, John and Judy Brauner. The love, support, and knowledge they have given me are the greatest gifts I could ever receive and I love them both. They taught me to believe that hard work can make all of your dreams come true and, without their love and encouragement, I could have never made it this far. I dedicate this work to them.

TABLE OF CONTENTS

TABLE OF CONTENTS - Continued

TABLE OF CONTENTS - Continued

LIST OF FIGURES

LIST OF FIGURES-Continued

LIST OF FIGURES-Continued

LIST OF FIGURES-Continued

LIST OF TABLES

CHAPTER 1. Introduction

1.1 Background

A major threat to groundwater resources is the release of gasoline and other fuels from leaking underground storage tanks (UST's). These fuels contain several aromatic hydrocarbons such as benzene, toluene, ethylbenzene, and xylenes (BTEX) and are a major health concern for both humans and wildlife (Dean, 1985). Recent studies indicate that gasoline additives such as methyl-tert-butyl-ether (MTBE), may also pose a significant risk to humans (Hartley and Englande, 1992). Recognition of these health risks has promoted research into the collection and/or remediation of petroleum hydrocarbon contaminated soil and groundwater.

Leaks from UST sites usually occur over extended periods of time, producing plumes of large areal expanse. The size of these plumes often makes *ex situ* technology, where aquifer material is physically removed and cleaned, expensive or even impossible. The high cost associated with *ex situ* options has led to increased research into *in situ* remediation of these toxic compounds. *In situ* bioremediation, which uses intrinsic biological processes to breakdown complex compounds into simpler, non-toxic ones, has the potential to provide an efficient and cost effective method for groundwater remediation. In addition to reduced cost, *in situ* bioremediation has other advantages. As Baker and Herson (1994) indicate, *in situ* bioremediation minimizes site disruption and eliminates the contaminant permanently. With *in situ* methods, costs associated with transportation of waste materials and long term liability are also eliminated. Furthermore, recent research indicates that, in some instances, naturally occurring biodegradation can adequately reduce contaminant concentrations to acceptable levels before the plume reaches a potentially harmful location, thus eliminating the need for any form of engineered treatment.

Baker and Herson (1994) note that bioremediation is not a new technology, having been used in wastewater treatment for at least a century. The novel idea is applying this

technology to groundwater contaminants *in situ*. *In situ* bioremediation is divided into natural and enhanced/engineered methods. Enhancement procedures typically increase biodegradation by either pumping the limiting electron acceptor or appropriate microorganisms into the subsurface until the substrate becomes the limiting factor in the reaction kinetics. Recently, more emphasis has been placed on natural bioremediation, investigating whether the 'non-action' alternative is an environmentally sound option. Acceptance of the non-action alternative can be justified only if existing aquifer conditions are shown to prevent the contaminant from reaching the nearest potential contact with humans or wildlife, the so-called first point of contact (POC).

Natural *in situ* bioremediation is significantly impacted by the sequential use of electron acceptors. Early research into *in situ* bioremediation identified only aerobic degradation of most groundwater contaminants. More recent research has shown degradation of aromatic hydrocarbons under anaerobic conditions, with acceptable electron acceptors including nitrate, iron(III), and sulfate (for summary, see Baker and Herson, 1994) . Methanogenic contaminant reduction has also been demonstrated, but is significantly slower than the other degradation processes (Vogel and Grbic-Galic, 1986). The most recent discovery of iron(III) reduction is evidenced by reduced contaminant concentrations and increased levels of aqueous phase iron(II) under anaerobic conditions (Lovley and Lonergan, 1990; Landmeyer et al., 1994). Additional research shows that iron(III) is preferentially used over sulfate (Chapelle and Lovley, 1992), but also shows iron(III) utilization is inhibited by the presence of oxygen and nitrate. The discovery of solid phase, iron(III)-based oxidation of toluene and other aromatic hydrocarbons may significantly increase the number of sites where the non-action alternative of natural biodegradation is acceptable.

Concurrent with research into *in situ* bioremediation theory, mathematical models have been developed to predict the effects of biodegradation. Using standard advection-dispersion transport models, researchers have added various types of decay terms to account for natural and/or enhanced biodegradation. Although these models have met

with some success in enhanced *in situ* bioremediation simulations, the more complex natural degradation phenomena has created the need for models designed to predict the effects of both solid and aqueous phase sequential electron acceptors.

1.2 Problem Statement

The objectives of this research are to evaluate the extent with which solid phase, iron(III)-based biodegradation affects natural intrinsic bioremediation and to develop a mathmatical model which accurately and realistically represents iron(III)-based oxidation of petroleum hydrocarbons. The effects of iron(III)-based biodegradation are examined by developing and testing a natural *in situ* biodegradation model. The model presented here couples two-dimensional transport and biodegradation using sequential electron acceptors, allowing both aqueous and solid phase electron acceptor to be modeled. A three-phase approach is employed to reach this goal. First, an existing model (SEAM2D) is adapted to handle a solid phase electron acceptor. Next, the SEAM2D model is investigated to determine which input parameters most significantly impact model output (i.e. changes in substrate mass and concentration). Finally, a comparison of SEAM2D model predictions is compared with data received from a USGS study site in Laurel Bay, South Carolina where petroleum hydrocarbons have leaked from a UST into the subsurface.

Note that the SEAM2D model, developed by Widdowson (1992), is unique in that it is the first to couple two-dimensional transport with sequential electron acceptors. The primary electron acceptor used in the field simulations is aqueous phase dissolved oxygen, while the terminal electron acceptor is solid phase iron(III). The modeling sequence of oxygen reduction (redox) followed by iron reducing conditions is also unique to this research.

1.3 Scope

This research concentrates on one model of sequential electron acceptor utilization. Model simulations use only one or, at most, two electron acceptors, with the primary electron acceptor being dissolved oxygen and the terminal electron acceptor being solid-phase iron(III),

unless otherwise noted. For the Laurel Bay site, this assumption neglects any contaminant reduction due to nitrate reducing, sulfate reducing, or methanogenic microorganisms.

For aqueous phase electron acceptors, utilization rates are assumed to follow modified Monod kinetics. The solid phase, iron-reducing kinetics are assumed to be zero order with respect to iron, and follow regular Monod kinetics with respect to the hydrocarbon contaminant, with an inhibition term added. This inhibition function accounts for reduced anaerobic substrate consumption due to the presence of oxygen.

A sensitivity investigation is performed by varying non-dimensional parameters identified in dimensionless governing equations from minimum to maximum values, as calculated from a search of current literature. Values for these non-dimensional groupings are calculated from the individual parameters, with typical values defined through the literature search. The sensitivity of each parameter is evaluated on the basis of a substrate mass balance, plotted as a function of time, and selected cross sections, reported as substrate or electron acceptor concentration versus longitudinal distance, which are felt to be representative of the model's performance.

All simulations assume a uniform velocity distribution and background concentration of both substrate and electron acceptors. A line boundary condition is used to simulate contaminant inflow. Finally, electron acceptor concentration for oxygen at the line boundary source is set lower than background concentrations, creating the anoxic zone typically seen in the center of aromatic hydrocarbon plumes.

1.4 Approach

To accomplish the above goals, the following chapters are provided. Chapter 2 provides an overview of modeling *in situ* bioremediation. This overview consists of several sections including a brief description of *in situ* bioremediation, a survey of alternate electron acceptors, and a review of existing bioremediation models. Chapter 3 contains the conceptual framework for a biodegradation model by listing applicable phenomena and the equations used to describe this phenomena. Chapter 3 also contains

the development of the SEAM2D model and identifies the governing equations of SEAM2D, both in dimensional and non-dimensional form. From the governing equations, necessary input parameters are identified and discussed. A compilation of required input parameters, their range of values, and a list of sources are included in Chapter 3. Chapter 4 contains the methodology and results of a sensitivity investigation, conducted to determine which parameters have the most influence on substrate mass and concentration. Chapter 4 also lists recommendations on parameter determination. These recommendations are used in Chapter 5, which applies SEAM2D to a gasoline leak from a UST site in Laurel Bay, South Carolina. Chapter 5 also contains the results of measurements and modeling for the aromatic hydrocarbon, toluene. Model simulations are conducted for a variety of electron acceptor conditions and results are presented as both one dimensional concentration profiles and two dimensional contour plots. Chapter 6 summarizes the results and conclusions of this research, and suggests future areas of research.

CHAPTER 2. Literature Review

2.1 The Biodegradation Environment

As Wilson et al. (1986) indicate, biodegradation is limited by either the available microbial population, electron acceptor, or electron donor. The microbial population requires a carbon, energy, and respiratory source to survive and grow (Bedient et al., 1994). In bioremediation, a hazardous compound, such as an aromatic hydrocarbon, can serve as the energy and carbon source, or substrate, and respiration is satisfied by an electron acceptor, such as oxygen, nitrate, iron(III), or sulfate. Biodegradation occurs when microbes are found in the same location as a suitable substrate and electron acceptor. Wilson et al. (1986) also note that many aquifers support a microbial population capable of degrading various groundwater contaminants, and cite the work of Ghiorse and Balkwill (1983) as evidence that these aquifers are capable of supporting this population, even at deeper aquifer locations. Given an adequate microbial population with a suitable substrate and electron acceptor, substrate oxidation may occur, unless limited by an insufficient concentration of either the electron acceptor or substrate itself.

The recognition of a biologically active subsurface environment has led to increased research into subsurface microbial populations. Depending on their mode of respiration, microbes can be classified into three categories, as aerobic, anaerobic, or facultative organisms (Tchobanoglous and Schroeder, 1985). Aerobes, as the name suggests, thrive only in oxygen environments, using dissolved oxygen as an electron acceptor. Strict anaerobes grow only under highly reduced conditions, where oxygen is effectively absent, and use an electron acceptor, such as sulfate, or carbon dioxide, as a respiratory source. Facultative organisms adapt to both aerobic and anaerobic conditions, but are typically more active in the presence of oxygen (Hutchins, 1991a). Microbes using nitrate as an electron acceptor tend to be facultative (Firestone, 1992), whereas sulfate reducing and methanogenic organisms are strict anaerobes (Oremland, 1988; Jørgensen, 1989; Baker and Herson, 1994). Iron reducers were originally shown in pure culture (Lovely and Lonergan, 1990), while recent evidence suggests

that facultative oxygen/iron(III) reducing organisms also exist and can significantly oxidize groundwater contaminants (F. Chapelle, pers. comm.).

The order of electron acceptor utilization is dependent on both the microbial population's respiratory preferences and the availability and quantity of each electron acceptor. Stumm and Morgan (1981) note that microbes tend to oxidize organic substrate by using the electron acceptor which provides the most energy. Figure 2.1, from Zehnder and Stumm (1988), displays the free energy associated with the various natural redox processes. Suflita and Sewell (1991) report the electron acceptor utilization order shown schematically as Figure 2.2(a) by examining the energy potential for each reduction process. Jørgensen (1989) uses the Gibbs free energies for the electron acceptor half reactions, calculated by Stumm and Morgan (1981), to support a similar electron acceptor sequence. Figure 2.2(b), adapted from Jørgensen (1989), illustrates the sequence and products of electron acceptor utilization for organic carbon oxidation.

As Lyngkilde et al. (1991) demonstrate, natural *in situ* bioremediation may employ different electron acceptors at various locations throughout a given site. These researchers determined a utilization order by measuring field concentrations for each electron acceptor. Figure 2.3 schematically shows the results of their work, depicting respiratory conditions for a plume which varies from highly reactive aerobic conditions, through anoxic nitrate and iron reduction, to highly reduced sulfate and methanogenic conditions. The work of Lyngkilde et al. (1991) provides an example of multiple electron acceptor utilization, illustrating spatial variation in electron acceptor use due to utilization order, source, and initial aquifer conditions.

Much of the original work on *in situ* bioremediation was conducted by Raymond and coworkers at Suntech during the 1970's (see Jamison et al., 1975; Raymond et al. 1976 & 1978). Initial research into organic compound degradation recognized only the importance of oxygen-based or aerobic respiration. Lee et al. (1987) indicate that, petroleum hydrocarbons, such as gasoline, aviation fuels, and heating oils, are some of the most aerobically biodegradable found in the subsurface environment. These researchers also note that the BTEX compounds are particularly degradable under aerobic conditions. Severe limits

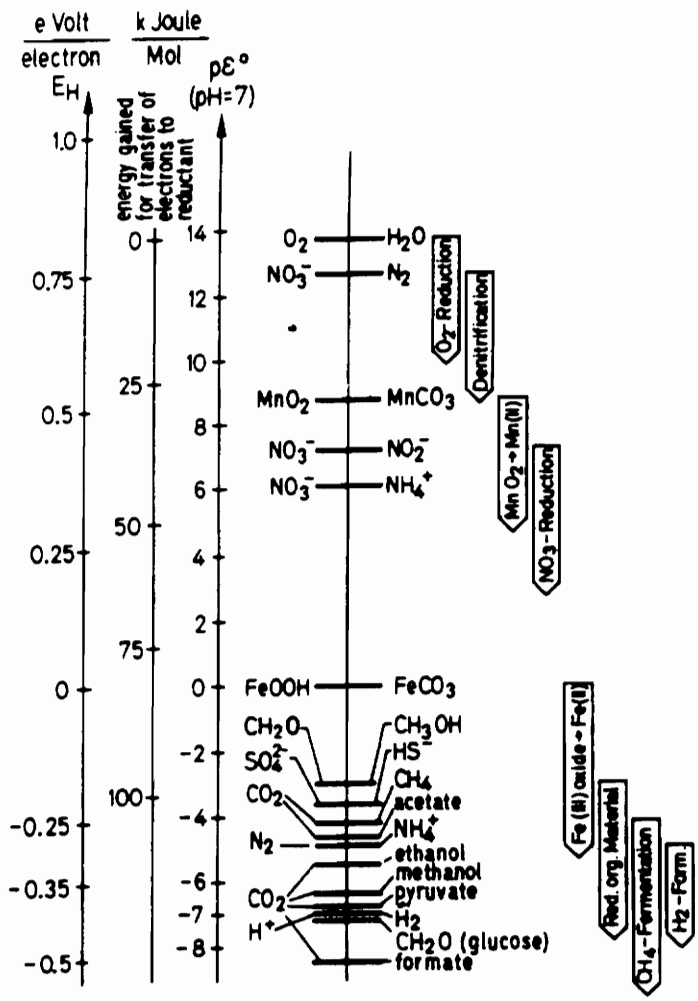

Figure 2.1. Electron-free energy diagram. (from Zehnder and Stumm, 1988)

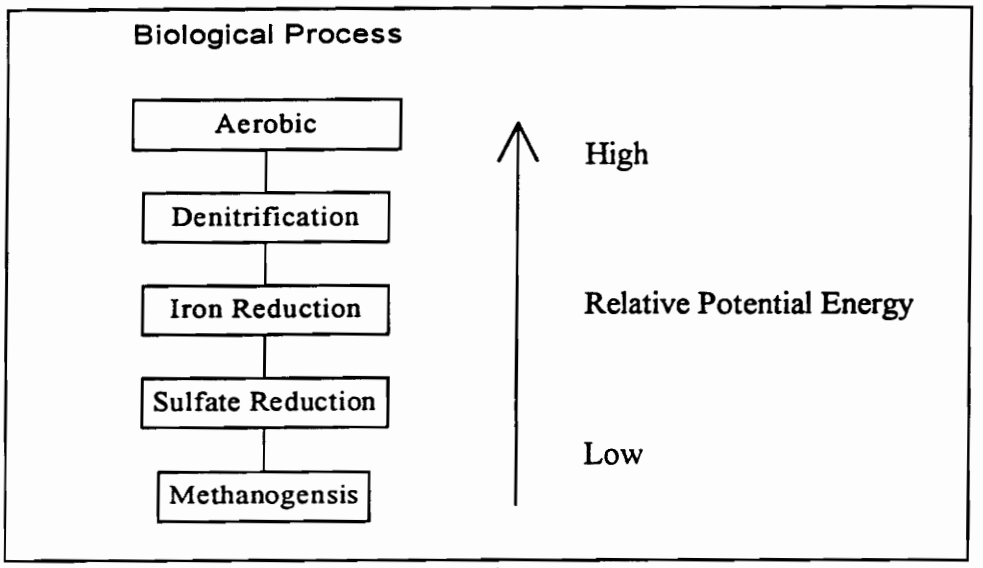

(a)

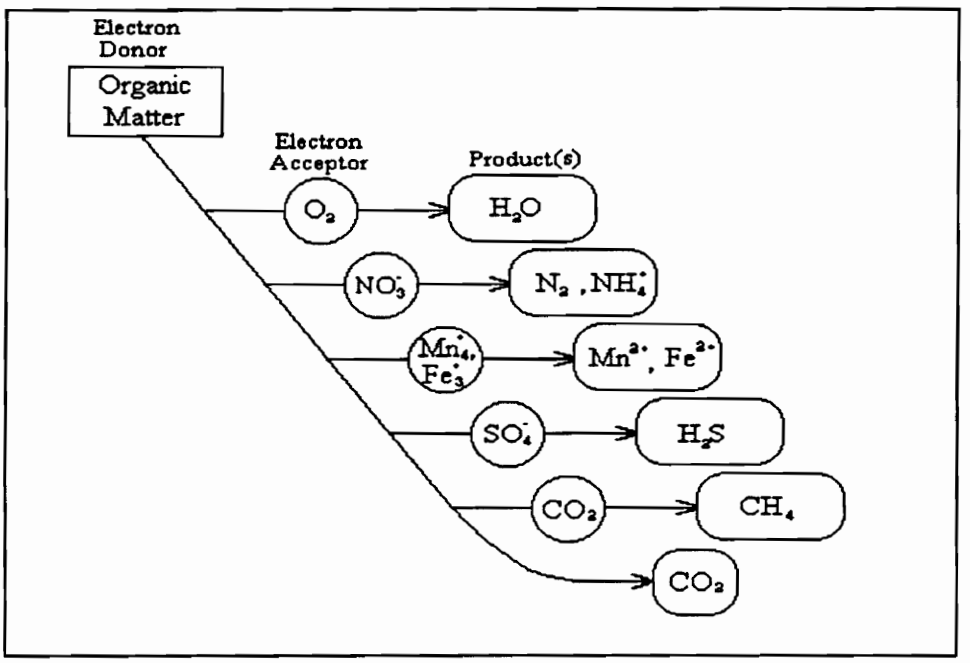

(b)

Figure 2.2(a) Electron acceptor utilization sequence determined by electron potential energies. (After Suflita and Sewell, 1991)

(b) Sequence and products for alternate electron acceptors reduction of organic compounds. (Adapted from Jørgensen, 1989)

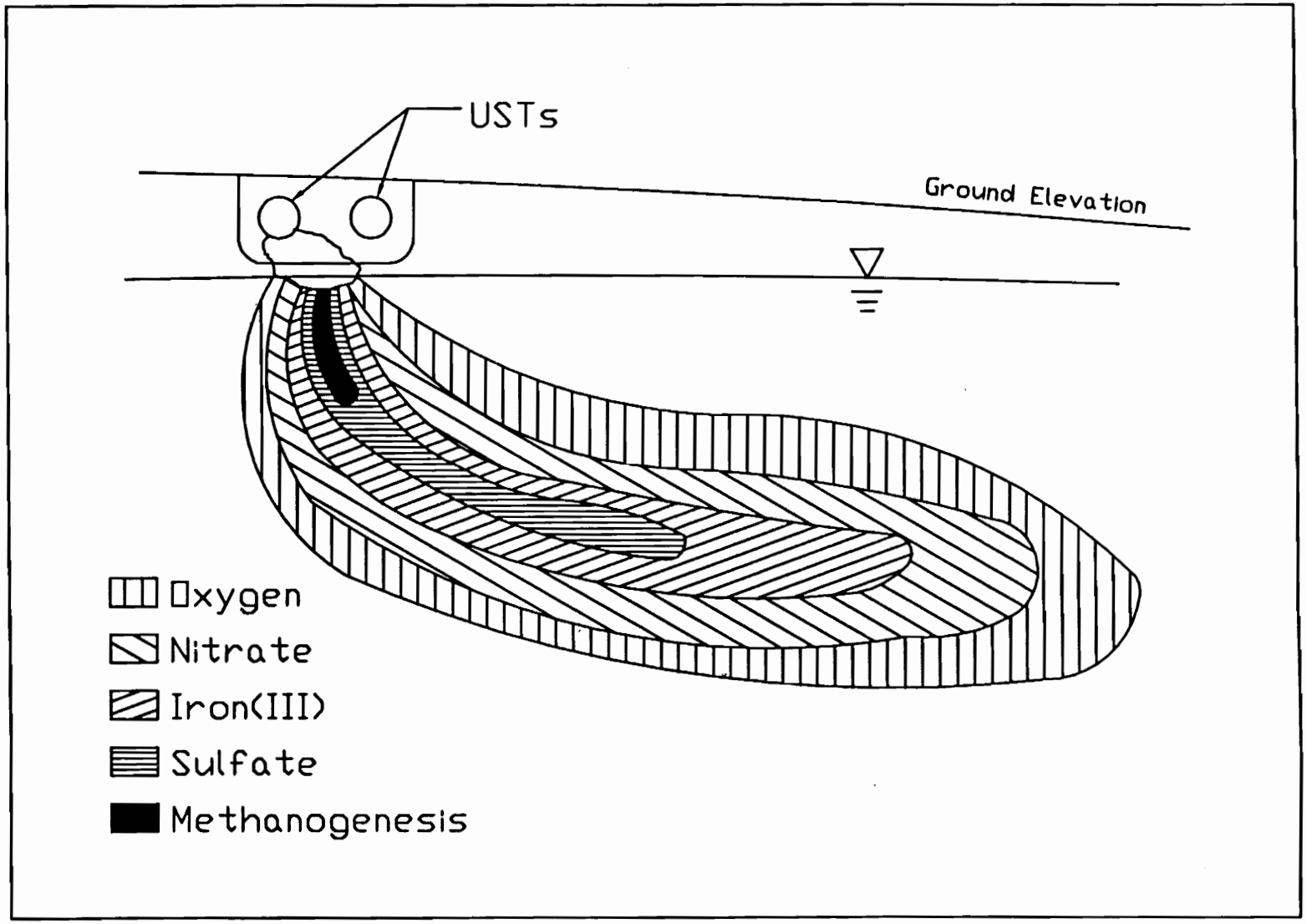

Figure 2.3. Spatial variation in electron acceptor conditions. (Adapted from Lynkilde et al., 1991)

may be placed on aerobic biodegradation of petroleum and other hydrocarbons, however, due to the low solubility of oxygen and the rapid reaction rates typical of oxygen reducing environments (Wilson et al., 1986; Zeyer et al. 1986; Barker et al., 1987). Note also that some aromatic hydrocarbons, for example the gasoline additive, methyl-tert-butyl-ether (MTBE), are recalcitrant to biological transformation (Landmeyer et al, 1994).

Although natural or artificial recharge may stimulate aerobic biodegradation by reintroducing oxygen to anaerobic regions, more recent investigations have led researchers to recognize the significance of anaerobic degradation of aromatic hydrocarbons. Investigation of aromatic hydrocarbon oxidation using nitrate-reducing (Zeyer et al., 1986; Hutchins, 1991a; Arcangeli and Arvin, 1994), iron-reducing (Lovley and Lonergan, 1990), sulfate-reducing (Haag et al., 1991; Edwards and Grbic-Galic, 1992) and methanogenic (Wilson and Rees, 1985; Grbic-Galic and Vogel, 1987) organisms has helped generate the current interest into natural *in situ* bioremediation. In particular, toluene, ethylbenzene and some of the xylenes have been shown to degrade anaerobically (e.g. Zeyer et al., 1986; Lovely and Lonergan, 1990; Hutchins, 1991a; Barbaro et al. 1992; and others). Arcangeli and Arvin (1991) note that toluene is the most anaerobically degradable compound of the BTEXs and also suggest that ethylbenzene and xlyene degradation is most significant when these compounds are cometabolized with toluene. Evidence of anaerobic benzene oxidation has been mixed. Hutchins' (1991b) study, which focuses on nitrate reduction, indicates previous investigations have shown benzene to be recalcitrant in some instances, but degradable under other anaerobic conditions. Hutchins provides two possible explanations for these conflicting reports by suggesting that either oxygen intrusion occurred during the microcosm studies, accounting for the reported degradation, or that the previous exposure of the microbial populations was sufficiently different to account for the discrepancies. Table 2.1 provides a partial listing of studies reporting biodegradation of the BTEX compounds under both aerobic and anaerobic conditions.

Anaerobic biodegradation rates for aromatic hydrocarbons are typically an order of magnitude or more less than aerobic conditions, but still may significantly influence substrate

Table 2.1. Research supporting biodegradation of BTEX compounds. (Modified from Bedient et al., 1994)

Compound	Conditions	Test	Reference
Benzene	Aerobic	In situ	Wilson et. al., 1986b
	Methanogenic, microcosm	Field simulation	Wilson et. al., 1986c
	Aerobic, batch study	Laboratory	Tabak et al., 1990
Ethylbenzene	Methanogenic, microcosm	Laboratory	Wilson et al., 1986
	Anaerobic, continuous flow column	Field sample	Kuhn et al., 1988
	Aerobic batch study	Laboratory	Tabak et al., 1990
	Nitrate reducing	Laboratory	Arcangeli and Arvin, 1994.
Toluene	Aerobic, microcosm	Field sample	Wilson et al., 1983b
	Aerobic	In situ	Wilson et al., 1986a
	Aerobic	In situ	Wilson et al., 1986b
	Methanogenic, microcosm	Field sample	Wilson et al, 1986c
	Anaerobic, continuous flow column	Field sample	Zeyer et al., 1986
	Aerobic, batch study	Field sample	Swindoll et al., 1988
	Anaerobic, continuous flow column	Field sample	Kuhn et al., 1988
	Iron reducing, batch study	Laboratory, pure culture	Lovley and Lonergan, 1990
	Aerobic, batch study	Laboratory	Tabak et al., 1990
	Methanogenic, microcosm	Field sample	Beller et. al., 1991
	Nitrate reducing microcosm and field stugy	Field sample	Barbaro et al., 1992
m-xylene	Aerobic	In situ	Wilson et al., 1986b
	Anaerobic, continuous flow column	Field sample	Kuhn et al., 1988
	Aerobic, batch study	Laboratory	Tabak et al., 1990

reduction due to longer reaction times (Wilson et al., 1986; Hutchins, 1991a; Landmeyer et al., 1994). The slower reaction rates are attributable to two phenomena. First, anaerobic microbes are less efficient at using the available electron acceptors to reduce groundwater contaminants (Zehnder and Stumm, 1988; Baker and Herson, 1994). Second, presence of one electron acceptor may inhibit the utilization of a second electron acceptor, especially if the first electron acceptor is oxygen (Hutchins, 1991a; Chang et al. 1993). The most important factor in determining if a contaminant plume can be successfully remediated may be identification of the terminal electron accepting process. Chapelle (1995) states that iron(III) and sulfate terminal electron accepting process may exhibit a rate constant two to three orders of magnitude less than aerobic conditions, but still adequately contain the contaminant plume if the groundwater velocity is slow relative to the rate of substrate biodegradation.

2.2 Iron(III) as an Electron Acceptor

This research gives particular emphasis to understanding and modeling the newly recognized iron(III) reducing condition found in some aquifer locations. Lovley and Lonergan (1990) were first to demonstrate pure culture iron(III)-based oxidation of toluene and show that aqueous phase iron(II) is a product of this reaction. Field measurements of large iron reducing zones in polluted aquifers have been documented by Nicholson et al. (1983) and Lyngkilde et al. (1991). Further evidence of iron reduction in the presence of groundwater contaminants is demonstrated by the reduction potential of aquifer soils containing iron(III) (Barcelona and Holm 1991; Heron et al., 1994). Chapelle and Lovley (1992) examined the inhibitory effects of iron(III) on other electron acceptors and found that sulfate reduction was severely limited by the presence of iron(III) oxyhydroxides. Lovely et al. (1994) demonstrate that iron(III)-based biodegradation of aromatic hydrocarbons can be significantly enhanced by the addition of organic ligands to the subsurface environment, suggesting that the rates of enhanced iron(III) degradation approach those of oxic environments. All of this research has led to our investigation of modeling iron(III) reduction in the groundwater environment.

Lovley et al. (1994) suggest that shallow aquifers are likely to have an abundance of insoluble iron(III) oxides, providing a major alternate electron acceptor source. Heron et al. (1994) provide a list of the most prevalent oxidized iron species, given here as Table 2.2. These researchers also list the possible electron acceptor half reactions for iron reduction shown in Table 2.3. Table 2.3 also contains the stoichiometric equations developed by Lovley and Lonergan (1990) for biologically mediated toluene-iron redox reactions. Lovley and Lonergan (1990) note that their experimental results closely match the theoretical 1:36 ratio of oxidized toluene to iron(II) production shown in Table 2.3.

Several sites in the coastal Carolina aquifer system have exhibited significant contaminant reduction under iron(III) reducing conditions. One such site is located in South Carolina's coastal aquifer, underlying the Laurel Bay Exchange, Marine Corps Air Station, Laurel Bay, South Carolina. Once the available oxygen has been consumed, Landmeyer, et al. (1994) provide evidence of significant iron(III)-based hydrocarbon reduction via measurements of high concentrations of iron(II), the end product of iron(III) reduction. Through monitoring well samples of contaminant (BTEX and MTBE), electron acceptor, and end product concentrations, Landmeyer et al. (1994) attempt to monitor and predict the fate of groundwater contaminants at the Laurel Bay site.

2.3 Previous Modeling Studies

From the remediation perspective, the existence of aromatic hydrocarbon degradation under multiple electron acceptor conditions is very promising. From the modeling perspective, however, inclusion of multiple electron acceptors and/or microbial populations adds complexity to models attempting to simulate groundwater contaminant degradation. Widdowson (1992) notes that various researchers have developed models to predict the fate and transport of biodegradable groundwater contaminants. Early models typically consisted of one-dimensional transport with single electron acceptors and single substrates (e.g. Molz et al., 1986; Borden et al., 1986). As research into *in situ* biodegradation increased, more complex models were developed, incorporating two-dimensional transport (Borden and Bedient, 1986), multiple

Table 2.2. Oxidized iron species. (Adapted from Heron et al., 1993)

Name	Formula	Color
Ferrihydrite (rust)	$Fe(OH)_3$	reddish-brown
Lepidocrocite	γ-FeOOH	orange
Akageneite	β-FeOOH	yellowish-brown
Maghemite	γ- Fe_2O_3	reddish-brown
Magnetite	Fe_3O_4	black
Hematite	α-Fe_2O_3	bright red
Goethite	α-FeOOH	yellowish-brown

Table 2.3. Iron reducing half and full redox reactions.

Half-Reactions (from Heron et al., 1994)	Electron Acceptor Phase
$Fe(OH)_3 + 3H^+ + e^- \rightarrow Fe^{2+} + 3H_2O$	(Solid)
$FeOOH + 3H^+ + e^- \rightarrow Fe^{2+} + 2H_2O$	(Solid)
$Fe_2O_3 + 6H^+ + 2e^- \rightarrow 2Fe^{2+} + 3H_2O$	(Solid)
Toluene(C_7H_8)-Iron Redox Reactions (modified from Lovley and Lonergan, 1990)	
$C_7H_8 + 36Fe(OH)_3 + 21H_2O \rightarrow 36FeO + 7H_2CO_3 + 72\ H_2O$	
$C_7H_8 + 108Fe(OH)_3 \rightarrow 36Fe_3O_4 + 7H_2CO_3 + 159\ H_2O$	

electron acceptors (Widdowson et al., 1988), and multiple substrates (Celia et al., 1989). Baveye and Valocchi (1989) provide a discussion of conceptual and mathematical models for biodegradation, while Bedient et al. (1994) provide an overview of existing biodegradation models.

When developing a model for biodegradation, two major decisions need to be made. The first decision is on the type of kinetics expression. Many models use modified Monod kinetics to determine utilization rates (e.g. Molz et al, 1986; Widdowson et al., 1988), but first order kinetic expressions have also been investigated (Tucker et al 1986; Domenico, 1987). First order kinetics are defined by a single parameter, the decay rate coefficient, with this coefficient considered constant and independent of substrate or electron acceptor concentration. Modified Monod kinetics account for variations in utilization rates due to changes in both substrate and electron acceptor concentrations. Rifai et al. (1988) take a unique approach of modeling biodegradation by superimposing transport of the substrate and electron acceptor, and assuming instantaneous reaction between the compounds. The second modeling decision is to define the structure of the microbial population. Biofilm models, as proposed for the groundwater environment by McCarty et al. (1984), assume that microbes are fixed to aquifer sediments in a continuous culture, and are often idealized as uniform in thickness and cell density (Bedient et al., 1994). Microcolony models, as an alternative to biofilms, assume discrete microbial communities which can generally be expressed as surface area available for diffusion per volume biomass (Widdowson et al., 1988). Baveye and Valocchi (1989) conclude that the microcolony approach is closer to reality in the existing subsurface environment, while biofilms are seen more often in wastewater and other engineered biological systems.

Although many biodegradation models have been proposed, very few of them have been tested by through naturally attenuating field simulations. Borden et al. (1986) test an aerobic, instantaneously reacting, one-dimensional transport model on a aromatic hydrocarbon contaminated site in Conroe, Texas and report reasonable predictions of observed conditions. Chiang et al. (1989) examine two dimensional transport and first

order decay for aerobic biodegradation of a BTX plume in Traverse City, Michigan. After calibrating the model with data from two temporally spaced data sets, BTX concentrations are predicted reasonably well for a third data set, even though significant differences were observed between predicted and actual oxygen concentrations. Klecka et al. (1990) apply a one dimensional, first order decay model to the Cliffs-Dow superfund site using kinetics parameters determined through a microcosm study. The simulations for this site account for the full range of representative values for the major input parameters (i.e. groundwater velocity and parent compound half life) leading to a worst case estimation that the contaminant is predicted to be contained to within 75m of the source.

Landmeyer et al. (1994) provide a unique modeling study at the Laurel Bay Exchange site in Laurel Bay, South Carolina. Site investigation led the research team to identify both aerobic an iron(III) based biodegradation of the BTEX contaminants. These researchers simulate plume migration and natural attenuation by using a model, developed by Voss (1984), which combines two dimensional transport with adsorption and first order biodegradation kinetics. Landmeyer et al.'s modeling effort examines the acceptability of natural attenuation by questioning if the worst case biodegradation simulation will prevent a potential POC. Their 'worst case' biodegradation rate was determined through a laboratory microcosm study of an iron-reducing aquifer sample, making their work unique as the first reported attempt to match model simulations with field data for iron(III)-based biodegradation. Although their effort is a significant advance in site modeling of biodegradation, the model employed in their investigation does not allow for either modified Monod kinetics or multiple electron acceptors.

Few researchers have published information on the development and application of multiple electron acceptor models. Widdowson et al. (1988) develop a one dimensional transport model coupled with sequential electron acceptors and provide a series of hypothetical simulations for aerobic, anaerobic (nitrate reducing), and sequential electron accepting conditions. Widdowson and Aelion (1991) extend this model to two dimensions and applied the model to a site in Hanahan, South Carolina. The model simulations for the

Hanahan site were performed to evaluate the effects of oxygen-nitrate sequential electron acceptor utilization on an enhanced *in situ* bioremediation plan to remediate the existing BTEX plume. Most recently, Rifai et al. (1995) have updated their model to incorporate a variety of kinetics expressions and multiple electron acceptors. As of the writing of this thesis, Rifai and colleagues are in the process of collecting data and to calibrate and verify their updated model.

The model examined in this thesis was developed by Widdowson (1988, 1992) and accounts for two dimensional transport, adsorption, and biodegradation of groundwater contaminants. This thesis extends Widdowson's model by developing the equations and coding for the solid phase electron acceptor, iron(III). Based on the field data collected by Landmeyer et al. (1994), a site application is also provided, where substrate and electron acceptor utilization is calculated using modified Monod kinetics, coupled with a multiple electron acceptor sequence of aqueous phase dissolved oxygen followed by solid phase iron(III).

CHAPTER 3. Model Development

3.1 Microbial Processes

3.1.1 Representation and Kinetics of Microbial Populations

In theory, the distribution, density, and characteristics of the subsurface microbial population change constantly in response to changes in electron donor, electron acceptor, and carbon source availability in the subsurface. One method of modeling the changes in microbial population size and characteristics is to divide the heterotrophic microbial population into several smaller populations which share common characteristics. As noted in the previous chapter, the heterotrophic microbial population can be divided into three distinct populations based on their mode of respiration (i.e. aerobic, facultative, and anaerobic). Another possibility is to divide the microbial population into different categories based on electron acceptor utilization, characterizing the microbes as oxygen-reducers, nitrate-reducers, iron-reducers, and so forth. The model used in this research employs both of these classification systems by first dividing the microbial population based on mode of respiration and then subdividing these populations based on electron acceptor utilization.

Regardless of the classification system selected, changes in the microbial populations can be accounted for using a simple mass balance composed of both a growth and a decay term. According to Herbert (1958), microbial population growth is proportional to the substrate utilization rate, r_s [$M_S/M_B/T$], defined as mass of substrate per biomass per time. Herbert (1958) suggests using a decay term corresponding to energy maintenance, while Pirt (1975) advocates a decay term representing death of cells in the microbial population. Although Pirt (1975) and Herbert (1958) disagree on the physical meaning of the decay rate, Harvey and Widdowson (1992) correctly indicate that either theory produces the same solution. A simple mass balance equation can thus be written for each microbial population as:

$$Yr_s - k_d = \frac{1}{M}\frac{dM}{dt} \tag{3.1}$$

where M is the biomass population per unit volume of porous medium [M_B/L^3], t is time [T], Y is the yield coefficient [M_B/M_S], and k_d is the decay, or death, rate for the population. The yield coefficient is defined for each electron acceptor as biomass per mass of substrate consumed, with a decrease in yield coefficient indicating an decrease in the microbes' utilization efficiency. Formulation of r_s is provided in the next section where the kinetics of substrate (and electron acceptor) utilization are discussed.

3.1.2 Growth Rates

Biodegradation kinetics are most commonly expressed in terms of a hyperbolic saturation-type function known as Monod or Michaelis-Menten kinetics. Monod (1942) first investigated the effects of substrate concentration on growth rate and the results of his work produced the now widely accepted Monod equation, given by:

$$\mu = \mu_{max}\left[\frac{s}{K_s + s}\right] \tag{3.2}$$

where μ is the specific growth rate [M_B/M_B /T], μ_{max} is the maximum specific growth rate [M_B/M_B/T], s is the microbial phase substrate concentration [M_S/L^3], and K_s is the half-saturation (Monod) constant [M_S/L^3]. The Monod equation is shown graphically in Figure 3.1. For high substrate concentrations ($s >> K_s$), growth is limited by the maximum specific growth rate. For lower substrate concentrations, substrate concentration becomes limiting and causes growth to tend to zero.

Harvey and Widdowson (1992) cite Harris and Hanford (1976) as evidence that growth rates for aerobic microorganisms may be subject to either single or dual limitation. As derived by Harris and Hanford (1976), the modified Monod equation for either substrate (electron donor), oxygen (electron acceptor), or dual limiting conditions may be written as:

$$\mu_{so} = \mu_o\left[\frac{s}{K_{so} + s}\right]\left[\frac{o}{K_o + o}\right] \tag{3.3}$$

where μ_{so} is the aerobic substrate growth rate [M_B/M_B /T], μ_o is the maximum specific

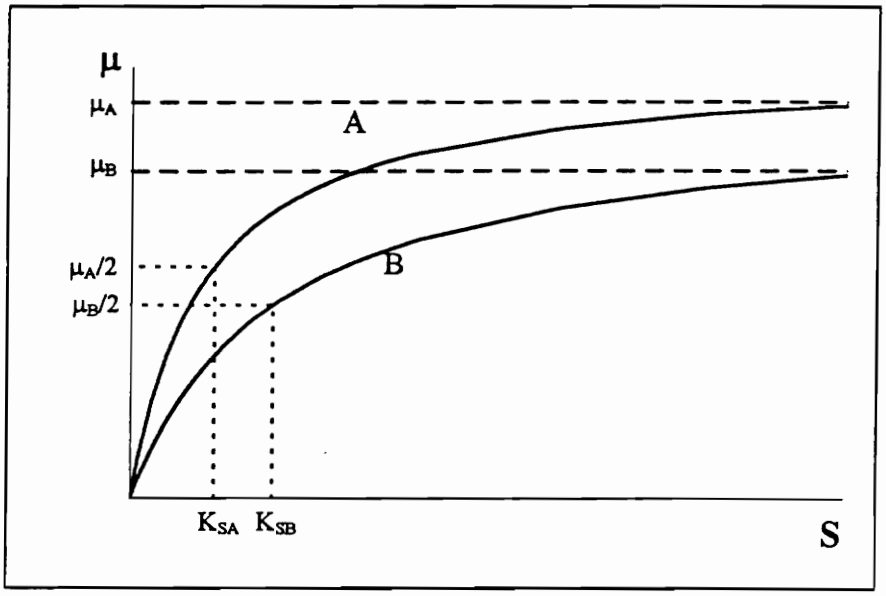

(a)

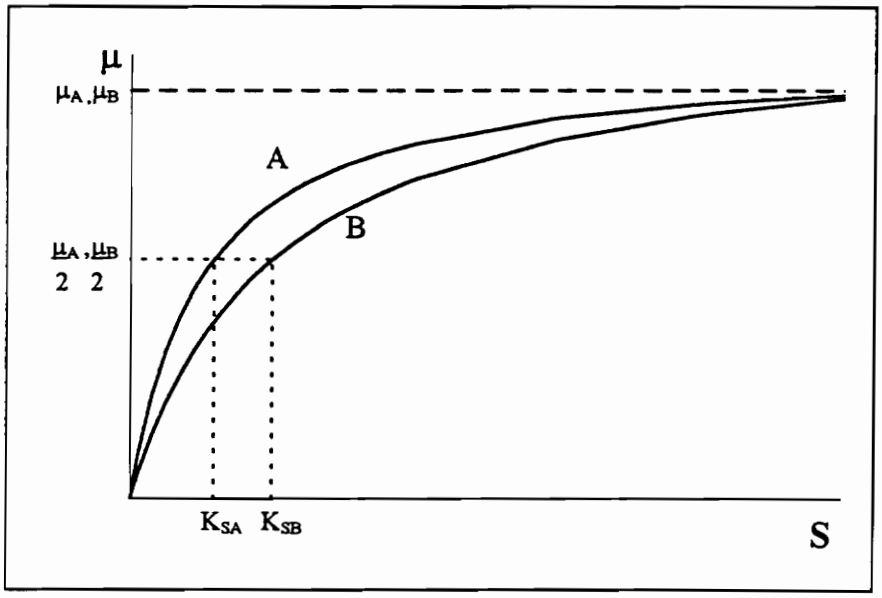

(b)

Figure 3.1. The Monod relationship, graphed as specific growth rate (μ) versus substrate concentration (S) for (a) compound A more biodegradable than compound B ($\mu_A > \mu_B$) and (b) for compound A with a smaller Monod constant than compound B ($K_{SB} > K_{SA}$). (After Rifai and Bedient, 1990)

growth rate under aerobic conditions [M_B/M_B /T], s and o are the microbial phase concentration for substrate [M_S/L^3] and oxygen [M_{O2}/L^3] respectively, K_{so} is the half saturation constant for substrate by oxygen-reducing organisms [M_S/L^3], and K_o is the half saturation constant for oxygen [M_{O2}/L]. Equation (3.2) is valid for growth when a single substrate limits growth, while the modified Monod equation (Equation (3.3)) may be used for dual limiting conditions. Molz et al. (1986) also use this form of the modified Monod equation, relating their conceptual model of microbial metabolism to the equations developed by Bailey and Ollis (1977).

Harvey and Widdowson (1992) also summarize various models used to simulate inhibited substrate growth. As noted by these researchers, Widdowson et al. (1988) proposes a growth rate expression for oxygen-inhibited, anaerobic, nitrate-based respiration given by:

$$\mu_{sn} = \mu_n \left[\frac{s}{K_{sn} + s} \right] \left[\frac{n}{K_n + n} \right] I(o) \tag{3.4}$$

where μ_{sn} is the growth rate due to anaerobic, nitrate-based respiration [$M_B/M_B/T$], μ_n is the maximum specific growth rate under nitrate-based respiration [$M_B/M_B/T$], n is the nitrate concentration in the microbial phase [M_{NO3}/L^3], K_{sn} is the half saturation constant for nitrate based substrate utilization [M_S/L] and K_n is the half saturation constant for nitrate-based respiration [M_{NO3}/L^3]. The inhibition function, I(o), is given by:

$$I(o) = \frac{K_c}{K_c + o} \tag{3.5}$$

where K_c is a coefficient of inhibition [M_{O2}/L^3]. Bouwer and Cobb (1987), also cited by Harvey and Widdowson, note that inhibition models have the advantages of rapid numerical method convergence and adjustable control over oxygen concentration influence on alternate electron acceptor utilization.

3.1.3 Utilization Rates

Conversion of the aforementioned specific growth rate to a substrate utilization rate, r_s, is accomplished via the yield coefficient mentioned in the discussion of microbial kinetics. Using modified Monod kinetics, the substrate utilization rate equations for oxygen and nitrate-based respiration are given by Equations (3.6) and (3.7), respectively:

$$r_{so} = \frac{\mu_{so}}{Y_o} \tag{3.6}$$

$$r_{sn} = \frac{\mu_{sn}}{Y_n} \tag{3.7}$$

where Y_o and Y_n are the yield coefficients [M_B/M_S] for oxygen and nitrate-reducing conditions, respectively.

Similar to substrate utilization, a type of yield coefficient is used to convert microbial growth rate to a rate of electron acceptor utilization. When developing equations for electron acceptors, the conversion factor is referred to as a use coefficient, γ, as illustrated for oxygen (Equation (3.8)) and nitrate (Equation (3.9)) below:

$$r_o = \gamma_o \mu_{so} \tag{3.8}$$

$$r_n = \gamma_n \mu_{sn} \tag{3.9}$$

where r_o is the oxygen utilization rate [$M_{O2}/M_B/T$], r_n is the oxygen utilization rate [$M_{NO3}/M_B/T$], γ_o is the oxygen use coefficient [M_{O2}/M_B], and γ_n is the nitrate use coefficient [M_{NO3}/M_B].

3.1.4 Modeling Solid Phase Electron Acceptors

The modified Monod equations (Equations (3.3) and (3.4)) are applicable for aqueous phase substrates and electron acceptors, as are found in many *in situ* bioremediation applications. The recognition of solid phase, iron(III)-based respiration creates a need for a utilization kinetics model capable of handling an aqueous phase substrate and solid phase electron acceptor. Chapelle (pers. comm.) recommends using the standard Monod relationship for a solid phase electron acceptor, such as iron(III), yielding

an equation for the microbial growth rate under iron-reducing conditions, μ_{sf} [$M_B/M_B/T$], in the form of:

$$\mu_{sf} = \mu_f \left[\frac{s_f}{K_{sf} + s_f} \right] I(o) \tag{3.10}$$

where μ_f and K_{sf} are the maximum specific growth rate [$M_B/M_B/T$] and half saturation constant [M_S/L^3] for iron-reducing conditions, respectively, and s_f is the microbial phase concentration of substrate under iron-reducing conditions. Although Equation (3.10) implies that iron(III)-based respiration is limited solely by the electron donor (i.e. substrate), μ_{sf} is set to zero when iron(III) becomes limiting or depleted during biodegradation. Chapelle suggests that iron(III)-based respiration subsides for iron(III) concentrations less than 10 μg Fe(III)/g of porous medium, corresponding to the concentration where the iron(III) is no longer accessible to the microbial population. Conversion of the iron(III)-based growth rate to a substrate utilization rate equation is accomplished by dividing Equation (3.10) by a yield coefficient for iron(III)-based respiration, Y_f [M_B/M_S], as was done for the aqueous phase electron acceptors in Equations (3.6) and (3.7), and is given here as:

$$r_{sf} = \frac{\mu_{sf}}{Y_f}. \tag{3.11}$$

The electron acceptor utilization rate for iron(III), r_f, [$M_{Fe3}/M_B/T$] is similarly developed, this time by multiplying Equation (3.10) by the iron(III) use coefficient, γ_f, [M_{Fe3}/M_B], yielding:

$$r_f = \gamma_f \mu_{sf}. \tag{3.12}$$

3.1.5 Biodegradation Rates

Biodegradation rates per unit volume of liquid may simply be expressed by summing up the amount of contaminant removal by the aerobic, facultative, and anaerobic microbial populations:

$$R_{bio} = R_{aer} + R_{fac} + R_{ana} \tag{3.13}$$

where R_{bio} is the total rate of substrate removal due to biodegradation [$M_S/L^3/T$] and R_{aer}, R_{fac}, and R_{ana} are the substrate removal rates [$M_S/L^3/T$] by the aerobic, facultative, and anaerobic microbial populations, respectively. These rates of removal are a function of both the number of microbes present and the rate with which these microbes consume the contaminant. The individual rates of substrate removal due to biodegradation may then be written as:

$$R_{aer} = \frac{M_{aer} r_{s,aer}}{\theta} \tag{3.14}$$

$$R_{fac} = \frac{M_{fac} r_{s,fac}}{\theta} \tag{3.15}$$

$$R_{ana} = \frac{M_{ana} r_{s,ana}}{\theta} \tag{3.16}$$

where M refers to the biomass per volume of porous medium [M_B/L^3], r_s refers to the rate of substrate consumption per biomass per time [$M_S/M_B/T$], and the subscripts 'aer', 'fac', and 'ana' correspond to the aerobic, facultative, and anaerobic populations, respectively. θ represents the porosity of the porous medium as the volume of voids per total volume [L^3/L^3].

As mentioned above, the facultative and anaerobic microbial populations may be further divided, based on electron acceptor utilization. The SEAM2D model calculates substrate biodegradation for three sequential electron acceptors, namely oxygen (primary), nitrate (secondary), and iron(III) (terminal). By expanding Equations (3.15) and (3.16) by electron acceptor utilization, the facultative and anaerobic substrate removal rate equations may be written as:

$$R_{fac} = \frac{M_{fac}}{\theta}\left(r_{so,fac} + \phi_{o,n} r_{sn,fac} + \phi_{o,f} r_{sf,fac}\right) \tag{3.17}$$

$$R_{ana} = \frac{M_{ana}}{\theta}\left(\phi_{n} r_{sn,ana} + \phi_{f} r_{sf,ana}\right) \tag{3.18}$$

where r_{so}, r_{sn}, and r_{sf} are the substrate utilization rates [$M_S/M_B/T$] for oxygen, nitrate, and iron(III)-based respiration, respectively, and the 'fac' and 'ana' subscripts refer to

facultative and anaerobic conditions, respectively. The ϕ factors used in Equations (3.17) and (3.18) correspond to the percentage of each microbial population which is capable of using a given electron acceptor. $\phi_{o,n}$ is the fraction of the facultative population which can respire on both oxygen and nitrate, $\phi_{o,f}$ is the fraction of the facultative population which can respire on both oxygen and iron(III), ϕ_n is the fraction of the anaerobic population which respires on nitrate, and ϕ_f is the fraction of the anaerobic population which respires on iron(III). Equation (3.17) inherently assumes that all facultative organisms use oxygen as the primary electron acceptor and either nitrate or iron(III) as the terminal electron acceptor, but not both. Equation (3.18) assumes, for simplicity, that the strictly anaerobic organisms are either nitrate- or iron(III)-reducers and admittedly does not account for the presence of other anaerobic microbes such as sulfate-reducing or methanogenic organisms. These assumptions lead to the following ϕ factor relationships:

$$\phi_{o,n} + \phi_{o,f} \leq 1 \tag{3.19}$$

$$\phi_n + \phi_f = 1. \tag{3.20}$$

3.2 Transport Processes

3.2.1 Advection and Dispersion

Models which describe solute transport in porous media are developed by combining two macroscopic mass transport processes, advection and hydrodynamic dispersion. Advection refers to the bulk movement of fluid through the porous medium and equals the average rate of solute transport. Hydrodynamic dispersion accounts for both the mechanical mixing which occurs during advection and molecular diffusion due to the presence of a concentration gradient. Based on the work of Ogata (1970) and Bear (1972), the mass balance equation for two-dimensional transport of a non-conservative substance, dissolved in ground water, is given by:

$$-\bar{v}_x \frac{\partial C}{\partial x} - \bar{v}_z \frac{\partial C}{\partial z} + D_x \frac{\partial^2 C}{\partial x^2} + D_z \frac{\partial^2 C}{\partial z^2} - R_{ad} - R_{bio} = \frac{\partial C}{\partial t} \tag{3.21}$$

where C is the solute concentration [M_S/L^3], x is a distance measured along the flow path [L], z is a distance measured perpendicular to the flow path [L], $\bar{v}_x$ and $\bar{v}_z$ are the average longitudinal and transverse groundwater velocities [L^2/T], respectively, D_x is the longitudinal dispersion coefficient [L/T], D_z is the transverse dispersion coefficient [L^2/T], and R_{ad} and R_{bio} are sink terms [$M_S/L^3/T$] accounting for adsorption and biodegradation, respectively. The right side of Equation (3.21) describes changes in solute mass with time. The first two terms on the left side of Equation (3.21) account for advection while the third and fourth terms calculate hydrodynamic dispersion in the longitudinal and transverse directions, respectively. By assuming that the transverse groundwater velocity is negligible in comparison to the longitudinal groundwater velocity, hydrodynamic dispersion in the longitudinal direction is calculated by:

$$D_x = \alpha_x \bar{v}_x + D^* \tag{3.22}$$

and in the transverse direction is given by:

$$D_z = \alpha_z \bar{v}_x + D^* \tag{3.23}$$

where α_x and α_z are the transverse and longitudinal dispersivities [L] and D^* is the diffusion coefficient [L^2/T]. The first term of these two equations accounts for mechanical mixing while the second term represents the effects of molecular diffusion.

3.2.2 Adsorption

Adsorption, in its most general definition, is the accumulation of a substance at a phase interface. In subsurface applications, adsorption is the movement of a groundwater constituent from solution to the solid phase of the porous medium, retarding the movement of the reactive constituent. Freeze and Cherry (1979) supply the most common expression for adsorption, given by an adsorption sink term, R_{ad}, as:

$$R_{ad} = \frac{\rho_b}{\theta} K_d \frac{\partial C}{\partial t} \tag{3.24}$$

where ρ_b is the bulk mass density [M_{SOLID}/L^3] and K_d is the distribution coefficient [L^3/M_{SOLID}]. The assumptions underlying Equation (3.24) are that the adsorption is instantaneous, reversible, and follows a simple linear isotherm.

A mathematically convenient way to represent the effects of adsorption on solute transport is through the use of a retardation factor, R. The retardation factor, as defined by Freeze and Cherry (1979) is expressed as a ratio of groundwater velocity to solute velocity and is given by:

$$R = \frac{\overline{v}}{\overline{v}_c} = 1 + \frac{\rho_b}{\theta} K_d \tag{3.25}$$

where $\overline{v}$ is the average groundwater velocity [L/T] and $\overline{v}_c$ is the average solute velocity [L^2/T].

By substituting the retardation factor into Equation (3.21), the solute mass balance equation can now be written as:

$$-\overline{v}_x \frac{\partial C}{\partial x} - \overline{v}_z \frac{\partial C}{\partial z} + D_x \frac{\partial^2 C}{\partial x^2} + D_z \frac{\partial^2 C}{\partial z^2} - R_{bio} = R \frac{\partial C}{\partial t} \tag{3.26}$$

3.2.3 Interphase Transport

Widdowson and Aelion (1991) note that equations are needed to relate the microbial phase and aqueous (i.e. pore fluid) phase substrate and electron acceptor concentrations. By assuming that the main transport process between the pore fluid and microbial phase is diffusion, the mass utilization rate in the biomass is considered equal to the rate of mass exiting the pore fluid and entering the biomass. Using the expressions developed by Molz et al. (1986) and refined by Widdowson et al. (1988), the following equations are defined for aerobic ($r_{s,aer}$), facultative ($r_{s,fac}$), and anaerobic ($r_{s,ana}$) substrate utilization:

$$r_{s,aer} = D_s \left[\frac{S - s_{aer}}{\delta_{aer}} \right] \beta_{aer} \tag{3.27}$$

$$r_{s,fac} = D_s \left[\frac{S - s_{fac}}{\delta_{fac}} \right] \beta_{fac} \tag{3.28}$$

$$r_{s,ana} = D_s \left[\frac{S - s_{ana}}{\delta_{ana}} \right] \beta_{ana} \tag{3.29}$$

where D_s is the diffusion coefficient [L^2/T] for substrate, S is the pore fluid substrate concentration [M_S/L^3], s_{aer}, s_{fac}, and s_{ana} are the microbial phase substrate concentrations [M_S/L^3], δ_{aer}, δ_{fac}, and δ_{ana} are the diffusion boundary layer thickness [L], and β_{aer}, β_{fac}, and β_{ana} are the surface areas available for diffusion per unit biomass[L^2/M_B] for each microbial population. Similar expression are also developed for oxygen (r_o) and nitrate (r_n) electron acceptor utilization:

$$r_o = D_o\left[\frac{\beta_{aer}}{\delta_{aer}}(O - o_{aer}) + \frac{\beta_{fac}}{\delta_{fac}}(O - o_{fac})\right] \tag{3.30}$$

$$r_n = D_n\left[\phi_{o,n}\frac{\beta_{fac}}{\delta_{fac}}(N - n_{fac}) + \phi_n\frac{\beta_{ana}}{\delta_{ana}}(N - n_{ana})\right] \tag{3.31}$$

where D_o and D_n are the diffusion coefficients [L^2/T] for oxygen and nitrate, respectively, O and N are the oxygen [M_{O2}/L^3] and nitrate [M_{NO3}/L^3] pore fluid concentrations, respectively, and o_{aer}, o_{fac}, n_{fac}, and n_{ana} are the microbial phase concentrations for oxygen [M_{O2}/L^3] and nitrate [M_{NO3}/L^3] for each microbial population. Note that solid phase iron(III) does not require an interphase transport equation, as the microbial population is attached directly to this electron acceptor.

3.3 Governing Equations

The SEAM2D model, developed by Widdowson (1992), couples two dimensional transport with adsorption and biodegradation by sequential electron acceptors to predict the fate of groundwater contaminants. The equations provided here are for two-dimensional flow through an anisotropic, homogeneous porous medium. As stated above, the sequential electron acceptors are oxygen (primary), nitrate (secondary), and iron(III) (terminal). For simplicity, it is assumed that oxygen and nitrate share a single facultative microbial population (i.e. $M_{aer} \approx 0$, $\phi_{o,n}=1$, $\phi_n=0$) whereas iron(III) supports an independent anaerobic microbial population (i.e. $\phi_{o,f}=0$, $\phi_f=1$). These assumptions also imply that the microbial phase substrate concentrations for oxygen and nitrate-based respiration are identical to the facultative microbial phase substrate concentration (i.e. $s_o=s_n=s_{fac}$), and that

the anaerobic microbial phase substrate concentration is equal to that of iron(III)-based respiration (i.e. $s_{ana}=s_f$). The governing equations for sequential oxygen-nitrate electron acceptor reduction have previously been developed by Widdowson (1992), while the equations for solid phase electron acceptor (e.g. iron(III)) based substrate utilization are unique to this thesis.

The mass balance equations developed here account for four phenomena, namely advection, hydrodynamic dispersion, adsorption, and biodegradation. The mass balance equation for substrate, as defined for a generic solute, is given by:

$$-\bar{v}_x \frac{\partial S}{\partial x} - \bar{v}_z \frac{\partial S}{\partial z} + D_x \frac{\partial^2 S}{\partial x^2} + D_z \frac{\partial^2 S}{\partial z^2} - R_{bio} = R \frac{\partial S}{\partial t} \tag{3.26}$$

Recall that R_{bio} is calculated by summing the effects of each microbial population, expressed as:

$$R_{bio} = R_{aer} + R_{fac} + R_{ana} \tag{3.13}$$

Using the simplifying assumptions defined above, the substrate removal rate by strict aerobes is zero, while the facultative and anaerobic removal rate equations are now defined by:

$$R_{fac} = \frac{M_{fac}}{\theta} r_{s,fac} = \frac{M_{fac}}{\theta}\left(r_{so} + r_{sn}\right) \tag{3.32}$$

$$R_{ana} = \frac{M_{ana}}{\theta} r_{s,ana} = \frac{M_{ana}}{\theta} r_{sf} \tag{3.33}$$

where the substrate utilization rate equations are defined in terms of utilization kinetics as:

$$r_{so} = \frac{\mu_o}{Y_o}\left[\frac{s_{fac}}{K_{so} + s_{fac}}\right]\left[\frac{o_{fac}}{K_o + o_{fac}}\right] \tag{3.34}$$

$$r_{sn} = \frac{\mu_n}{Y_n}\left[\frac{s_{fac}}{K_{sn} + s_{fac}}\right]\left[\frac{n_{fac}}{K_n + n_{fac}}\right] I(o) \tag{3.35}$$

$$r_{sf} = \frac{\mu_f}{Y_f}\left[\frac{s_{ana}}{K_{sf} + s_{ana}}\right] I(o). \tag{3.36}$$

Substrate utilization can also be written in terms of interphase transport, as shown in Equations (3.28) and (3.29), and given here as:

$$r_{s,fac} = r_{so} + r_{sn} = D_s\left[\frac{S - s_{fac}}{\delta_{fac}}\right]\beta_{fac} \tag{3.37}$$

$$r_{s,ana} = r_{sf} = D_s\left[\frac{S - s_{ana}}{\delta_{ana}}\right]\beta_{ana} \tag{3.38}$$

Substituting Equations (3.32) and (3.33) into Equations (3.14) and (3.15), respectively, the mass balance for substrate (Equation (3.26)) takes the form of:

$$-\bar{v}_x\frac{\partial S}{\partial x} - \bar{v}_z\frac{\partial S}{\partial z} + D_x\frac{\partial^2 S}{\partial x^2} + D_z\frac{\partial^2 S}{\partial z^2} - \left(\frac{M_{fac}}{\theta}(r_{so} + r_{sn}) + \frac{M_{ana}}{\theta}r_{sf}\right) = R\frac{\partial S}{\partial t} \tag{3.39}$$

The mass balance equations for oxygen and nitrate are similarly written as:

$$-\bar{v}_x\frac{\partial O}{\partial x} - \bar{v}_z\frac{\partial O}{\partial z} + D_x\frac{\partial^2 O}{\partial x^2} + D_z\frac{\partial^2 O}{\partial z^2} - \frac{M_{fac}}{\theta}r_o = \frac{\partial O}{\partial t} \tag{3.40}$$

$$-\bar{v}_x\frac{\partial N}{\partial x} - \bar{v}_z\frac{\partial N}{\partial z} + D_x\frac{\partial^2 N}{\partial x^2} + D_z\frac{\partial^2 N}{\partial z^2} - \frac{M_{fac}}{\theta}r_n = \frac{\partial N}{\partial t} \tag{3.41}$$

where the simplifying assumptions lead to the aqueous phase electron acceptor utilization rates given by:

$$r_o = D_o\left[\frac{(O - o_{fac})}{\delta_{fac}}\right]\beta_{fac} = \gamma_o\mu_o\left[\frac{s_{fac}}{K_{so} + s_{fac}}\right]\left[\frac{o_{fac}}{K_o + o_{fac}}\right] \tag{3.42}$$

$$r_n = D_n\left[\frac{(N - n_{fac})}{\delta_{fac}}\right]\beta_{fac} = \gamma_n\mu_n\left[\frac{s_{fac}}{K_{sn} + s_{fac}}\right]\left[\frac{n_{fac}}{K_n + n_{fac}}\right]I(o) \tag{3.43}$$

Note that the retardation factor associated with dissolved oxygen and nitrate is effectively one, as both of these electron acceptors are found predominantly in the aqueous phase.

The solid phase, iron(III) mass balance equation does not include the transport terms and is written solely in terms of utilization:

$$-\frac{M_{ana}}{\rho_s(1-\theta)}r_f = \frac{dF_3}{dt} \tag{3.44}$$

where F_3 is the iron(III) concentration [M_{Fe3}/L^3], ρ_s is the particle mass density [M_{PART}/L^3], and r_f is given by:

$$r_f = \gamma_f \mu_f \left[\frac{s_{ana}}{K_{sf} + s_{ana}} \right] I(o) \tag{3.45}$$

Field monitoring of iron(III) reduction is accomplished by measuring aqueous phase iron(II) concentrations, the product of the reduction reaction. To match field measurements of iron(II) production, an additional mass balance equation is required to simulate the production and transport of iron(II). This equation is given as:

$$-\bar{v}_x \frac{\partial F_2}{\partial x} - \bar{v}_z \frac{\partial F_2}{\partial z} + D_x \frac{\partial^2 F_2}{\partial x^2} + D_z \frac{\partial^2 F_2}{\partial z^2} + \zeta \frac{M_{ana}}{\theta} r_f = R_{F2} \frac{\partial F_2}{\partial t} \tag{3.46}$$

where F_2 is the iron(II) concentration [M_{Fe2}/L^3], ζ is a iron(II) production coefficient, expressed as mass of iron(II) produced per mass of iron(III) consumed [M_{Fe2}/M_{Fe3}], and R_{F2} is the retardation factor for iron(II).

Mass balance equations are also developed for the both the facultative and anaerobic biomass populations. Since oxygen and nitrate are the electron acceptors which support the facultative biomass population, both oxygen and nitrate based substrate utilization rates appear as growth terms in Equation (3.47). The mass balance equations for the facultative and strictly anaerobic organisms are thus given by:

$$Y_o r_{so} + Y_n r_{sn} - k_{d,fac} = \frac{1}{M_{fac}} \frac{dM_{fac}}{dt} \tag{3.47}$$

$$Y_f r_{sf} - k_{d,ana} = \frac{1}{M_{ana}} \frac{dM_{ana}}{dt} \tag{3.48}$$

respectively, where $k_{d,fac}$ and $k_{d,ana}$ are the decay rates for the facultative and strictly anaerobic microbial populations, respectively.

3.4 Dimensionless Form of the Governing Equations

The governing equations displayed in the previous section are expressed in dimensionless form, allowing evaluation of which parameters most significantly affect the

solution of this system of equations. Conversion to dimensionless form is accomplished by defining the following dimensionless terms, then substituting these terms into the governing equations developed above. The dimensionless independent variables are defined as:

$$X = \frac{x}{L_x} \quad \partial x = L_x \partial X \quad \partial x^2 = L_x^2 \partial X^2$$

$$Z = \frac{z}{L_z} \quad \partial z = L_z \partial Z \quad \partial z^2 = L_z^2 \partial Z^2 \tag{3.49}$$

$$T = \frac{t}{\tau} \quad \partial t = \tau \partial T$$

where L_x and L_z are characteristic lengths in the longitudinal and transverse directions, respectively, and τ is a characteristic time. L_x and L_z may be taken as the x and z coordinate, respectively, of an observation point (e.g. a monitoring well) down-gradient of the contaminant source. The characteristic time, τ, is then taken as the time for travel from the source area to the point of observation. The dimensionless dependent variables (concentration terms) are defined by:

$$S^* = \frac{S}{S_B} \; ; \; O^* = \frac{O}{O_B} \; ; \; F_3^* = \frac{F_3}{F_B}$$

$$s_{fac}^* = \frac{s_{fac}}{S_B} \; ; \; s_{ana}^* = \frac{s_{ana}}{S_B} \; ; \; o_{fac}^* = \frac{o_{fac}}{O_B} \; ; \; n_{fac}^* = \frac{n_{fac}}{N_B} \tag{3.50}$$

$$M_{fac}^* = \frac{M_{fac}}{M_{B,fac}} \; ; \; M_{ana}^* = \frac{M_{ana}}{M_{B,ana}}$$

where S_B, O_B, N_B, and F_B are the reference substrate, oxygen, nitrate, and iron(III) concentrations (e.g. source or initial conditions), respectively, and $M_{B,fac}$ and $M_{B,ana}$ are the initial facultative and anaerobic microbial populations. The electron acceptor utilization equations are now converted to dimensionless form and given by:

$$r_o^* = \left[\frac{s_{fac}^*}{K_{so}^* + s_{fac}^*}\right]\left[\frac{o_{fac}^*}{K_o^* + o_{fac}^*}\right] \tag{3.51a}$$

$$r_n^* = \left[\frac{s_{fac}^*}{K_{sn}^* + s_{fac}^*}\right]\left[\frac{n_{fac}^*}{K_n^* + n_{fac}^*}\right] I(o_{fac}^*) \tag{3.51b}$$

$$r_f^* = \left[\frac{s_{ana}^*}{K_{sf}^* + s_{ana}^*}\right] I(o_{fac}^*) \tag{3.51c}$$

where the half saturation constants are also non-dimensionalized to:

$$K_{so}^* = \frac{K_{so}}{S_B};\ K_o^* = \frac{K_o}{O_B};\ K_{sn}^* = \frac{K_{sn}}{S_B};\ K_n^* = \frac{K_n}{N_B};\ K_{sf}^* = \frac{K_{sf}}{S_B}. \tag{3.52}$$

The non-dimensional inhibition function is given by:

$$I(o_{fac}^*) = \left[\frac{K_c^*}{K_c^* + o_{fac}^*}\right] \tag{3.53}$$

where the dimensionless inhibition coefficient given by:

$$K_c^* = \frac{K_c}{O_B}. \tag{3.54}$$

By substituting these dimensionless expressions into the SEAM2D governing equations, the following non-dimensional equations are developed. For substrate, the mass balance equation is converted to:

$$-\frac{\partial S^*}{\partial X} - \tau^* \frac{\partial S^*}{\partial Z} + (P_e)_x^{-1} \frac{\partial^2 S^*}{\partial X^2} + (P_e)_z^{-1} \frac{\partial^2 S^*}{\partial Z^2} - R_{bio}^* = R \frac{\partial S^*}{\partial T} \tag{3.55}$$

where the coefficients of the dispersion terms in Equation (3.55) are defined as Peclet Numbers with respect to the longitudinal velocity, and are defined as:

$$P_{ex} = \frac{\bar{v}_x L_x}{D_x} \tag{3.56}$$

$$P_{ez} = \frac{\bar{v}_x L_z^2}{D_z L_x} \tag{3.57}$$

for the longitudinal and transverse directions, respectively. The coefficient of the second term of Equation (3.55), τ^*, is defined as:

$$\tau^* = \frac{\bar{v}_z}{\bar{v}_x} \frac{L_x}{L_z}. \tag{3.58}$$

The non-dimensional biodegradation sink term, R^*_{bio}, is developed by substituting the non-dimensional terms defined in Equation (3.49) into the interphase transport expressions (Equations (3.37) and (3.38)), and is given here as:

$$R^*_{bio} = \frac{M^*_{fac}}{\theta} D^{III}_{fac}(S^* - s^*_{fac}) + \frac{M^*_{ana}}{\theta} D^{III}_{ana}(S^* - s^*_{ana}). \tag{3.59}$$

where the coefficients of Equation (3.59) are associated with non-dimensional groupings, defined for each microbial population, and given by:

$$D^{III}_{fac} = \frac{D_s \beta_{fac} M_{B,fac}}{\delta_{fac}} \tau \tag{3.60}$$

$$D^{III}_{ana} = \frac{D_s \beta_{ana} M_{B,ana}}{\delta_{ana}} \tau \tag{3.61}$$

where the characteristic time, τ [T], is calculated as $L_x / \overline{v}_x$.

A similar manipulation yields the dimensionless mass balance equations for the aqueous phase electron acceptors, oxygen and nitrate, given as Equations (3.62) and (3.63):

$$-\frac{\partial O^*}{\partial X} - \tau^* \frac{\partial O^*}{\partial Z} + (P_e)_x^{-1} \frac{\partial^2 O^*}{\partial X^2} + (P_e)_z^{-1} \frac{\partial^2 O^*}{\partial Z^2} - \frac{M^*_{fac}}{\theta} D^{III}_o (O^* - o^*_{fac}) = \frac{\partial O^*}{\partial T} \tag{3.62}$$

$$-\frac{\partial N^*}{\partial X} - \tau^* \frac{\partial N^*}{\partial Z} + (P_e)_x^{-1} \frac{\partial^2 N^*}{\partial X^2} + (P_e)_z^{-1} \frac{\partial^2 N^*}{\partial Z^2} - \frac{M^*_{fac}}{\theta} D^{III}_n (N^* - n^*_{fac}) = \frac{\partial N^*}{\partial T} \tag{3.63}$$

where the dimensionless groupings for oxygen and nitrate utilization are given by:

$$D^{III}_o = \frac{D_o \beta_{fac} M_{B,fac}}{\delta_{fac}} \tau \tag{3.64}$$

$$D^{III}_n = \frac{D_n \beta_{fac} M_{B,fac}}{\delta_{fac}} \tau, \tag{3.65}$$

respectively.

The dimensionless mass balance for solid phase iron(III) does not have the associated interphase transport terms, and is defined simply as:

$$-\frac{M^*_{ana}\, r^*_f}{(1-\theta)} D^{IV}_f = \frac{d\, F_3^*}{dT} \tag{3.66}$$

where the dimensionless grouping associated with iron utilization is given by:

$$D^{IV}_f = \frac{M_{B,ana}\, \gamma_f\, \mu_f}{F_B \rho_s} \tau \tag{3.67}$$

and r_f^* is previously defined as Equation (3.51c).

Dimensionless mass balance equations also need to be developed for the facultative and strict anaerobic biomass populations. By substituting the dimensionless parameters defined in Equations (3.49) through (3.51c) into the facultative biomass mass balance (Equation (3.43)), the non-dimensional form of the facultative biomass mass balance equation is given by:

$$(D^I_o\, r^*_o + D^I_n\, r^*_n - D_{k,fac}) = \frac{1}{M^*_{fac}} \frac{dM^*_{fac}}{dT} \tag{3.68}$$

where the D^I dimensionless number for oxygen and nitrate-based respiration is given by Equations (3.69) and (3.70), respectively:

$$D^I_o = \mu_o \tau \tag{3.69}$$

$$D^I_n = \mu_n \tau \tag{3.70}$$

and $D_{k,fac,}$, which relates the microbial population decay rate to travel time, is defined for the facultative population as:

$$D_{k,fac} = k_{d,fac} \tau \tag{3.71}$$

A similar manipulation of the anaerobic biomass mass balance equation yields a non-dimensional equation of the form:

$$(D^I_f r^*_f - D_{k,ana}) = \frac{1}{M^*_{ana}} \frac{dM^*_{ana}}{dT} \tag{3.72}$$

where D^I_f is defined by:

$$D^I_f = \mu_f \tau . \tag{3.73}$$

and $D_{k,ana}$ is given as:

$$D_{k,ana} = k_{d,ana} \tau . \tag{3.74}$$

The utilization equations are also converted to non-dimensional form by substituting dimensionless parameters into the governing utilization equations, and rewriting Equation (3.37) as:

$$r^*_{s,fac} = r^*_o + \frac{\mu_n}{\mu_o}\frac{Y_o}{Y_n} r^*_n = D^{II}_{so}(S^* - s^*_{fac}) \tag{3.75}$$

for facultative, substrate utilization dominated by oxygen-based respiration, where D^{II}_{so} is a dimensionless parameter defined as:

$$D^{II}_{so} = \frac{D_s \beta_{fac} S_B Y_o}{\delta_{fac} \mu_o}. \tag{3.76}$$

For facultative substrate utilization dominated by nitrate-based respiration, the substrate utilization rate can be expressed as:

$$r^*_{s,fac} \cong r^*_n = D^{II}_{sn}(S^* - s^*_{fac}) \tag{3.77}$$

where:

$$D^{II}_{sn} = \frac{D_s \beta_{fac} S_B Y_n}{\delta_{fac} \mu_n} \tag{3.78}$$

Iron(III)-based substrate utilization, as given in Equation (3.38), is also rewritten in dimensionless form, given by:

$$r^*_{s,ana} = r^*_f = D^{II}_{sf}(S^* - s^*_{ana}) \tag{3.79}$$

where the dimensionless term for iron(III)-based substrate utilization is defined here as:

$$D^{II}_{sf} = \frac{D_s \beta_{ana} S_B Y_f}{\delta_{ana} \mu_f}. \tag{3.80}$$

The aqueous phase electron acceptor (i.e. oxygen and nitrate) utilization equations are similarly converted to dimensionless form, as given by:

$$r_o^* = \frac{D_o \beta_{fac} O_B}{\gamma_o \mu_o \delta_{fac}}(O^* - o^*) = D^{II}_o(O^* - o^*) \tag{3.81}$$

for oxygen, and:

$$r^*_n = \frac{D_n \beta_{fac} N_B}{\gamma_n \mu_n \delta_{fac}}(N^* - n^*) = D^{II}_n(N^* - n^*) \tag{3.82}$$

for nitrate, where the dimensionless groupings for oxygen and nitrate utilization are defined as:

$$D_o^{II} = \frac{D_o \beta_{fac} O_B}{\gamma_o \mu_o \delta_{fac}} \tag{3.83}$$

$$D_n^{II} = \frac{D_n \beta_{fac} N_B}{\gamma_n \mu_n \delta_{fac}} . \tag{3.84}$$

The non-dimensional utilization equation for solid phase, iron(III) does not contain the interphase transport terms used for aqueous electron acceptors, and may simply be represented by the expression given in Equation (3.51c):

$$r_f^* = \frac{r_f}{\gamma_f \mu_f} = \left[\frac{s_{ana}^*}{K_{sf}^* + s_{ana}^*} \right] I(o^*) . \tag{3.51c}$$

3.5 Input Parameters

3.5.1 Independent Variables

Examination of the governing equations for the SEAM2D model leads to identification of the input parameters required for the model. As was done during the development of the governing equations, the input parameters can be divided into categories based on the process they are used to predict. These categories, as shown in Table 3.1, correspond to hydrodynamic transport, interphase transport, microbial population distribution, microbial kinetics, and utilization kinetics. Table 3.1 lists the input parameters required for the SEAM2D model by category, assuming that there are three microbial populations (aerobic, facultative, and anaerobic), three electron acceptors (oxygen, nitrate, and iron(III)), and one substrate. Hydrodynamic parameters are used to model the transport phenomena of advection, hydrodynamic dispersion, and adsorption, while biodegradation effects are calculated using a combination of the interphase transport, microbial, and utilization parameters.

Estimation of hydrodynamic variables, such as dispersivity and groundwater velocity, is accomplished by a combination of field measurements and a geologic survey of the subsurface environment. Freeze and Cherry (1979) note that groundwater velocity

Table 3.1. Input parameters for the SEAM2D Model.

Process	Symbol	Name	Phenomena Described
Transport	$\overline{V}_x, \overline{V}_z$	Groundwater Velocity	Advection
	α_x, α_z	Dispersivity	Mechanical Dispersion
	D^*	Diffusion Coefficient	Molecular Diffusion
	R	Retardation Factor	Adsorption
Interphase Transport	D_s, D_o, D_n	Diffusion Coefficient	Boundary Layer Diffusion
	$\delta_{aer}, \delta_{fac}, \delta_{ana}$	Boundary Layer Thickness	Boundary Layer Diffusion
	$\beta_{aer}, \beta_{fac}, \beta_{ana}$	Surface Area Available for Diffusion	Boundary Layer Diffusion
Microbial Population	$\phi_{o,n}, \phi_{o,f}$	Facultative Population Distribution Factor	Microbial Distribution
	ϕ_n, ϕ_f	Anaerobic Population Distribution Factor	Microbial Distribution
Microbial Kinetics	μ_o, μ_n, μ_f	Maximum Specific Growth Rate	Microbial Growth
	$k_{d,aer}, k_{d,fac}, k_{d,ana}$	Decay Rate	Microbial Decay
	K_c	Inhibition Coefficient	Inhibited Microbial Growth
Utilization	K_{so}, K_{sn}, K_{sf}	Monod Constant (Substrate)	Electron Donor Utilization
	K_o, K_n	Monod Constant (Electron Acceptor)	Electron Acceptor Utilization
	Y_o, Y_n, Y_f	Yield Coefficient	Substrate Utilization
	$\gamma_o, \gamma_n, \gamma_f$	Use Coefficient	Electron Acceptor Utilization

can be determined by methods which employ either the Darcy equation or groundwater tracers. Darcy's Law, written to calculate the average groundwater velocity, $\bar{v}$, is defined as:

$$\bar{v} = -\frac{K}{\Theta}\frac{dh}{dl} \tag{3.85}$$

where h is the hydraulic head [L], $\frac{dh}{dl}$ is the hydraulic gradient [L/L], K is a medium property known as the hydraulic conductivity [L/T], and negative sign indicates that water flows in the direction of decreasing hydraulic head. Hydraulic conductivity corresponds to a medium's ability to transmit water, with high K values corresponding to highly transmissive soils, such as gravels and sands, while lower K values are associated with confining units which are composed primarily of clays and unfractured rocks. Hydraulic conductivity is usually determined through field tests (e.g. pump, slug, or tracer tests) and may vary significantly with respect to both depth and location. Hydraulic gradients are also measured in the field by recording the hydraulic head at two or more points along a flow path and dividing the difference in hydraulic head by the distance between the wells. The hydraulic gradient can also very spatially and may be subject to temporal changes, especially in shallow aquifers and in aquifers which are well connected with surface waters. If a tracer method is used to estimate groundwater velocity, the effects of dispersion and adsorption must also be accounted for, as discussed in the following paragraphs.

Determination of the hydrodynamic dispersion parameters (α_x, α_z, D^*) is also important for transport modeling. The dominant process for hydrodynamic dispersion is a function of groundwater velocity, with mechanical mixing controlling high groundwater velocity conditions and diffusion becoming more significant for low groundwater velocities (Freeze and Cherry, 1980). Diffusion tends to be more influential in the transverse direction, and may play a significant role in the lateral spreading of a plume. The diffusion coefficient (D^*) is well defined for most groundwater constituents and can be found in a scientific handbook of chemistry. As noted by Domenico and Schwartz

(1990), laboratory experiments have helped establish a relationship between mechanical dispersion and the linear groundwater velocity in homogeneous porous media. The coefficient of mechanical dispersion [L^2/T] for the longitudinal (D_x)and transverse (D_z) directions is given by:

$$D_x = \alpha_x \bar{v}_x \tag{3.86}$$

$$D_z = \alpha_z \bar{v}_x \tag{3.87}$$

respectively, as seen previously on the right side of Equations (3.22) and (3.23).

Dispersivity can be estimated from either laboratory or field studies, with field measured dispersivities tending to be an order of magnitude or more greater than laboratory values and longitudinal values tending to be an order of magnitude larger than transverse values (Domenico and Schwartz, 1990). These researchers indicate that the discrepancy between field and laboratory results may be attributable to systematic errors in data collection and interpretation, but also note that field measurements of dispersivity may include variations in other transport phenomena, particularly advection. Domenico and Schwartz also indicate that dispersivity tends to increases with scale, citing the work of Gelhar (1985), Sudicky (1986), and others as evidence of this trend.

Adsorption effects, in the form of a retardation factor (R), also play a significant role in solute transport and may be measured by either field or laboratory methods. Bedient et al. (1994) indicate that field estimation techniques for the retardation factor tend to be very straightforward, as shown in Equations (3.88) and (3.89):

$$R = \frac{\text{Distance from source of nonreactive plume}}{\text{Distance from source of reacitve plume}} \tag{3.88}$$

or

$$R = \frac{\text{Time for reactive chemical to reach a given point}}{\text{Time for nonreactive chemical to reach a given point}} \tag{3.89}$$

Laboratory estimation of R requires three parameters (bulk mass density, porosity, and a partitioning or distribution coefficient), as identified in Equation (3.24). Porosity is

determined during the geologic survey of the site, while bulk mass density is simply measured as the oven-dried mass of a sample divided by its field volume and typically ranges between 1.6 and 2.1 g/cm^3. K_d is defined as the mass of solute on the solid phase per unit mass of solid per solute concentration in solution [L^3/M_{SOLID}], and is most commonly determined through laboratory studies, as summarized in Novotny and Olem (1994).

The interphase transport parameters (D^*,β,δ) quantify the accessibility of electron donors and acceptors for the microbial populations. Diffusion, as applied to interphase transport, accounts for the movement of a solute from the pore fluid phase into the microbial phase. This movement occurs through a diffusion layer, δ, as shown in Figure 3.2. β is the surface area available for diffusion per unit biomass and, when multiplied by the volume of biomass, yields the specific surface area available for diffusion per unit volume of aquifer. Although neither β nor δ are measurable *in situ* (Rittmann et al., 1980), a range of physically possible values can be defined for each parameter. For δ, the minimum thickness is essentially zero, while the maximum boundary layer thickness is equal to the pore space between the individual aquifer particles. For β, a maximum value can be assigned by assuming a geometric configuration for each microcolony (e.g. cylindrical, hemispherical, etc.), calculating of a specific surface area for each microcolony for the selected geometry, and then multiplying by the number of microcolonies to determine the specific surface area for diffusion. Alternately, β can be estimated in conjunction with the initial biomass (M_B). Harvey et al. (1984) indicates that the surface area available for diffusion is much less than one percent of the total specific surface area. Thus, by assuming a geometric configuration for the porous medium, the total specific surface area can be calculated and a maximum specific surface area for diffusion can be estimated.

Determination of the Monod kinetic parameters (μ_{max}, K_s) consists of a combination of laboratory, microcosm, and field data. Harris and Hanford (1976) report good agreement between recorded data and predicted results for various biofilm reactor

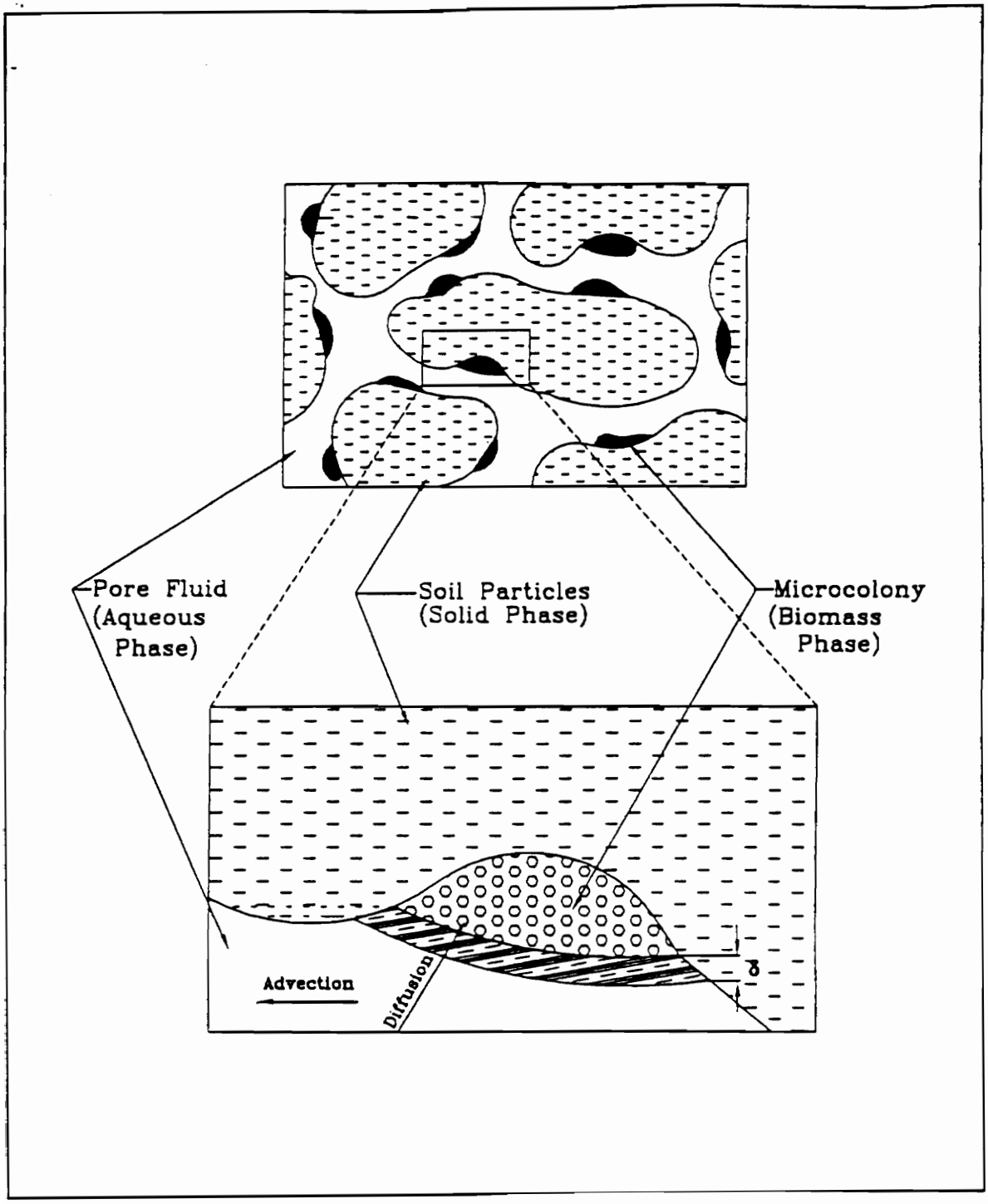

Figure 3.2. Boundary layer schematic with the microcolony concept. (from Baveye and Valocchi, 1989)

models using the modified Monod equation (Equation (3.3)). Research by Chang et al. (1993) and Oh et al. (1994), among others, has demonstrated in laboratory studies that degradation of the BTX compounds follow Monod kinetics under single substrate limiting conditions, modified Monod kinetics under dual limiting conditions, and inhibited Monod kinetics under competitive utilization. Rittmann et al. (1986) provide a method for estimating biofilm kinetics parameters in microcosm experiments while Button (1985) provides an extensive listing of kinetic parameter values for a variety of substrates and electron acceptors. Bedient et al. (1994) cite reports that laboratory studies of kinetic parameters result in significantly higher degradation rates than those found under field conditions, supporting their assertion that laboratory results are not always applicable to field simulations.

The remaining utilization parameters (Y, γ) relate to the efficiency with which the microbial populations utilize substrate and the electron acceptors. Both of these parameters are measurable in laboratory microcosms. The yield coefficient can be measured as the inverse of the amount of substrate consumed per unit biomass while the electron acceptor use coefficients are recorded as the mass of electron acceptor consumed per unit mass of substrate consumed. Maximum values for the electron acceptor use coefficient can be determined by examining the stoichiometric expressions like those given in Table 2.3. As an example, typical experimental results yield an oxygen use coefficient for toluene of around 3 mg/l while the stoichiometric equation for this reaction yields a maximum oxygen use coefficient of 3.5 mg/l.

3.5.2 Dependent Variables

Concentration variables for the SEAM2D model are listed in Table 3.2. For the equations of the three electron acceptor, single substrate model developed in this chapter, four aqueous phase concentrations, one solid phase concentration, and three microbial phase concentrations are determined as a function of space and time. The aqueous phase concentrations refer to the substrate, oxygen, nitrate, and iron(II) concentrations, while

Table 3.2. Dependent variables (macroscopic concentrations) in the SEAM2D model.

Variable	Symbol	Description	Phase
Substrate	S	Substrate Concentration	Aqueous
Electron Acceptors	O	Oxygen (O_2) Concentration	Aqueous
	N	Nitrate (NO_3^-) Concentration	Aqueous
	Fe(III)	Iron(III) (Fe^{3+}) Concentration	Solid
Reaction Product	Fe(II)	Iron(II) (Fe^{2+}) Concentration	Aqueous
Microbial Populations	M_{aer}	Aerobic Microbial Population	Microbial
	M_{fac}	Facultative Microbial Population	Microbial
	M_{ana}	Anaerobic Microbial Population	Microbial

the solid phase concentration is for the iron(III) electron acceptor. Changes in biomass population are also determined, yielding independent microbial phase concentrations for the aerobic, facultative, and anaerobic populations, respectively. Changes in the concentration variables due to changes in the independent variables can be reported in the form of both contour maps and graphs with respect to either time or location, with further discussion of model output capabilities provided in Chapters 4 and 5.

3.6 Dimensionless Parameters

3.6.1 Dimensionless Groupings

In an effort to better understand the phenomena of a mixed-culture biological film, Kissel et al. (1984) convert the mass balance equations for solute transport and biomass fractions to dimensionless form. Rifai and Bedient (1990) also convert the governing equations of their instantaneous reaction groundwater model to dimensionless form, attempting to establish the conditions under which their model is valid. The purpose of the dimensionless parameters defined in this research is twofold. First, the dimensionless parameters, as presented in Table 3.3, help characterize which phenomena control a given SEAM2D simulation. As shown in column 4 of Table 3.3, the dimensionless numbers represent a ratio of the phenomena accounted for in the SEAM2D model, yielding a quantifiable relationship between phenomena. Second, the dimensionless numbers combine related input parameters, thereby reducing the number of parameters which need to be analyzed in the sensitivity investigation of the SEAM2D model. This combination of parameters is particularly useful for the non-measurable input parameters such as the diffusion layer thickness and specific surface area available for diffusion. Commentary on the dimensionless groupings developed for the SEAM2D model is provided in the remainder of this section.

The first dimensionless grouping, the Peclet number, represents the ratio of the two primary mechanisms of solute mass transport, advection and hydrodynamic dispersion. Examination of the formula for the Peclet number shows that a decreasing

Table 3.3. Dimensionless Groupings.

Symbol	Formula	Nomenclature	Ratio	Process	Phenomena Described
P_{ex} P_{ez}	$v_x L_x / D_x$ $v_x L_z^2 / D_z L_x$	D_x, D_z = Dispersion coefficient L_x, L_z = Characteristic length v_x = Average ground water velocity	Advection / Dispersion	Transport	Indicates Dominant Transport Process
D_o^I D_n^I D_f^I	$\mu_o \tau$ $\mu_n \tau$ $\mu_f \tau$	μ = Maximum specific growth rate $\tau = L_x / v_x$ = Travel time	Growth Rate / Advection	Microbial Growth	Potential for microbial growth
$D_{k,fac}$ $D_{k,ana}$	$k_{d,fac} \tau$ $k_{d,ana} \tau$	$k_{d,ana}$, $k_{d,fac}$ = Decay coefficient	Decay Rate / Advection	Microbial Decay	Potential for microbial decay
D_{so}^{II} D_{sn}^{II} D_{sf}^{II} D_o^{II} D_n^{II}	$D_s \beta_{fac} S_B Y_o / \delta_{fac} \mu_o$ $D_s \beta_{fac} S_B Y_n / \delta_{fac} \mu_n$ $D_s \beta_{ana} S_B Y_f / \delta_{ana} \mu_f$ $D_o \beta_{fac} O_B / \gamma_o \delta_{fac} \mu_o$ $D_n \beta_{fac} N_B / \gamma_n \delta_{fac} \mu_n$	D_s, D_n, D_o = Diffusion coefficient N_B = Nitrate reference concentration O_B = Oxygen reference concentration S_B = Substrate reference concentration Y = Yield coefficient β = Surface area available for diffusion δ = Diffusion layer thickness	Diffusion Rate / Utilization Rate	Utilization	Substrate and aqueous phase electron utilization by each microbial population
D_{fac}^{III} D_{ana}^{III} D_o^{III} D_n^{III}	$D_s \beta_{fac} M_{B,fac} \tau / \delta_{fac}$ $D_s \beta_{ana} M_{B,ana} \tau / \delta_{ana}$ $D_o \beta_{fac} M_{B,fac} \tau / \delta_{fac}$ $D_n \beta_{fac} M_{B,fac} \tau / \delta_{fac}$	M_B = Biomass reference concentration	Diffusion Rate / Advection	Utilization	Time available for aqueous phase substrate and electron acceptor diffusion into each microbial population
D_f^{IV}	$M_{B,ana} \gamma_f \mu_f \tau / F_B$	F_B = Iron(III) reference concentration	Utilization Rate / Advection	Utilization	Time available for solid phase electron acceptor utilization
K_{so}^* K_{sn}^* K_{sf}^* K_o^* K_n^*	K_{so}/S_B K_{sn}/S_B K_{sf}/S_B K_o/O_B K_n/N_B	K = Monod Constant	Utilization Rate / Initial Condition	Utilization	Indicates either utilization rate or substrate/electron acceptor limited conditions
K_c^*	K_c/O_B	K_c = Inhibition Coefficient	Inhibition Rate / Initial Condition	Utilization	Inhibitory effect due to the presence of Oxygen

Subscripts: ana = anaerobic microbes; fac = facultative microbes; f = iron(III), n = nitrate, o = oxygen; s = substrate; so = substrate oxidation by oxygen-reducing microbes, sn = substrate oxidation by nitrate-reducing microbes, sf = substrate oxidation by iron(III)-reducing microbes; x = longitudinal direction; z = transverse direction

Peclet number implies an increase in the amount of dispersion, or spreading, of the plume as it moves through the aquifer. Figure 3.3 shows the effects of a change in the Peclet number along a longitudinal cross-section for a conservative tracer.

The next two dimensionless groupings, D^I and D_k, relate to changes in the microbial population with time. By representing advection by a characteristic travel time, τ, the time available for microbial growth (D^I) and microbial decay (D_k) is quantified. Under non-limiting conditions, microbial populations possess more potential for growth rather than decay, illustrated by the fact that D^I is generally an order of magnitude (or more) greater than D_k. Upon examination of Equations (3.43a) and (3.44a), periods of decline in the microbial population occur only when the substrate or electron acceptor becomes limiting, signified mathematically when the product of D^I times r^* is less than D_k.

For aqueous phase substrates and electron acceptors, the next two dimensionless groupings quantify the suitability of the subsurface conditions for utilization. The D^{II} dimensionless number quantifies the relationship between interphase transport and utilization. An increasing D^{II} number indicates either an increase in the rate of diffusion or a decrease in the ability of the microbial population to utilize the diffusing substance. Larger D^{II} numbers indicate utilization limiting conditions whereas smaller values of the D^{II} number indicate that boundary layer diffusion is limiting. The D^{III} number, like the Peclet number, relates two transport terms, but here the related phenomena are diffusion into the microbial phase versus advection. Once again representing advection as a characteristic travel time, decreases in this dimensionless grouping imply less time for diffusion of substrate and electron acceptors from the pore fluid phase into the microbial phase. Conversely, increases in D^{III} imply that more time is available for movement of the substrate and electron acceptors into the microbial phase, thereby increasing the likelihood of substrate and electron acceptor utilization.

The dimensionless grouping, D^{IV}, relates specifically to the solid phase electron acceptor iron(III), but is equally applicable to any other solid phase electron acceptor (or donor). Under non-substrate limiting conditions, this dimensionless grouping shows that

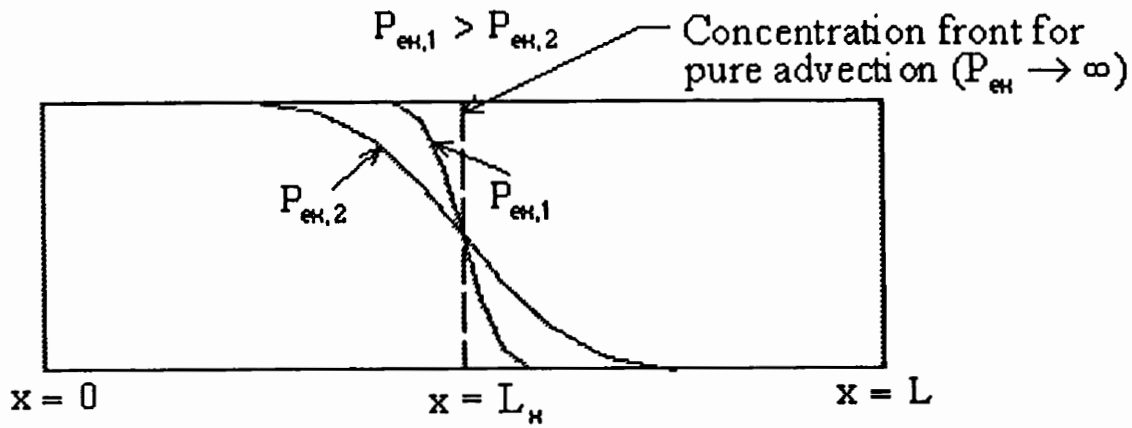

$$P_{ex} = \frac{\bar{v}_x L_x}{D_x}$$

Figure 3.3. Effects of varying Peclet number on solute transport for a typical conservative solute concentration profile.

the size (M_B) and efficiency (γ) of the microbial population along with the amount of available electron acceptor (F_B) controls the electron acceptor utilization rate, with increases in τ implying that more time is available for utilization to occur. By this reasoning, increases in the D^{IV} number imply increases in the rate of solid phase electron acceptor utilization.

The K^* dimensionless parameters represent a ratio between the initial condition and the utilization rate. Increases in this dimensionless number imply that the reaction kinetics are approaching first order, while decreases in K^* indicate that the kinetics are approaching zero order. First order kinetics are associated with substrate or electron acceptor limited conditions, whereas non-limited conditions follow zero order kinetics.

The final dimensionless grouping, K_c^*, quantifies the relationship between inhibition effects and the initial oxygen concentration. Examination of Equation (3.53) shows that an increase in K_c^* results in reduced inhibition effects, while a decrease in K_c^* implies an increase in oxygen-based inhibition of alternate electron acceptors.

3.6.2 Dimensionless Dependent Variables

As part of the conversion of the governing equation to dimensionless form, the concentration variables listed in Table 3.2 have also been non-dimensionalized. For substrate, the base concentration is taken as the concentration at the influent boundary, such that the highest dimensionless substrate concentration (i.e. the highest contaminant level) corresponds to unity. For the electron acceptors, the base concentration corresponds to the existing background concentration, where unity here signifies the most pristine areas of the domain. For the microbial populations, the base concentration is taken as the initial population, implying that dimensionless microbial concentrations greater than one represent an increase in the microbial population and values less than one represent a decrease in the population.

CHAPTER 4. Sensitivity Investigation

4.1 Evaluation Methodology

4.1.1 Introduction

Natural heterogeneity in the subsurface environment causes both spatial and temporal variation in the input parameters and boundary conditions required to model groundwater contaminant transport and biodegradation (Connor, 1994; Freeze et al., 1980). As Anderson and Woessner (1992) indicate, the purpose of a sensitivity analysis is to quantify the effects of input parameter uncertainty on model results. The purpose of this sensitivity investigation is to identify the input parameters and processes which significantly affect dependent variables in the SEAM2D model. By identifying which parameters are most influential, recommendations on SEAM2D modeling procedures may be developed and subsequently applied to an actual site (see Chapter 5 for site application).

Model results for this sensitivity analysis of the SEAM2D model are in the form of substrate and electron acceptor concentrations. Changes in total mass of substrate throughout the domain are also reported and graphed as a function of time. Evaluation of model sensitivity is based on changes in substrate concentration along a longitudinal profile and changes in substrate mass with time. Each axis on the graphs provided in this analysis is non-dimensionalized using an indicated reference value, allowing biodegradation effects to be evaluated on a percentage basis. Biodegradation effects are quantified by comparing each series of biodegradation simulations to a basic tracer simulation, plotted as a solid line on each graph.

4.1.2 Model Domain

The hypothetical model used to investigate input parameter sensitivity is a rectangular grid, 50 meters long and 25 meters wide. A line source extends 5m from one longitudinal boundary, supplying a steady-state substrate and aqueous phase electron acceptor influent concentration as shown in Figure 4.1. The domain is bounded by specified flow (Neumann) conditions along the longitudinal boundaries and by specified head (Dirichlet) conditions along

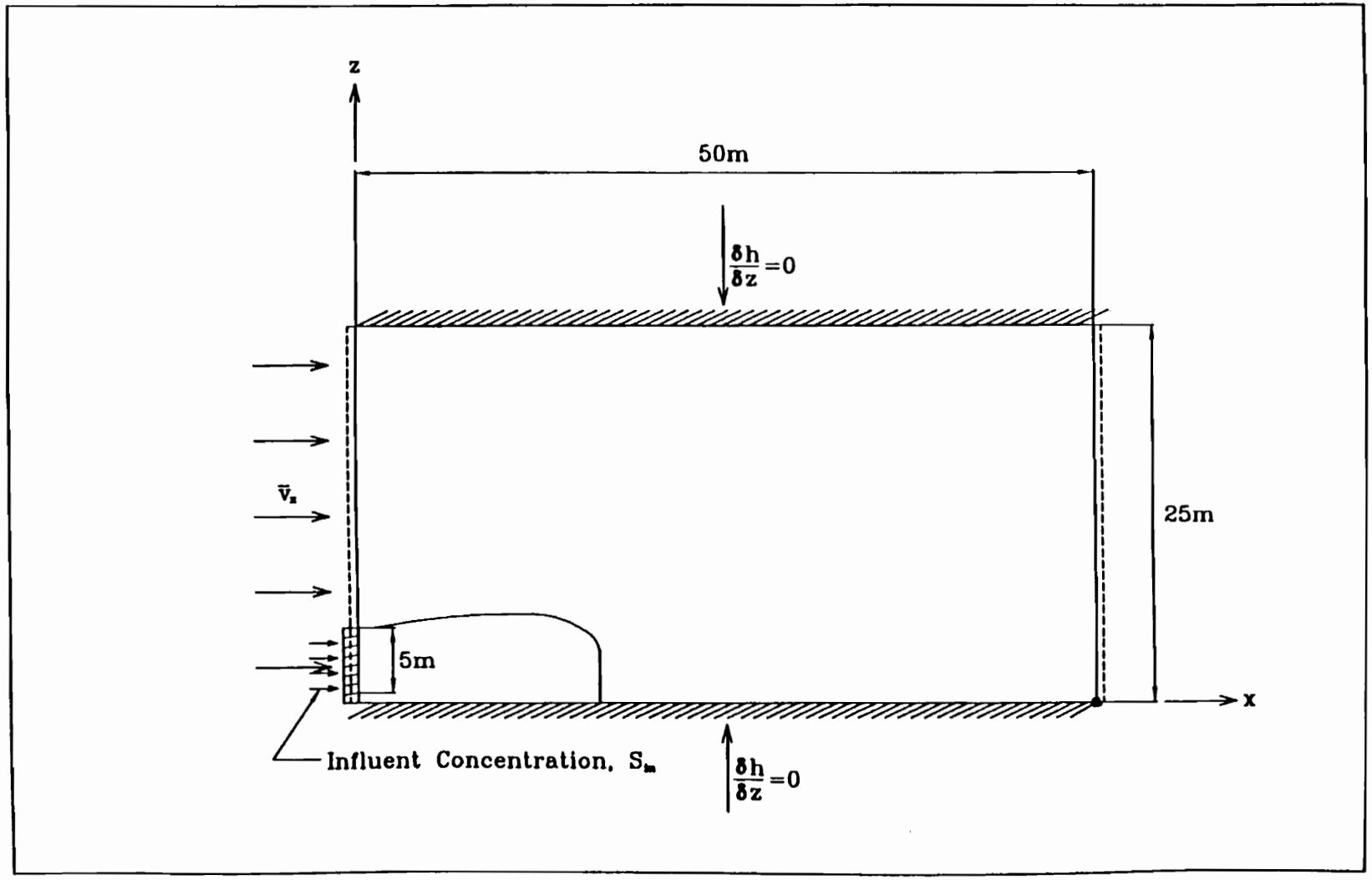

Figure 4.1. Model domain for sensitivity analysis.

the transverse boundaries. The longitudinal boundaries are specified as no flow, and the transverse boundaries are specified as hydraulic boundaries of uniform head, producing a uniform gradient along the x-axis. Two-dimensional transport is simulated for a uniform velocity field, oriented such that the direction of groundwater flow is parallel to the longitudinal axis. The symmetrical properties of this grid and source orientat.
ion allow the contaminant plume to be divided into two identical halves with respect to the longitudinal (x) axis. By dividing the plume in this fashion, more nodes are available to model a particular site with a finer grid and/or larger domain. A square, point-centered grid of 0.5 meters is used, with 200 time steps of 0.5 days, yielding a run time of 100 days. This combination of grid and time step size results in a uniform Courant number of 1.0, which limits the effects of numerical dispersion (Anderson and Woessner, 1992).

4.1.3 Biodegradation Conditions

A single, aqueous phase electron acceptor is used in all of the sensitivity analysis simulations, except when the solid phase electron acceptor (iron(III)) and the inhibition coefficient are investigated. The solid phase electron acceptor is investigated both as a single, primary electron acceptor and as a terminal electron acceptor under the influence of oxygen-based inhibition. The line source influent concentrations of substrate and aqueous phase electron acceptor are independently varied from expected maxima to minima. Substrate concentration variation simulates the range of possible contaminant concentrations that may be encountered at an actual site, while influent electron acceptor concentration variation simulates both optimal (i.e. high influent electron acceptor concentrations) and less than optimal (i.e. moderate to low electron acceptor concentrations) conditions typically seen in the heart of established contaminant plumes. Uniformly low background substrate concentrations and high background electron acceptor conditions are assumed, simulating pristine aquifer conditions. Excepting the oxygen-iron(III) sequential electron acceptor simulations, a single substrate, consumed by a single microbial population, is modeled with either an aqueous or solid phase electron acceptor. For the oxygen-iron(III) sequential electron acceptor model, two microbial

populations, one oxygen-reducing and one iron(III)-reducing, degrade the single substrate with oxygen as the primary and iron(III) as the terminal electron acceptor.

4.1.4 Input Parameters

A literature search of the various input parameters was conducted to establish the range of physically possible conditions. Table 4.1 lists the individual parameter ranges for an aqueous phase electron acceptor including the maximum, minimum, and typical values for each parameter, along with an list of sources used to establish these values. Figure 4.2 shows the conversion of these maximum and minimum input parameters to the full range of dimensionless parameter values, with the center hatch of Figure 4.2 indicating the base value used in the sensitivity simulations. The dimensionless groupings are evaluated both individually and in combination with other groupings to determine their impact on biodegradation. The arrows shown on Figure 4.2 define the minimum (▲) and maximum (Δ) dimensionless parameter values which can be independently tested, while the outside hatches represent the physically possible extremes for each dimensionless parameter. Table 4.2 lists the individual parameters for the solid phase electron acceptor simulations, including expected maxima and minima. The values in Table 4.2 are representative of the physically possible range of values for iron-reducing conditions and are converted to the corresponding dimensionless numbers in Figure 4.3. Table 4.3 lists the input parameters used in the sequential electron acceptor simulations, with the inhibition coefficient as the solely varied parameter. Figure 4.4 shows the relationships between the individual parameters and the dimensionless groupings. The individual dimensionless parameter analysis is accomplished by varying the input parameters shown on the left side of Figure 4.4. As illustrated in Figure 4.4, all of the dimensionless groupings can be varied individually except the D^I number, which must be evaluated in conjunction with other dimensionless parameters. The effects of varying two or more dimensionless parameters in combination are investigated by changing the variables which produce changes in multiple dimensionless groupings, as shown on the right side of Figure 4.4.

Table 4.1. Input parameter ranges for aqueous phase electron acceptor conditions.

Parameter	Maximum	Minimum	Base Value	Source
Microbial Parameters				
$k_{d,fac}$ (d^{-1})	0.100	0.001	0.01	Chen et al. (1992)
K_o, K_n ($mg_{e-(aq)}/L$)	1.00	0.01	0.1	Chen et al. (1992)
K_{so}, K_{sn} (mg/L)	100.0	0.1	10.0	Arcangeli and Arvin (1992) Chen et al. (1992) Kindred and Celia (1989)
$M_{B,fac}$ (g_{bio}/m^3)	10^3	10^{-3}	0.1933	
O_B, N_B (mg_e/L)	10.0	0.1	4.0	Arcangeli and Arvin (1992) Chen et al. (1992) Borden et al. (1984)
S_B (mg_S/L)	1,000	0.1	10.0	Site Specific
Y_o, Y_n(mg_S/mg_{bio})	0.50	0.01	0.25	Arcangeli and Arvin (1992) Chen et al. (1992) Kindred and Celia (1989)
β_{fac} (m^2/g_{bio})	30.0	1.0	30.0	
δ_{fac} (m)	10^{-3}	10^{-5}	10^{-4}	
γ_o, γ_n ($mg_{e-(aq)}/mg_S$)	5.0	0.5	1.0	Arcangeli and Arvin (1992) Chen et al. (1992) Borden et al. (1984)
μ_o, μ_n (d^{-1})	10.0	0.1	1.0	Arcangeli and Arvin (1992) Kindred and Celia (1989)
Hydrodynamic Parameters				
D_o,D_n (m^2/d)			$2x10^{-4}$	
D_s (m^2/d)			10^{-4}	Chen et al. (1984)
$\overline{v}_x$ (m/d)	2.5	0.001	1.0	
α_L (m)	1.0	0.001	0.1	
α_T (m)	0.1	0.0001	0.01	

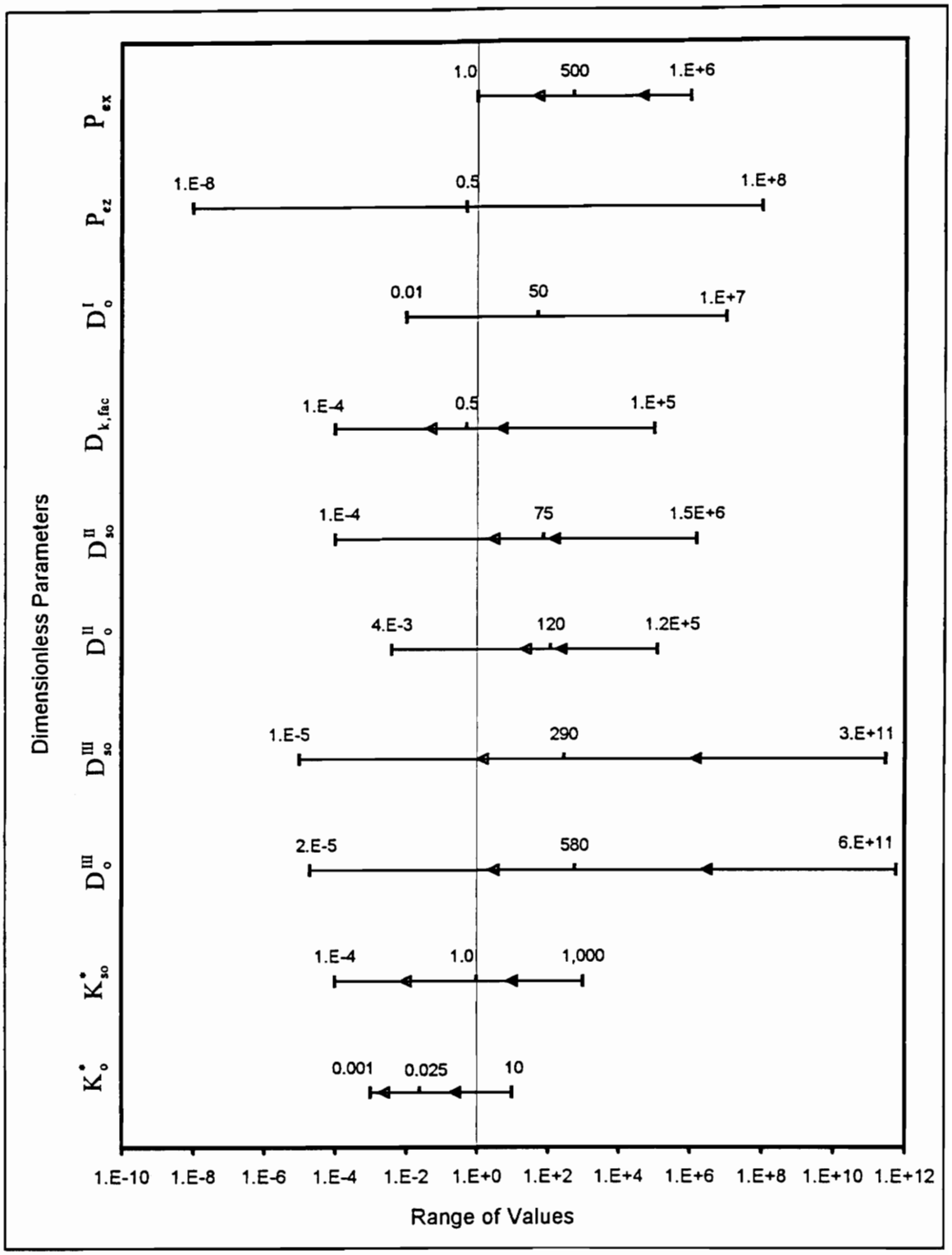

Figure 4.2. Dimensionless parameter ranges for aqueous phase electron acceptor conditions.

Table 4.2. Input parameter ranges for solid phase electron acceptor conditions.

Parameter	Maximum	Minimum	Base Value
Microbial Parameters			
$k_{d,ana}$ (d^{-1})	0.100	0.001	0.01
K_{sf} (mg/L)	1,000	1.0	10.0
S_B (mg_S/L)	1,000	0.1	10.0
F_B ($\mu g_{e^-(so)}$/g)	100.0	15.0	100.0
$M_{B,ana}$ (g_{bio}/m^3)	1.0	10^{-3}	0.1
Y_f(mg_S/mg_{bio})	0.50	0.05	0.5
β_{ana} (m^2/g_{bio})	30.0	1.0	10.0
δ_{ana} (m)	10^{-3}	10^{-5}	10^{-4}
γ_f ($mg_{e^-(so)}/mg_S$)	100.0	1.0	10.0
μ_f (d^{-1})	5.0	0.05	0.5
ζ($mg_{Fe(II)}/mg_{Fe(III)}$)			0.01
Hydrodynamic Parameters			
D_s (m^2/d)			10^{-4}
$\overline{v}_x$ (m/d)	2.5	0.001	1.0
α_L (m)	1.0	0.001	0.1
α_T (m)	0.1	0.0001	0.01

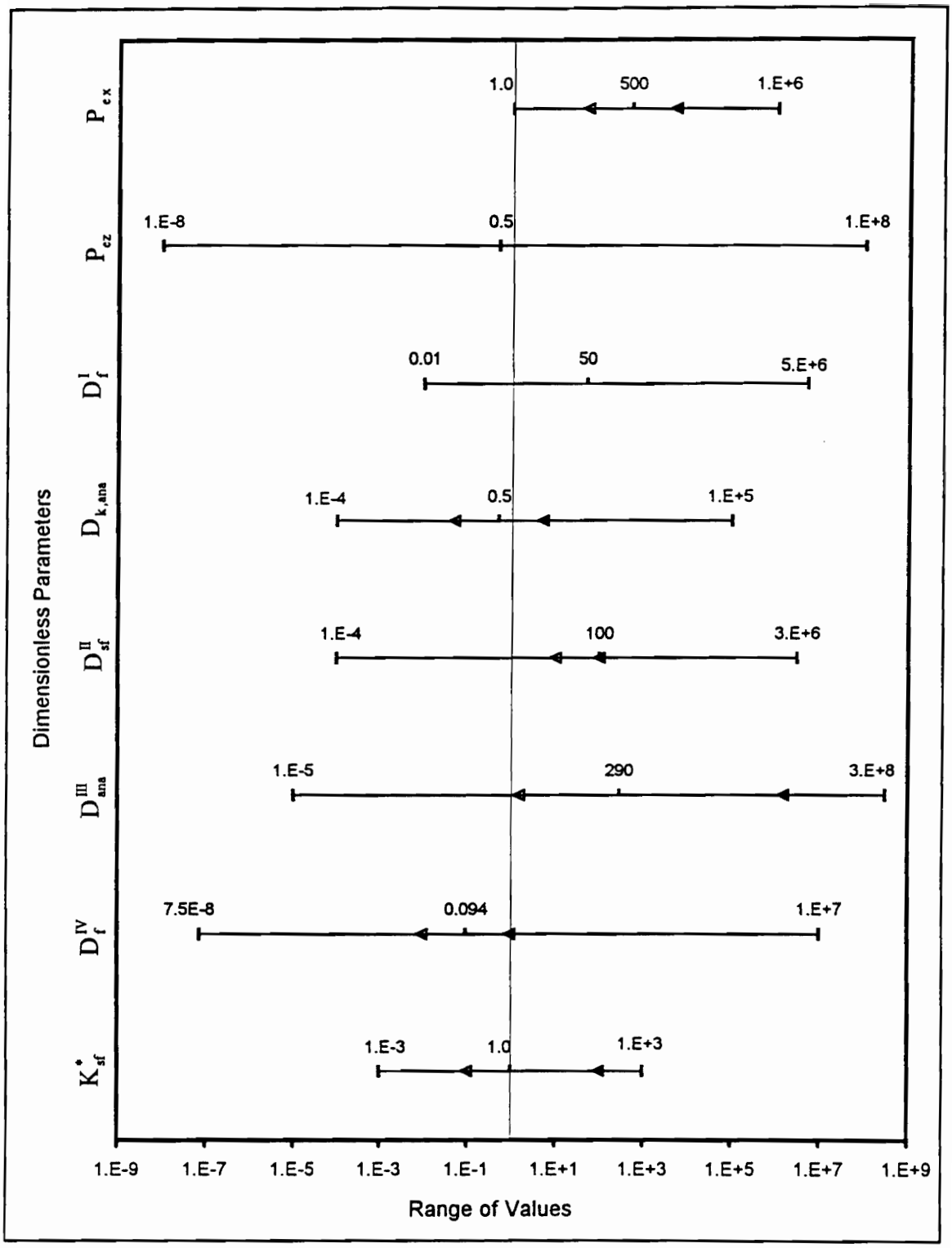

Figure 4.3. Dimensionless parameter ranges for solid phase electron acceptor conditions.

Table 4.3. Input parameter ranges for sequential electron acceptor conditions.

Parameter	Primary Electron Acceptor (Aqueous)	Terminal Electron Acceptor (Solid)
Microbial Parameters		
K_c (mg_{O2}/L)		1.0-0.001
k_d (d^{-1})	0.01	0.01
K_s (mg/L)	10.0	10.0
F_B ($\mu g_{e^-(so)}/g$)	n/a	100.0
O_B (mg_S/L)	4.0	n/a
M_B (g_{bio}/m^3)	0.2	0.1
S_B (mg_S/L)	10.0	10.0
Y(mg_S/mg_{bio})	0.25	0.50
β (m^2/g_{bio})	10.0	10.0
δ (m)	10^{-4}	10^{-4}
γ (mg_{e^-}/mg_S)	10.0	10.0
μ_{max} (d^{-1})	1.0	0.5
ζ($mg_{Fe(II)}/mg_{Fe(III)}$)		0.01
Hydrodynamic Parameters		
D_o (m^2/d)	$2x10^{-4}$	n/a
D_s (m^2/d)	10^{-4}	10^{-4}
$\overline{v}_x$ (m/d)	1.0	1.0
α_L (m)	0.1	0.1
α_T (m)	0.01	0.01

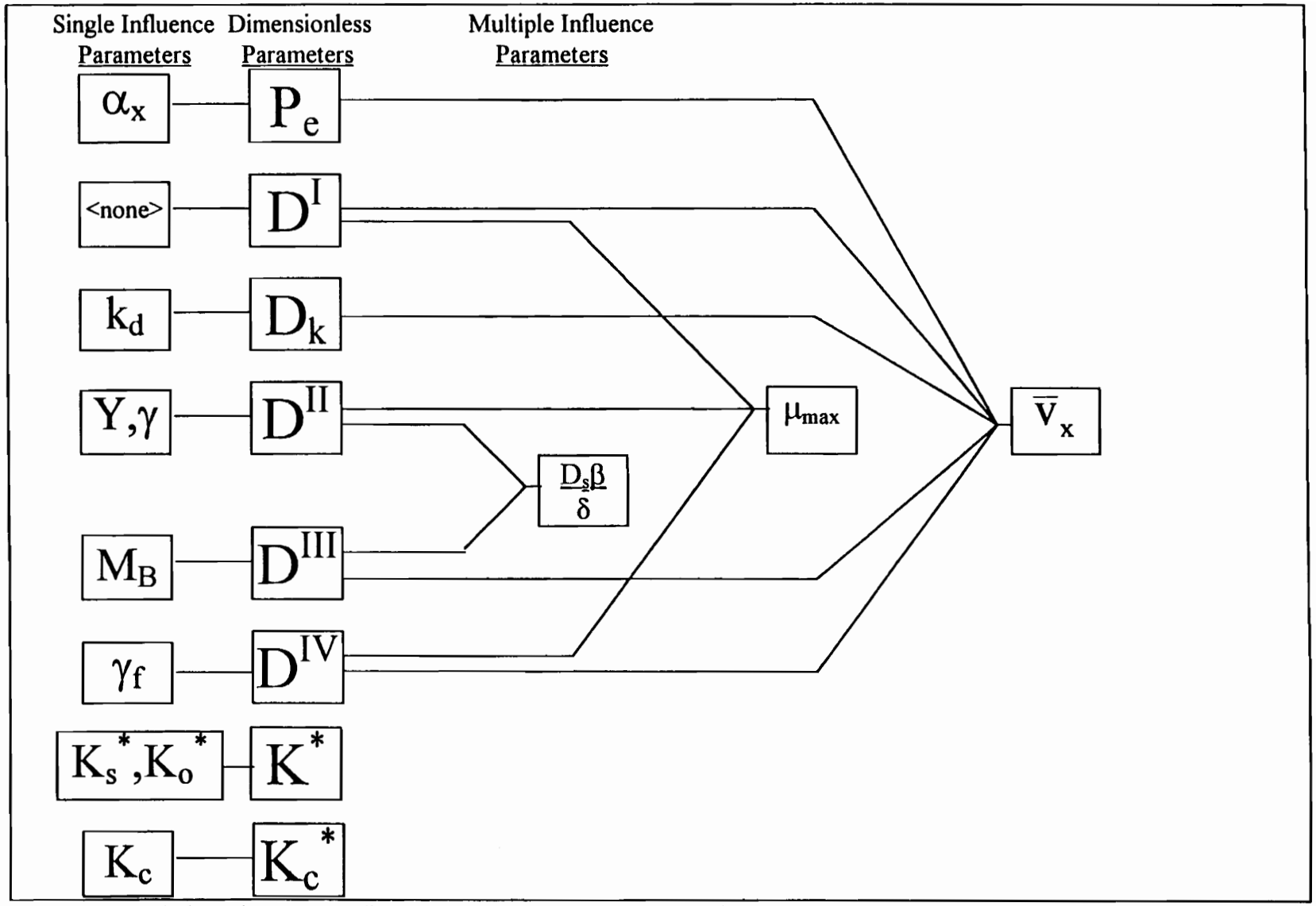

Figure 4.4. Relationship between dimensionless groupings and the individual input parameters.

4.1.5 Reference Values

As mentioned above, the graphs presented in this sensitivity analysis are non-dimensionalized using specified reference concentrations, lengths, or times. The reference longitudinal distance, L_x, is taken as the model domain length of 50 meters. The characteristic time, τ, is then formulated as the reference longitudinal distance divided by the average groundwater velocity and calculated as 50 days. The reference substrate concentration, S_B, is taken as the influent substrate concentration while the reference electron acceptor concentration, O_B or F_B, is set equal to the specified initial concentration for the model domain. Finally, the reference biomass concentration, M_B, is taken as the initial biomass concentration.

4.2 Results for Aqueous Phase Electron Acceptor Simulations

4.2.1 Graphical Representation

For each parameter examined in this sensitivity analysis, a plot of dimensionless substrate concentration (S^*) versus dimensionless longitudinal distance (X) is provided at a dimensionless time (T) of 0.5. This concentration profile is taken along the longitudinal axis corresponding to the centerline of the contaminant plume, as illustrated in Figure 4.5. A plot of dimensionless substrate mass (M^*) versus dimensionless time is also provided for each simulation, depicting changes in substrate mass throughout the domain with time. By calculating the mass flux into and out of the domain, a substrate mass balance is performed by summing the substrate mass in each individual cell after biodegradation has occurred. The substrate mass is then non-dimensionalized by dividing this mass of substrate by a mass balance performed without biodegradation. When indicated, a longitudinal profile of dimensionless oxygen concentration (O^*) versus dimensionless longitudinal distance for T equal to 0.5 and/or a substrate concentration profile and mass balance at T = 0.2 is also provided.

4.2.2 Influent Concentrations

The effects of varying the influent concentration of either the substrate or aqueous

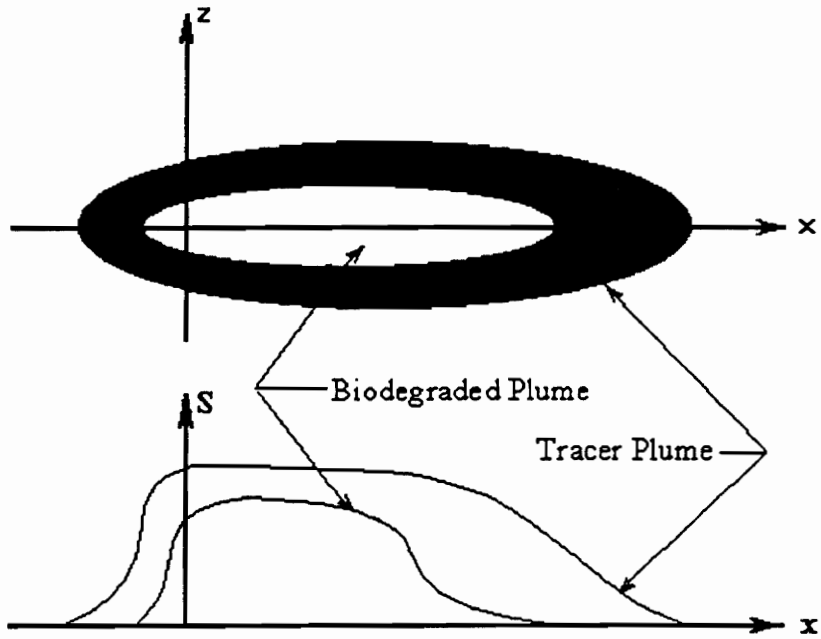

Figure 4.5. Schematic representation of a typical substrate concentration profile.

electron acceptor significantly impact the potential for biodegradation. Increases in the influent substrate concentration produce proportional increases in both D_{so}^{II} and K_{so}^{*}. Figures 4.6a and 4.6b indicate that, on a percentage basis, substrate consumption increases for decreases in the influent substrate concentration. For large substrate concentrations (i.e. large D_{so}^{II} and K_{so}^{*}), the electron acceptor is completely consumed, thus limiting biodegradation. For low substrate concentrations (i.e. low D_{so}^{II} and K_{so}^{*}), however, the aqueous phase electron acceptor, oxygen, is no longer limiting and a large percentage of the influent substrate is consumed.

Changes in the influent oxygen concentration also impact model results even though none of the dimensionless parameters listed in Table 3.3 change. As indicated in Figures 4.7a and 4.7b, increases in the influent aqueous phase electron acceptor (oxygen) concentration result in increased biodegradation. Figure 4.7c indicates that large influent oxygen concentrations produce substrate-limiting conditions, while low influent oxygen concentrations produce electron acceptor-limiting conditions.

4.2.3 The Peclet Number

The Peclet number, representing the ratio of advective to hydrodynamically dispersive transport processes, may be independently varied by using dispersivity. The dispersivity is varied for both the longitudinal and transverse directions concurrently, such that the ratio of α_x to α_z stays at 1 to 10. This ratio corresponds to the ratio typically seen in field conditions for horizontal subsurface transport (Domenico and Schwartz, 1990). In the hypothetical model used here, the Peclet number is reported in longitudinal direction (i.e. P_{ex}) only, as the concentration profiles presented here focus on transport in the longitudinal direction. Note that P_{ez} varies proportionally to P_{ex}, with the characteristic width defined as the source width. For the tracer simulations shown in Figure 4.8a and 4.8b, a decrease in the Peclet number produces a more disperse plume edge. The biodegrading simulations presented in Figure 4.8a indicate that changes in the Peclet number may produce local variations in biodegradation but Figure 4.8b indicates that

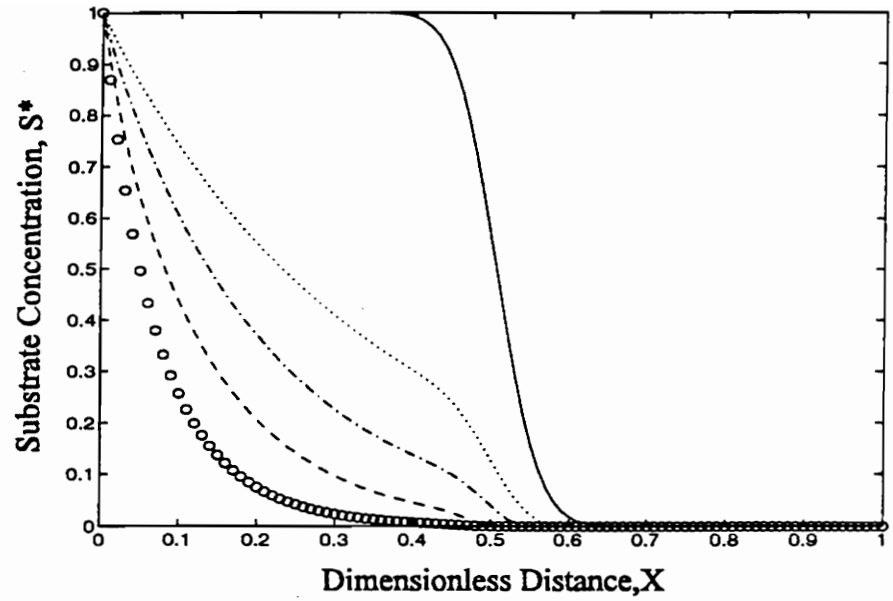

(a)

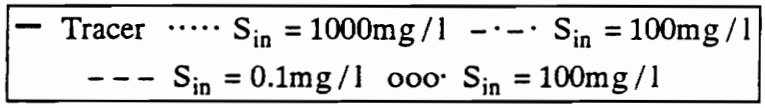

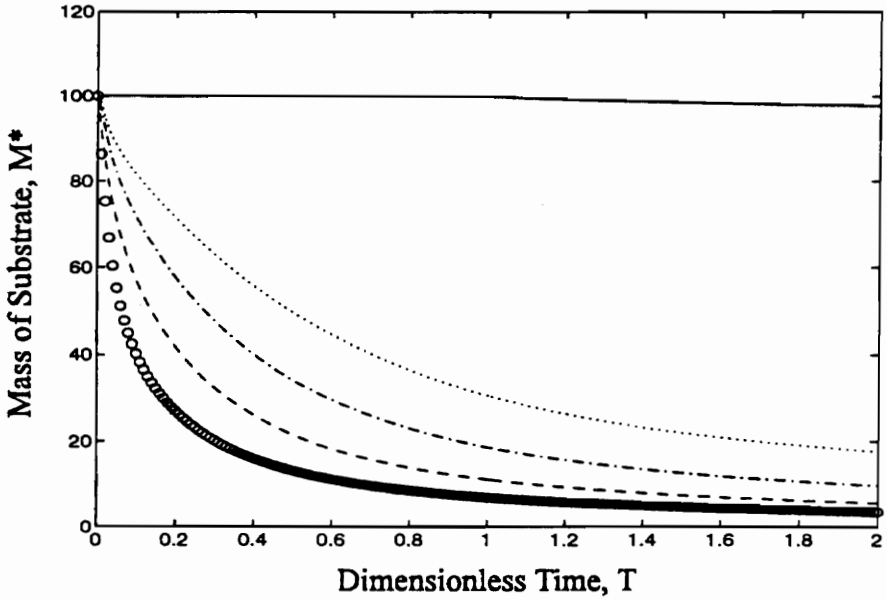

(b)

Figure 4.6. Substrate concentration profile and mass balance for varying influent substrate concetrations.

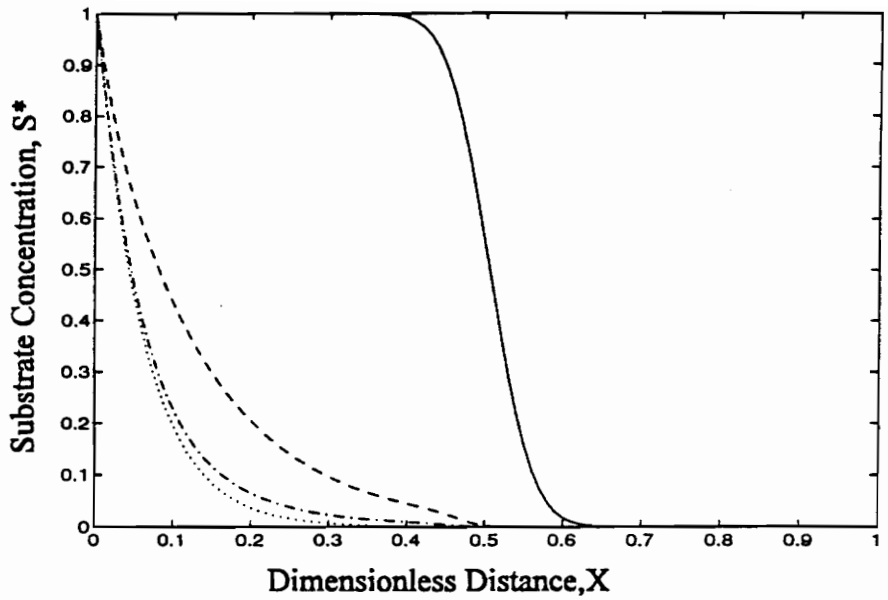

(a)

— Tracer ····· $O_{in} = 4.0 mg/l$ –·–· $O_{in} = 1.0 mg/l$ – – – $O_{in} = 0.1 mg/l$

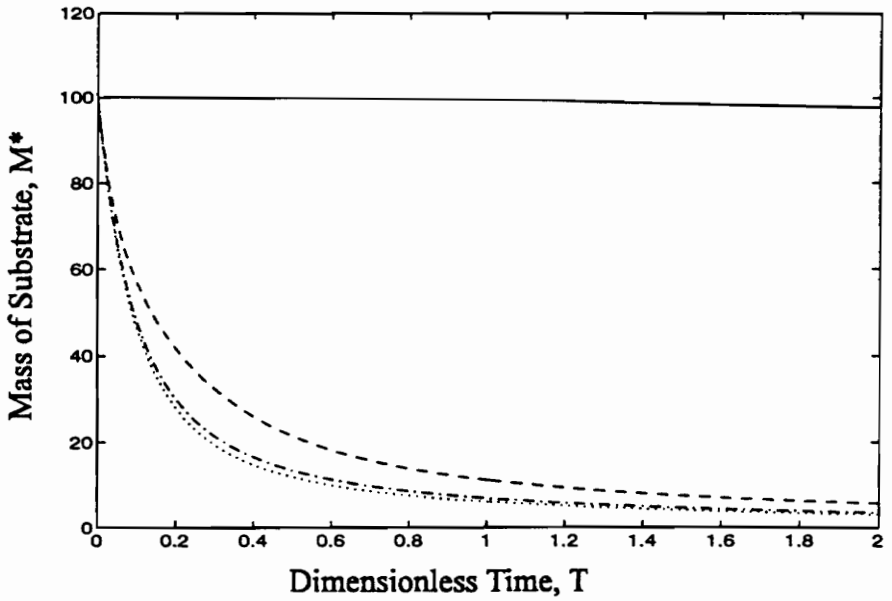

(b)

Figure 4.7. Substrate concentration profile and mass balance for varying influent oxygen concetrations.

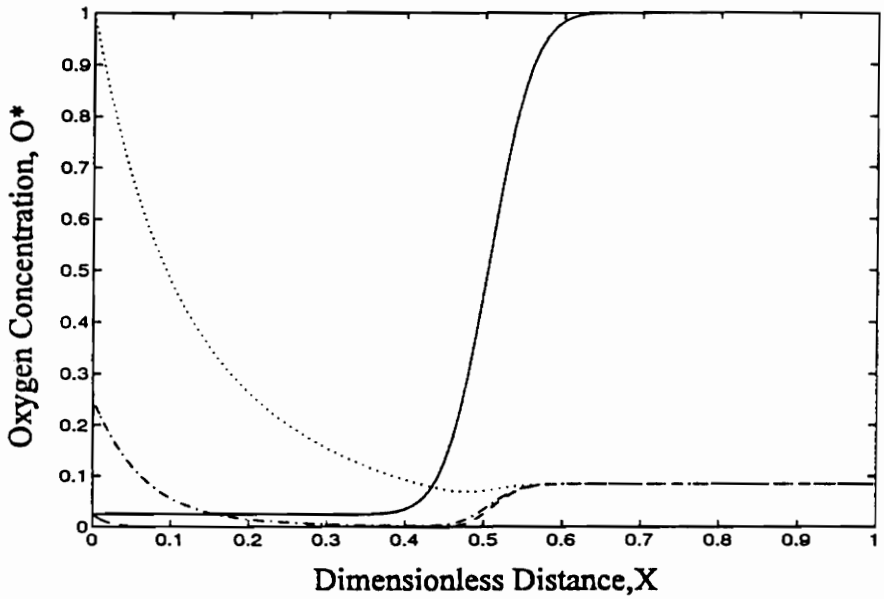

(c)

— Tracer ····· $O_{in} = 4.0 mg/l$ –·–· $O_{in} = 1.0 mg/l$ – – – $O_{in} = 0.1 mg/l$

Figure 4.7. Oxygen concentration profile for varying influent oxygen concentrations.

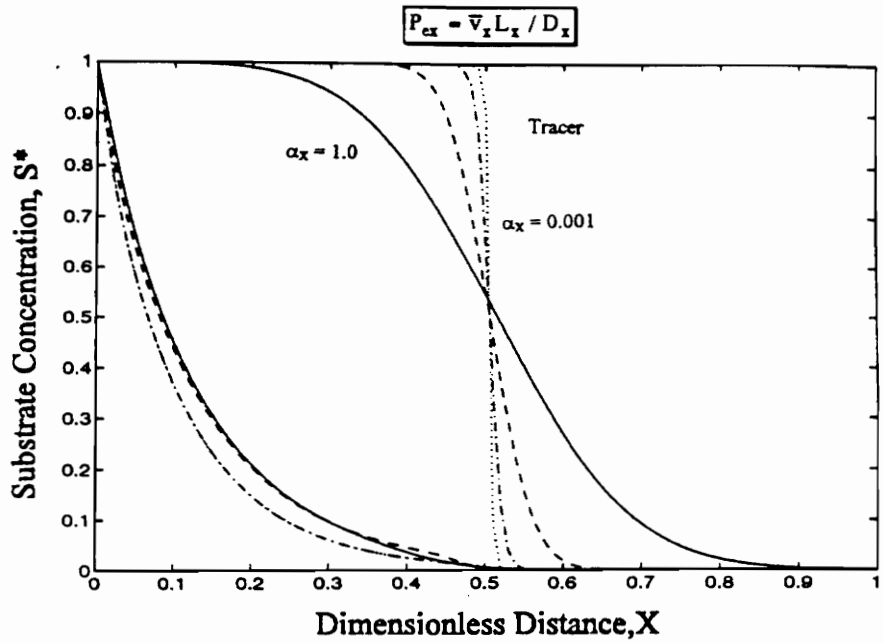

(a)

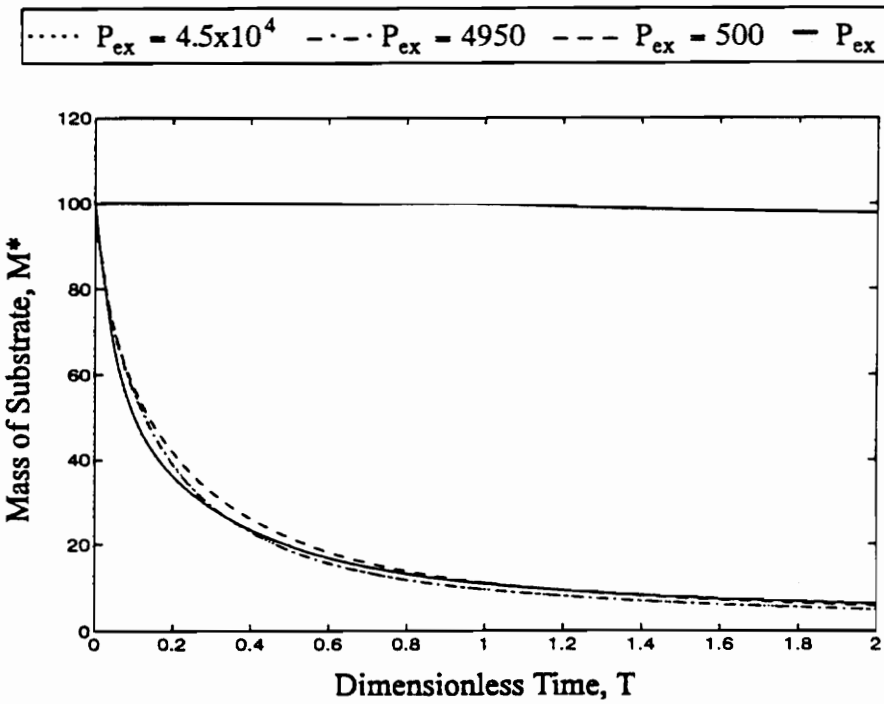

(b)

Figure 4.8. Substrate concentration profile and mass balance for varying Peclet number.

variation of the Peclet number does do not produce major changes in the total mass of biodegraded substrate.

4.2.4 The D_k Number

The $D_{k,fac}$ dimensionless grouping, which relates microbial decay to the characteristic travel time, may be varied by changing the decay coefficient, $k_{d,fac}$. Increases in $D_{k,fac}$ imply an increase in either the microbial decay rate or the time available for decay and are expected to decrease substrate biodegradation. Figures 4.9a and 4.9b show that variation of $D_{k,fac}$ has little impact on biodegradation, with increases in $D_{k,fac}$ producing a small decrease in the amount of substrate consumed.

4.2.5 The D^{II} Number

Model sensitivity to the D^{II} dimensionless grouping may be evaluated by varying the yield coefficient for substrate and by varying the use coefficient for an aqueous phase electron acceptor. As noted in Chapter 3, decreases in the yield coefficient are indicative of less efficient substrate utilization by the microbial population. By decreasing the yield coefficient, the microbial population requires more substrate to sustain growth, increasing the rate of substrate utilization. By this reasoning, decreases in D^{II}_{so} which varies directly with Y_o, are expected to produce increases in biodegradation. Figures 4.10a and 4.10b confirm this hypothesis, depicting a decrease in both substrate concentration and total mass for a decrease in D^{II}_{so}.

D^{II}_{o} is independently varied by changing the use coefficient, γ_o, where γ_o represents the ratio of aqueous phase electron acceptor utilization to biomass production. The use coefficient varies inversely with D^{II}_{o}, with decreases in γ implying more efficient electron acceptor utilization. Since more efficient electron acceptor utilization implies that less oxygen is required to degrade a given quantity of substrate, increases in D^{II}_{o} are expected to increase biodegradation. Figures 4.11a and 4.11b confirm that an increase in D^{II}_{o}

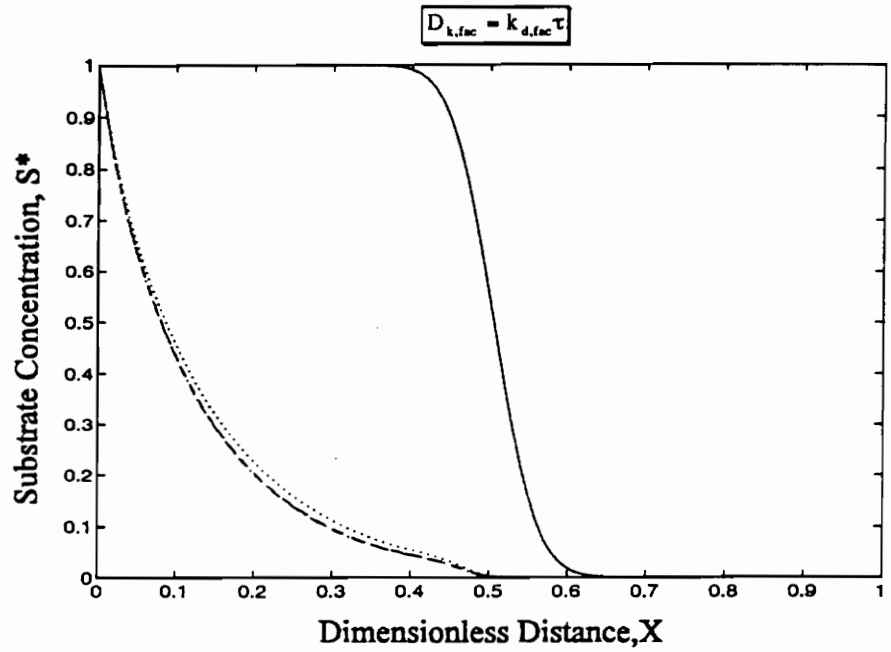

(a)

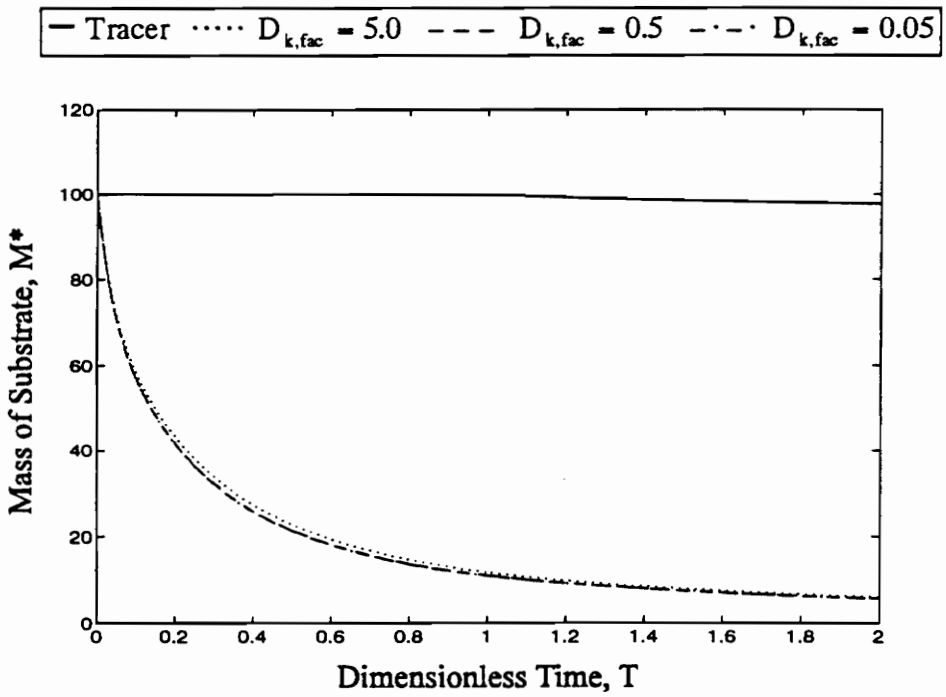

(b)

Figure 4.9. Substrate concentration profile and mass balance for varying $D_{k,fac}$.

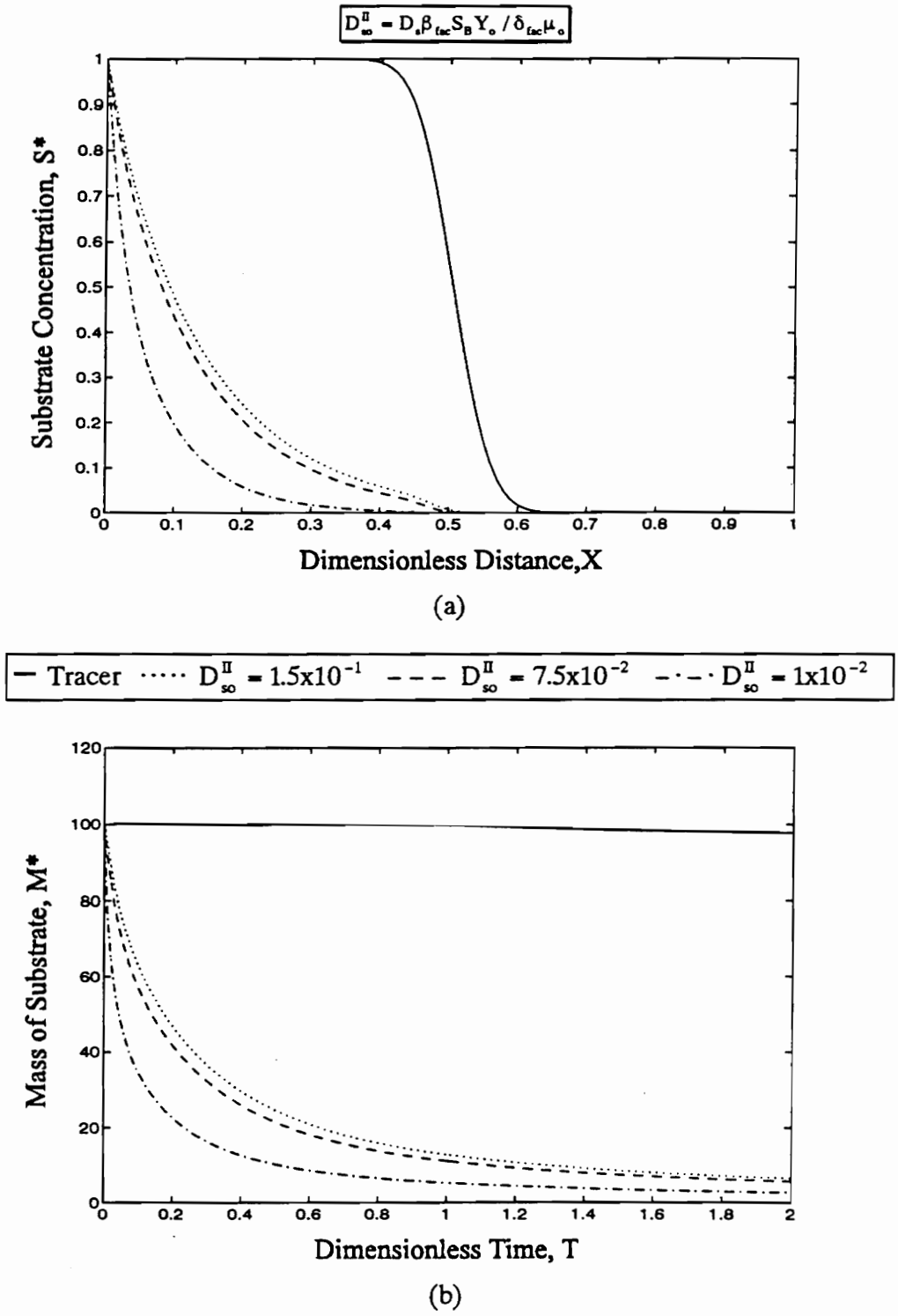

Figure 4.10. Substrate concentration profile and mass balance for varying D_{so}^{II}.

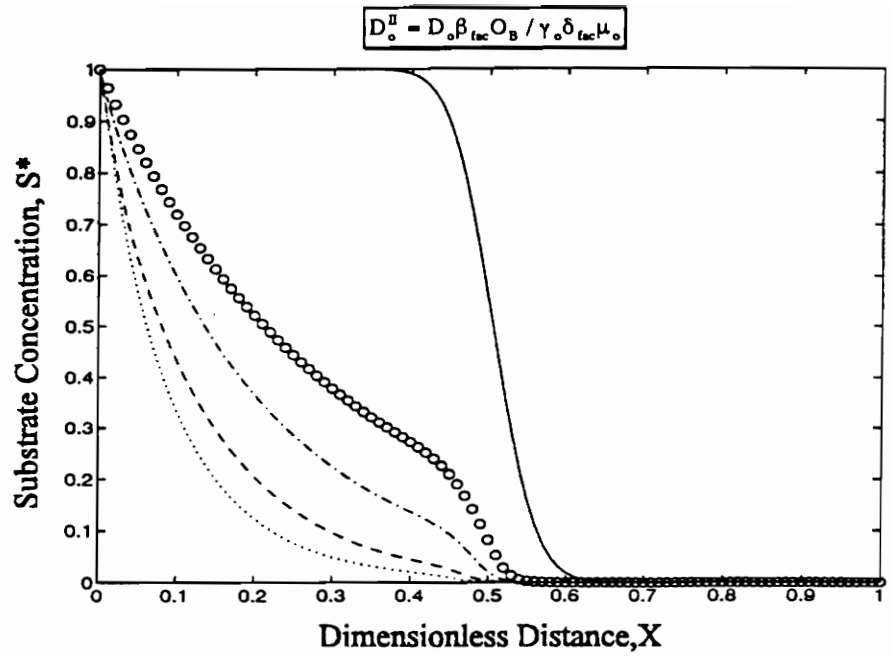

(a)

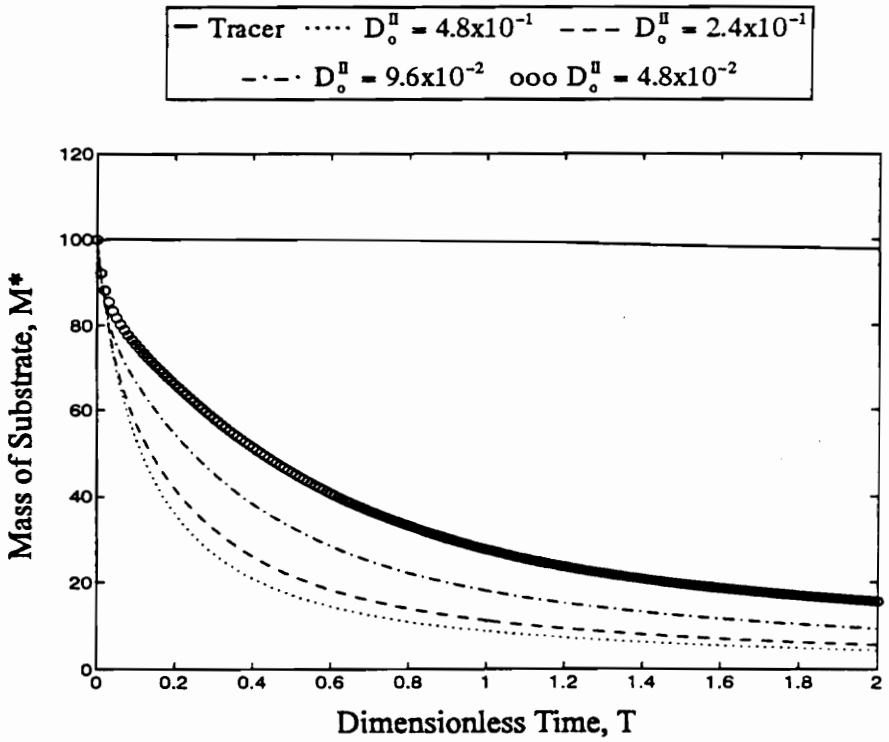

(b)

Figure 4.11. Substrate concentration profile and mass balance for varying D_o^{II}.

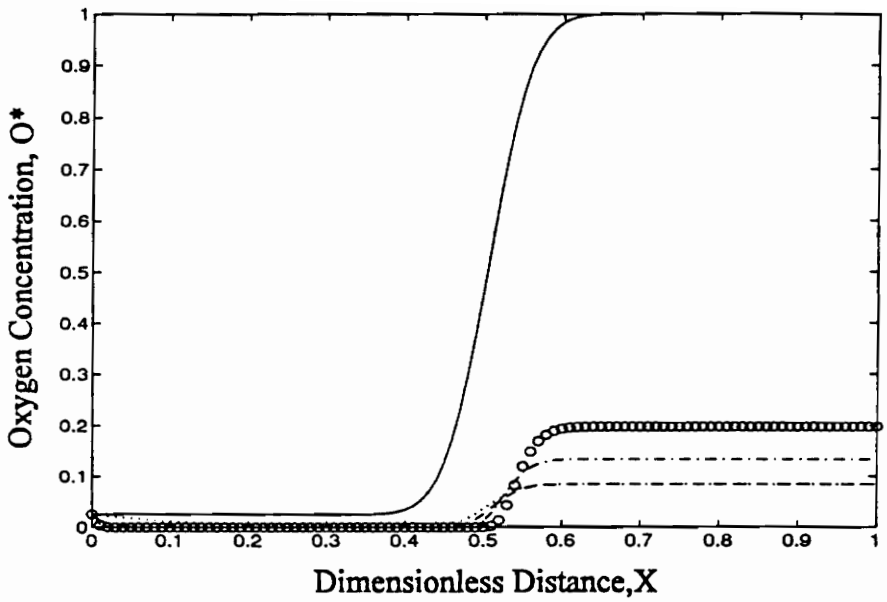

(c)

— Tracer ····· $D_o^{II} = 4.8x10^{-1}$ - - - $D_o^{II} = 2.4x10^{-1}$
-·-· $D_o^{II} = 9.6x10^{-2}$ ooo $D_o^{II} = 4.8x10^{-2}$

Figure 4.11. Oxygen concentration profile for varying D_o^{II}.

results in increased biodegradation. Figure 4.11c indicates that, for larger D_o^{II} values, oxygen within the plume is not completely consumed (by T = 0.5), thus providing further evidence that increased electron acceptor utilization efficiency results in improved biodegradation conditions.

4.2.6 The D^{III} Number

The D^{III} dimensionless grouping quantifies the relationship between interphase transport and the characteristic travel time. Increases in either the travel time and/or the diffusion rate parameters produce an increase in D^{III}, and are expected to produce increased substrate and electron acceptor consumption. The initial biomass population, M_B, varies proportionally with D^{III} groupings, and is used to independently examine the D^{III} dimensionless grouping. Figures 4.12a and 4.12b confirm that increasing D^{III} does produce increased biodegradation. Further investigation of these figures indicates that changes in D^{III} have a major impact on biodegradation results, especially for small D^{III} numbers.

4.2.7 The K^* Number

The K^* dimensionless parameters represent a ratio between the initial condition and the utilization rate. Increases in this dimensionless number imply that the reaction kinetics are approaching first order, while decreases in K^* indicate that the kinetics are approaching zero order. First order kinetics are associated with substrate or electron acceptor limited conditions, whereas non-limited conditions follow zero order kinetics. Increases in K^* also imply that both the microbial growth and utilization rates decrease. Examination of Figures 4.13a and 4.13c indicates inconsistent changes in substrate concentration for changes in K_{so}^*. Figures 4.13b and 4.13d explain this apparent inconsistency by portraying an increase in biodegradation for decreasing K_{so}^* for the high growth conditions seen here at early times. Once all of the available electron acceptor is

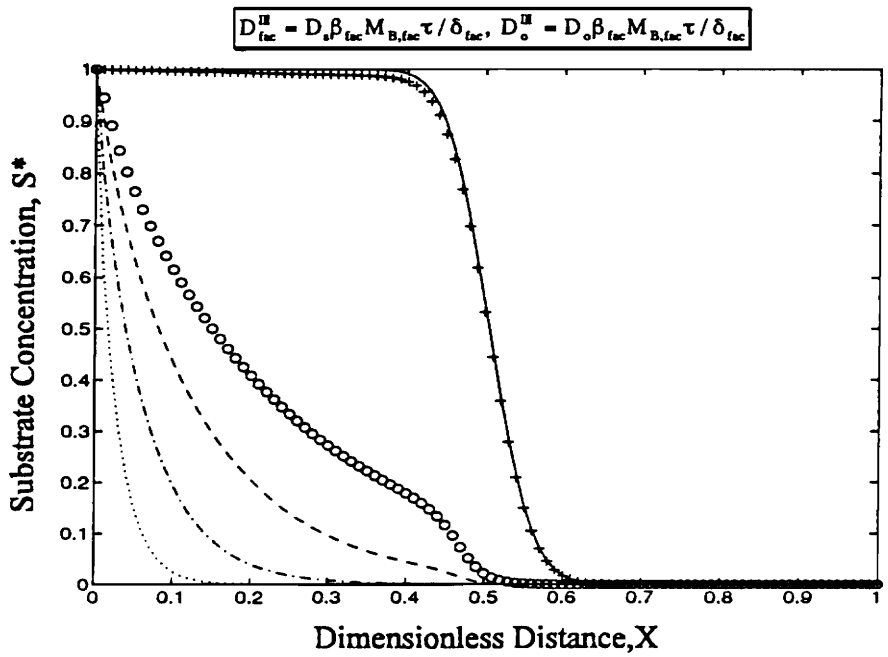

(a)

— Tracer ····· $D^{III}_{fac} = 1.5x10^6, D^{III}_o = 3.0x10^6$ –·–· $D^{III}_{fac} = 1.5x10^3, D^{III}_o = 3.0x10^3$
– – – $D^{III}_{fac} = 290, D^{III}_o = 580$ ooo $D^{III}_{fac} = 150, D^{III}_o = 300$ + + + $D^{III}_{fac} = 1.5, D^{III}_o = 3.0$

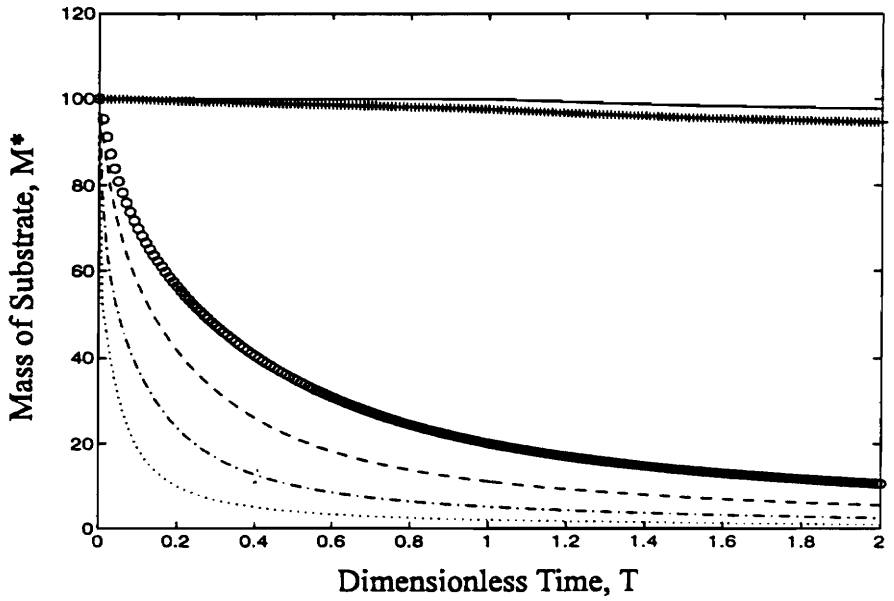

(b)

Figure 4.12. Substrate concentration profile and mass balance for varying D^{III}.

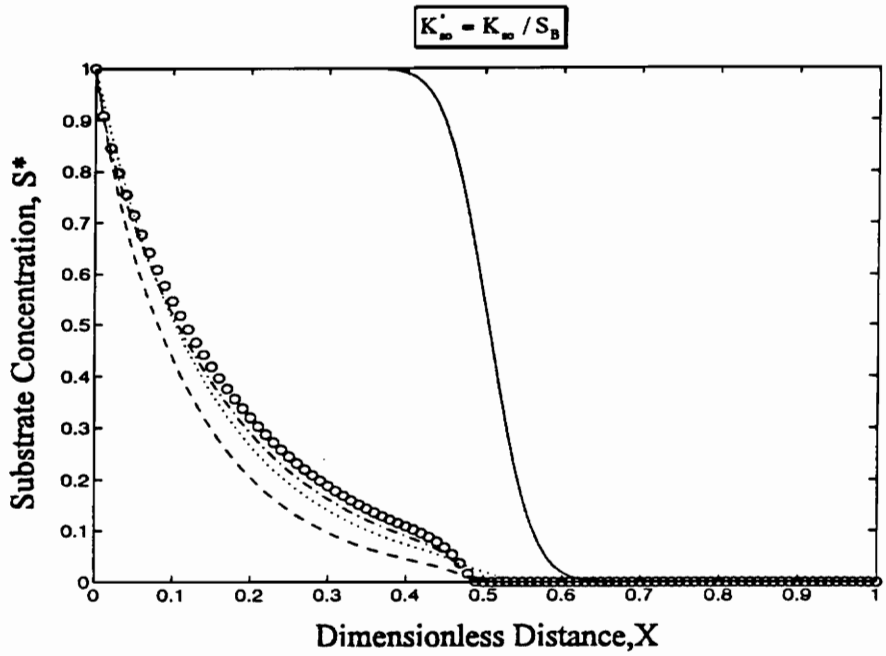

(a)

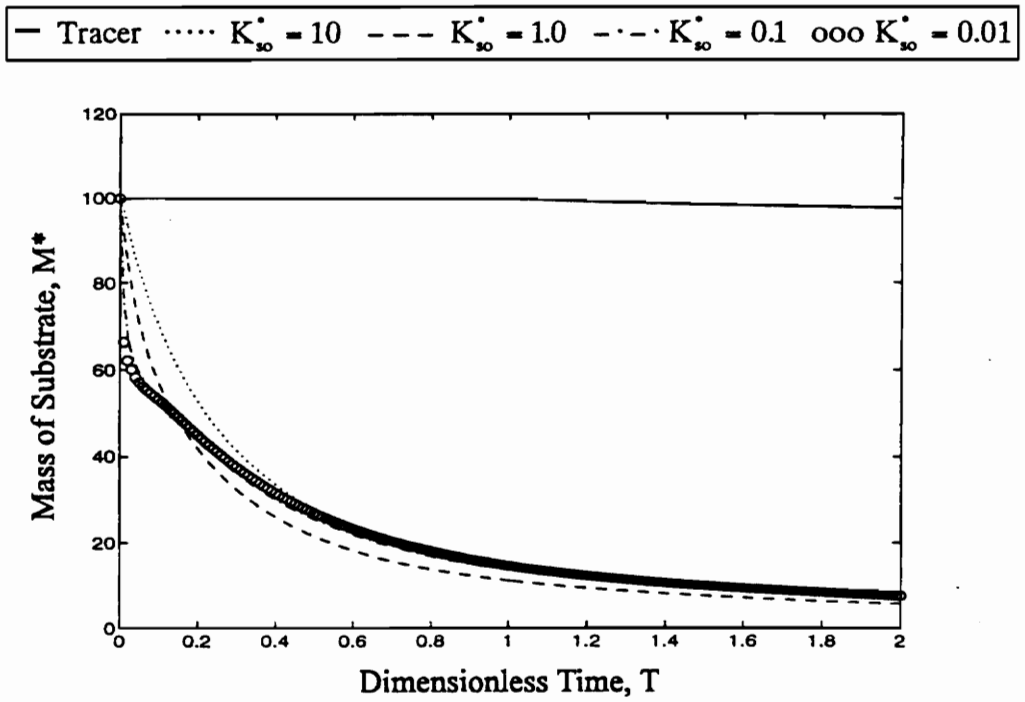

(b)

Figure 4.13. Substrate concentration profile and mass balance for varying K^*_{so}.

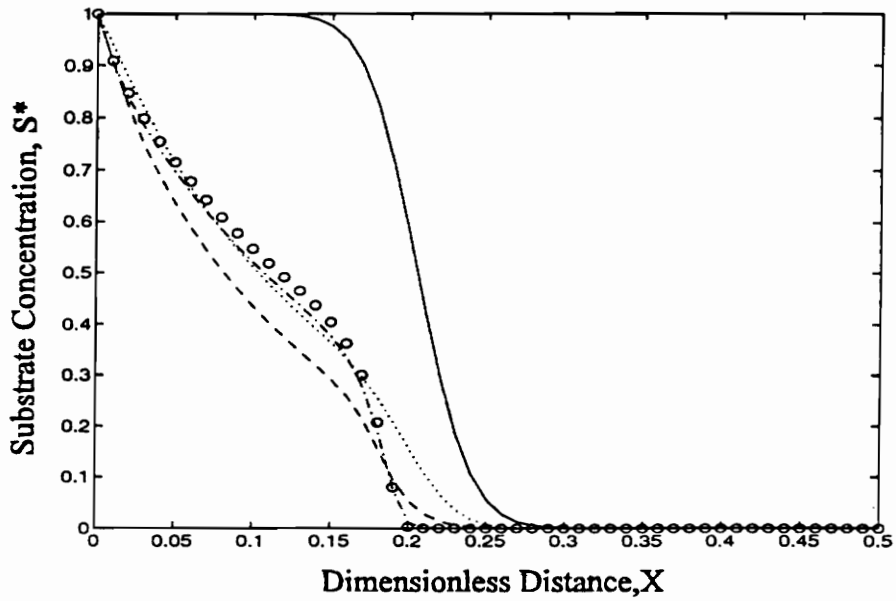

(c)

— Tracer ····· $K^*_{so} = 10$ – – – $K^*_{so} = 1.0$ –·–· $K^*_{so} = 0.1$ ooo $K^*_{so} = 0.01$

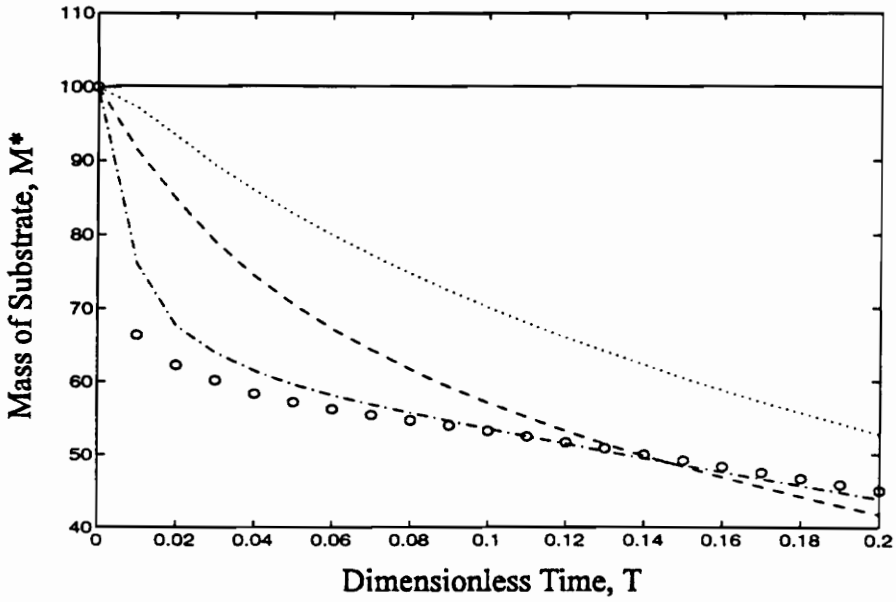

(d)

Figure 4.13. Substrate concentration profile at $\tau = 0.2$ and mass balance at early time for varying K^*_{so}.

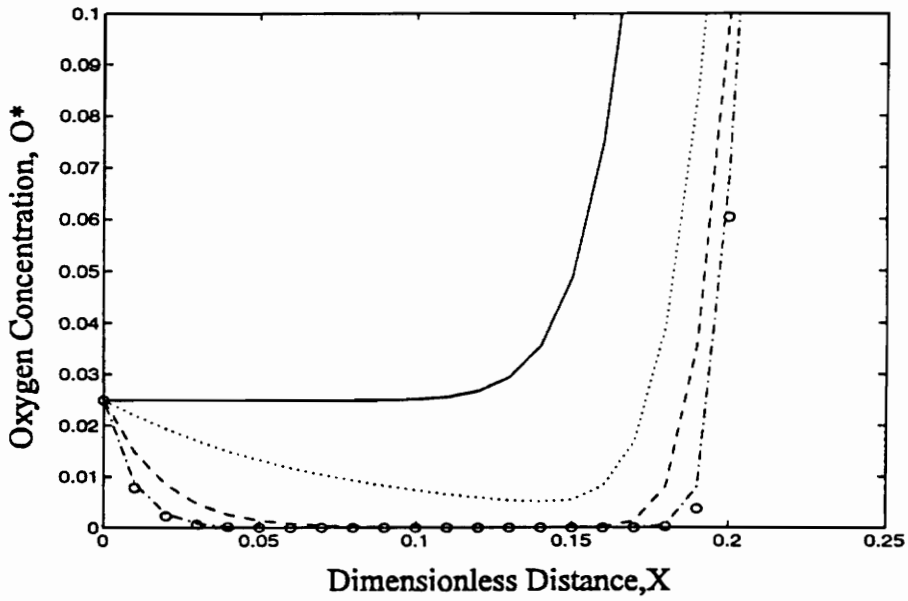

(e)

— Tracer ····· $K^*_{so} = 10$ – – – $K^*_{so} = 1.0$ –·–· $K^*_{so} = 0.1$ ooo $K^*_{so} = 0.01$

Figure 4.13. Oxygen concentration profile at $\tau = 0.2$ for varying K^*_{so}.

consumed, the substrate utilization rate slows considerable due to electron acceptor limited conditions. Figure 4.13e, showing the oxygen concentration profile at T = 0.2, indicates that the lower utilization rates (i.e. higher K^*_{so} values) do not fully deplete the available electron acceptor, allowing continuous biodegradation and producing the increased substrate removal at high K^*_{so} values, as shown in Figure 4.13b.

K^* for the aqueous electron acceptor (i.e. oxygen) behaves similarly to K^*_{so} in that small K^*_o values produce increased biodegradation at early times, as shown in Figures 4.14a and 4.14b. Figure 4.14c shows that, for high K^*_o, the electron acceptor is fully depleted, producing electron acceptor limited conditions and allowing moderate K^*_o values to induce increased biodegradation with increasing time, as illustrated in Figure 4.14b.

4.2.8 Biofilm Parameters β and δ

The specific surface area for diffusion (β) and diffusion layer thickness (δ) are always used in combination in the SEAM2D model, allowing these two parameters to be analyzed concurrently as the ratio, β/δ. This ratio is a component of both the D^{II} and D^{III} numbers for substrate and aqueous phase electron acceptors, with increases in β/δ producing proportional increases in both of these dimensionless parameters. Considering that β/δ increases for an increase in either the specific surface area available for diffusion or a decrease in the boundary layer thickness, an increase in this ratio implies a faster rate of diffusion for substrate and electron acceptor into the biomass, producing more favorable conditions for biodegradation. As shown in Figures 4.15a and 4.15b, biodegradation does increase with β/δ, yielding a trend that is consistent with the results found for the D^{III} dimensionless grouping, but is opposite to the trend witnessed earlier for the D^{II}_{so} number. The apparent inconsistency noted here is accounted for by examining which phenomena are varied during each individual sensitivity analysis. When D^{II}_{so} is

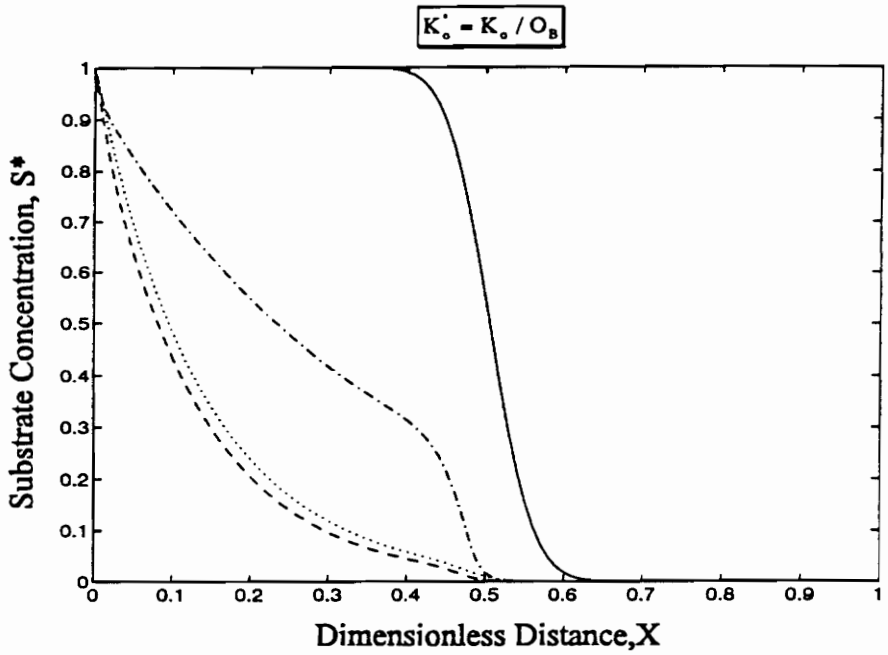

(a)

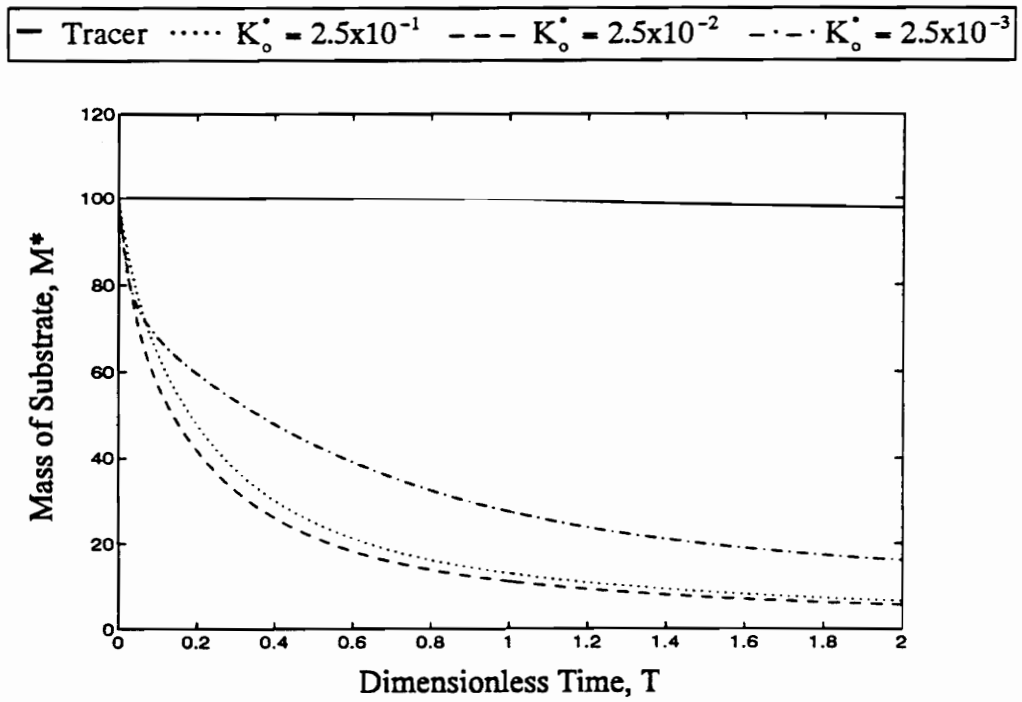

(b)

Figure 4.14. Substrate concentration profile and mass balance for varying K_o^*.

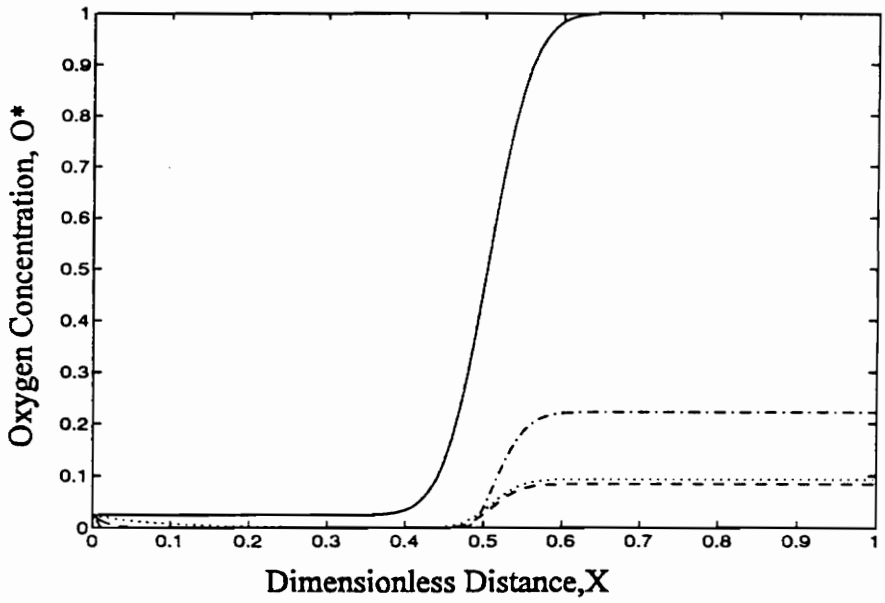

(c)

— Tracer ····· $K_o^* = 2.5x10^{-1}$ – – – $K_o^* = 2.5x10^{-2}$ –·–· $K_o^* = 2.5x10^{-3}$

Figure 4.14. Oxygen concentration profile for varying K_o^*.

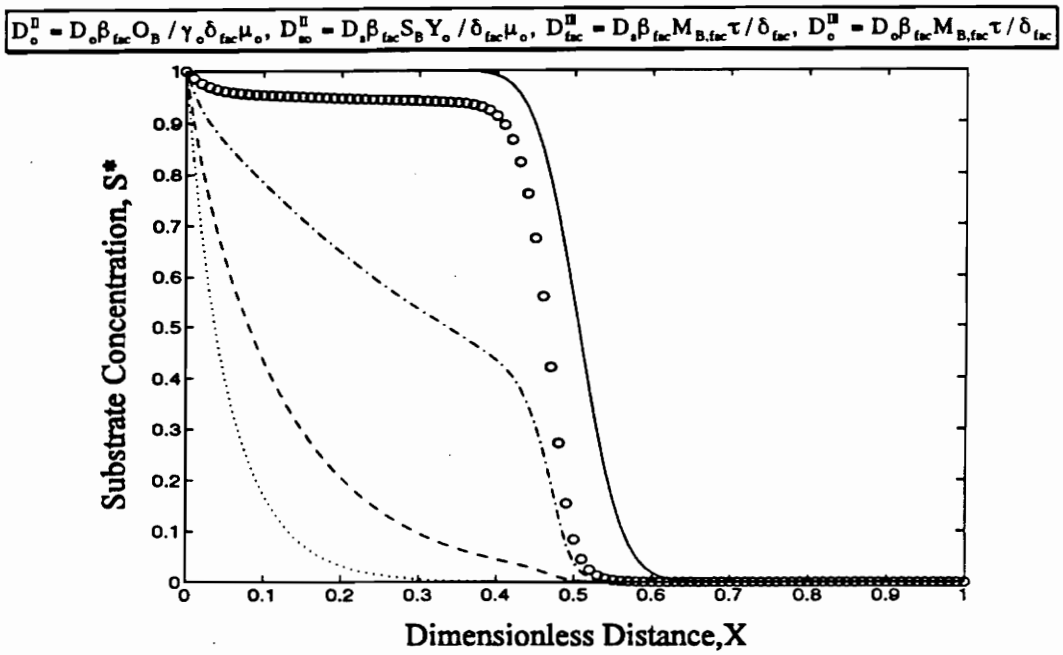

(a)

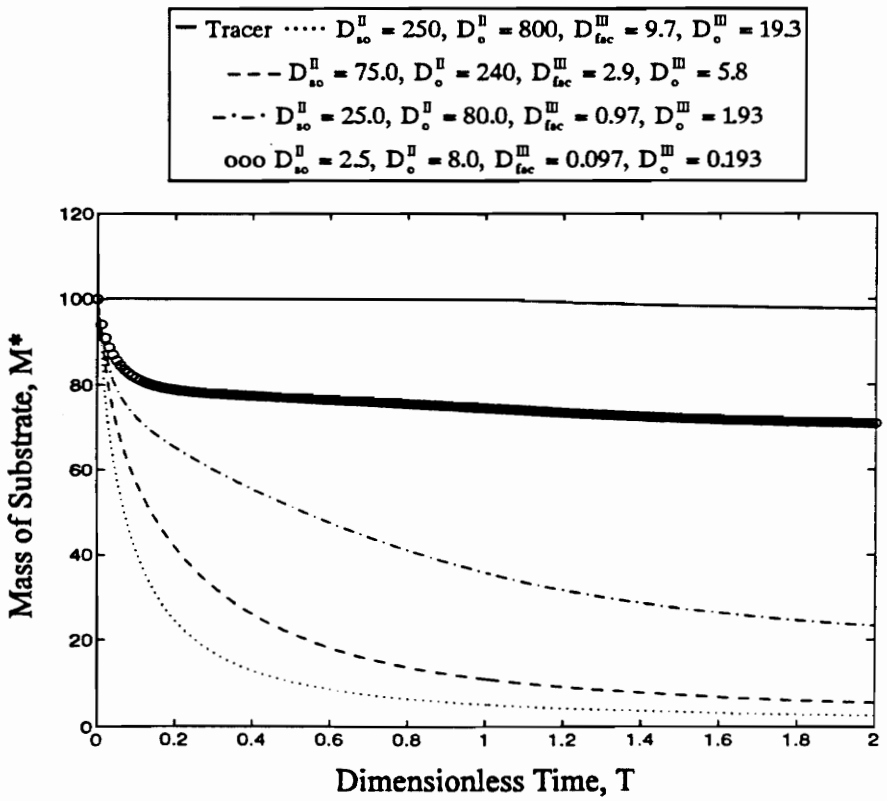

(b)

Figure 4.15. Substrate concentration profile and mass balance for varying β_{fac}/δ_{fac}.

examined independently, decreases in the yield coefficient, pertaining to less efficient substrate utilization, produced a decrease in D^{II}_{so} but an increase in biodegradation. For the β/δ analysis of D^{II}_{so}, however, the utilization rate is not varied, with increases in β/δ enhancing the condition for biodegradation, allowing increased biodegradation to occur when both D^{II} and D^{III} are increased.

4.2.9 The D^{I} Number and μ_o

For aqueous phase electron acceptors, the maximum specific growth rate affects the D^{I} number and the D^{II} numbers. The maximum specific growth rate varies directly with the D^{I} number and varies inversely with the D^{II} numbers. As seen for low K^{*} numbers and shown in Figures 4.16a and 4.16b, a large maximum specific growth rate produces rapid aqueous phase electron acceptor-based biodegradation for early time, depleting the available oxygen and creating electron acceptor limiting conditions. Figures 4.16a and 4.16b also demonstrate that moderate μ_o values degrade a larger mass of substrate for increasing time. Large μ_o values produce increases in both the microbial growth rate and utilization rate, supporting the witnessed trend of increased biodegradation for increasing μ_o, and shown in Figures 4.16a and 4.16b for early time (i.e. high growth conditions). These trends support the hypothesis that increased biodegradation occurs for an increase in D^{I} or a decrease in D^{II}_{so}, when D^{II}_{so} is decreased by an increase in a utilization rate parameter.

4.3 Results for Solid Phase Electron Acceptor Simulations

4.3.1 Graphical Representation

As with the solid phase electron acceptor simulations, a longitudinal profile of the substrate concentration at a dimensionless time (T) of 0.5 is provided for each dimensionless parameter. Changes in substrate mass with time are also plotted for each analysis. When necessary, plots of iron(III) consumption and iron(II) production are also

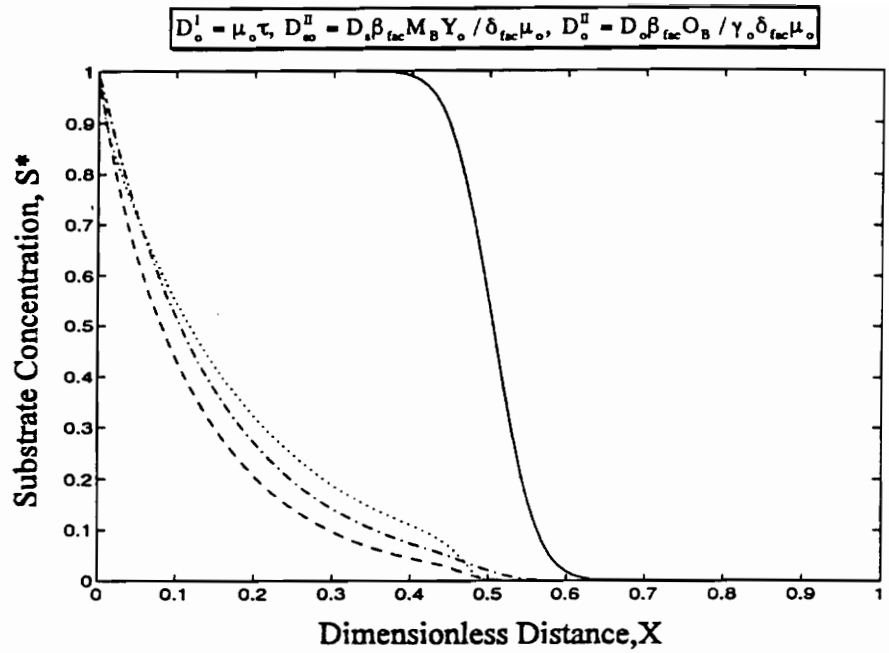

(a)

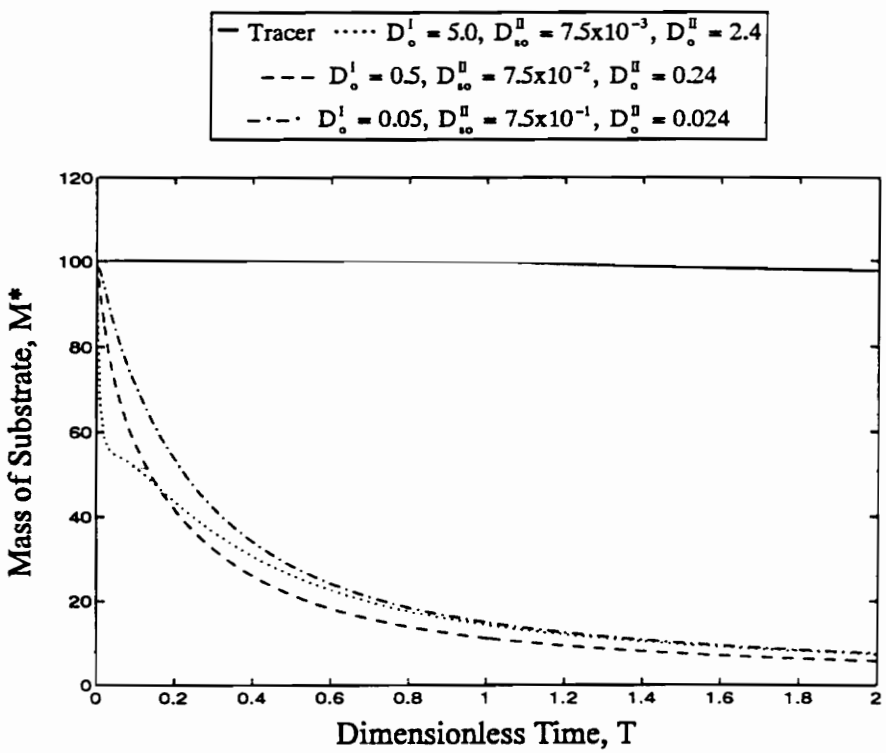

(b)

Figure 4.16. Substrate concentration profile and mass balance for varying μ_o and aqueous phase electron acceptor conditions.

provided at T = 0.5, with solid phase iron(III) plotted as a change in mass versus dimensionless distance and aqueous phase iron(II) plotted as concentration versus time.

4.3.2 Influent Concentrations

Changes in the influent substrate concentration affect both the D_{sf}^{II} and K_{sf}^{*} dimensionless groupings. The influent substrate concentration varies proportionally with D_{sf}^{II} and inversely with K_{sf}^{*}. As shown in Figures 4.17a and 4.17b, decreases in the influent substrate concentration produce increased biodegradation when evaluated on a dimensionless basis. Increases in the influent substrate concentration also result in increased iron(III) consumption and iron(II) production as shown in Figures 4.17c and 4.17d, respectively. Figure 4.17c also indicates that the solid phase electron acceptor does not limit biodegradation.

Considering a solid phase electron acceptor is immobile, the mass of available electron acceptor changes only during biodegradation or chemical reaction. Given that neither of these processes produces more of the electron acceptor and an adequate microbial population and substrate mass is available, a solid phase electron acceptor is expected to become limiting as the time for biodegradation increases. By decreasing the background concentration, the effects of solid phase electron acceptor limited conditions can be simulated and observed. Figures 4.18a and 4.18b depict the results of such a simulation and illustrate that substrate concentration and total mass will increase as the solid phase electron acceptor becomes limiting.

4.3.3 The Peclet Number

Increasing the Peclet number produces a sharper breakthrough curve for both the tracer and biodegrading simulations, as shown in Figure 4.19a. Figure 4.19b, however, indicates that variation of the Peclet number has little impact on the overall mass of degraded substrate.

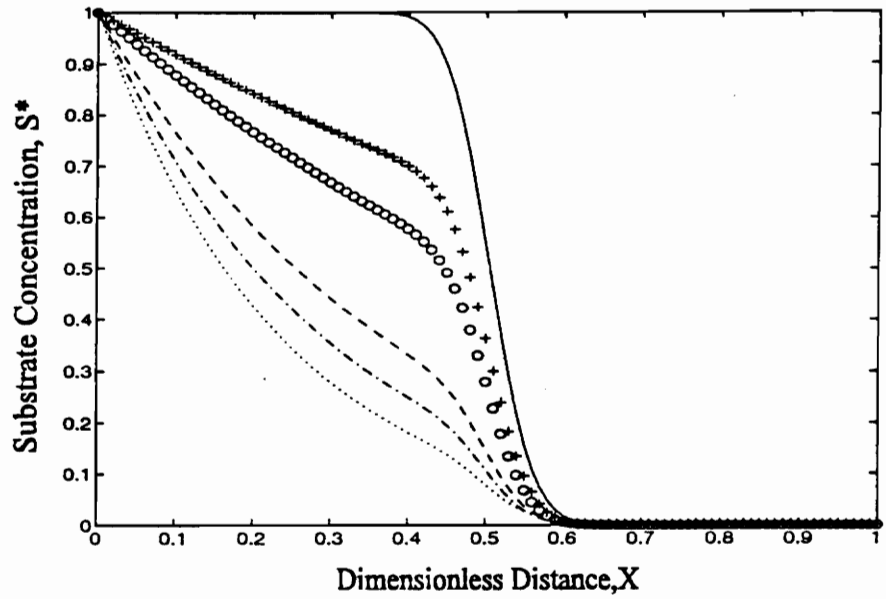

(a)

— Tracer +++ S_{in} = 1000 ooo S_{in} = 100
– – – S_{in} = 10.0 –·–· S_{in} = 1.0 ····· S_{in} = 0.1

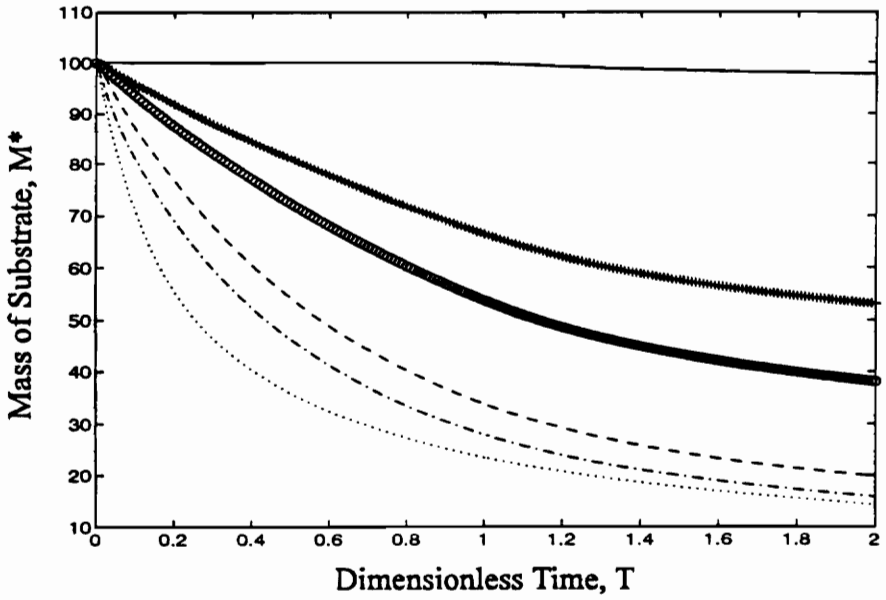

(b)

Figure 4.17. Substrate concentration profile and mass balance for varying influent substrate concentrations.

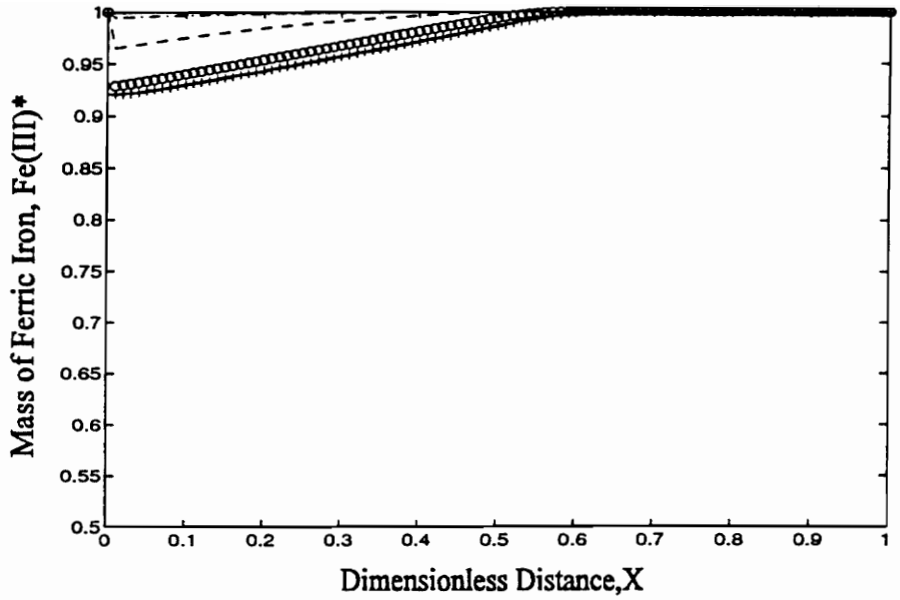

(c)

— Tracer +++ S_{in} = 1000 ooo S_{in} = 100
– – – S_{in} = 10.0 –·–· S_{in} = 1.0 ····· S_{in} = 0.1

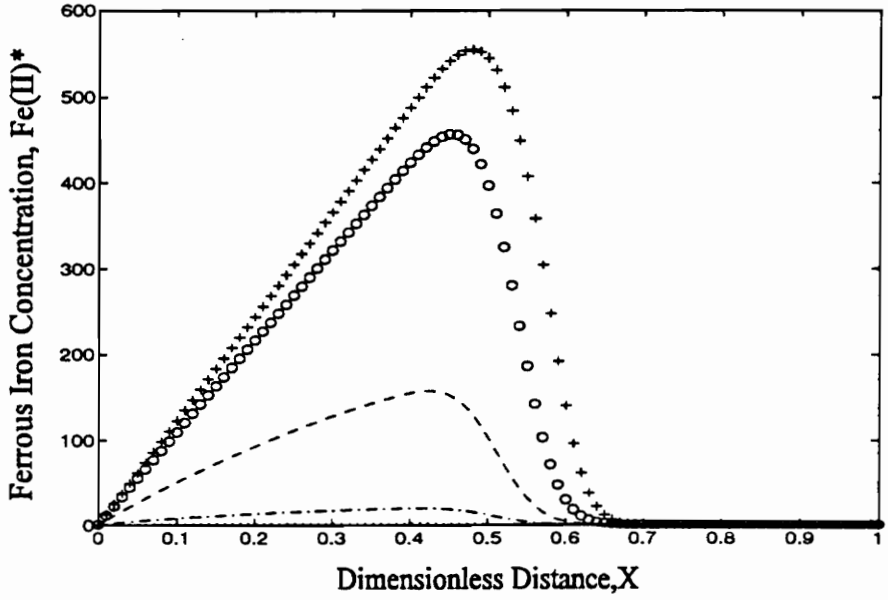

(d)

Figure 4.17. Iron(III) and Iron(II) concentration profiles for varying influent substrate concentrations.

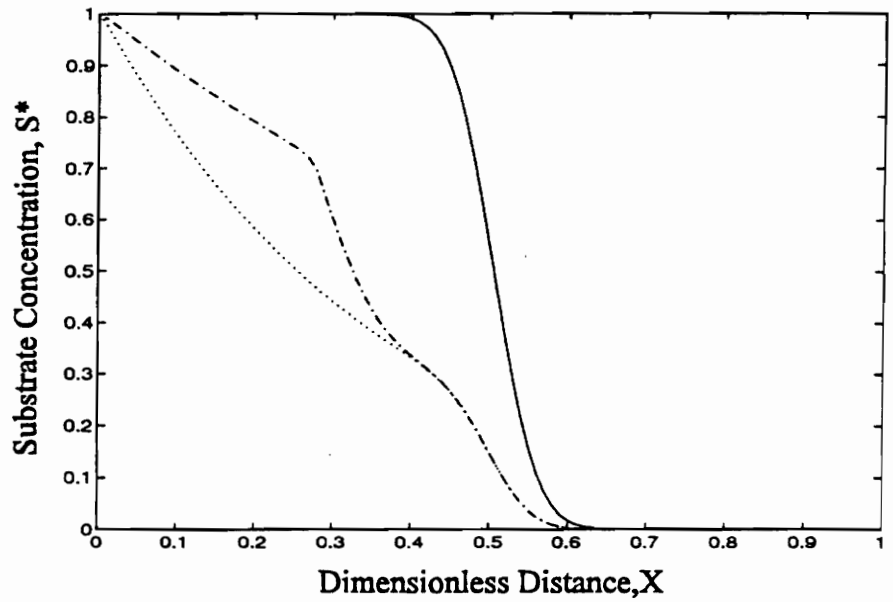

(a)

— Tracer ····· $Fe(III)_B = 100\mu g/g$ –·–· $Fe(III)_B = 15\mu g/g$

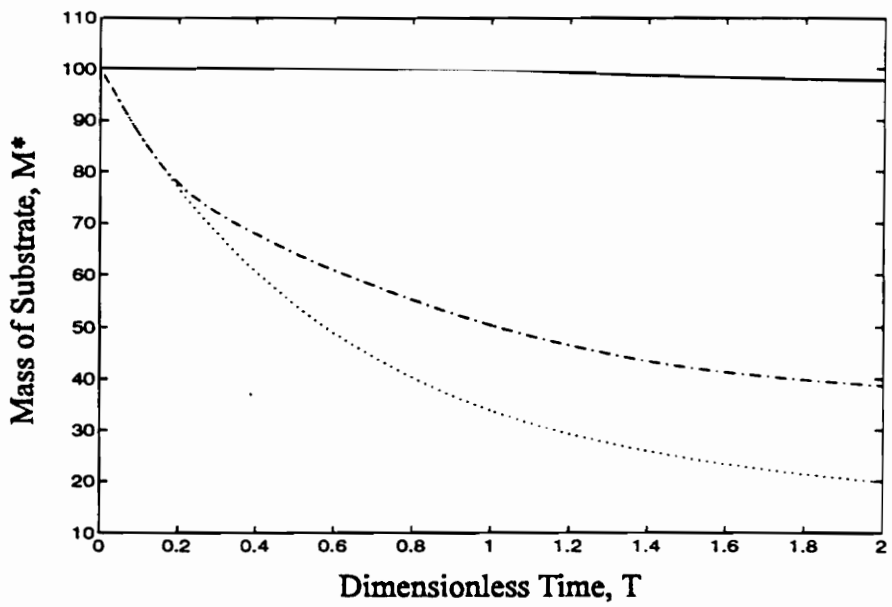

(b)

Figure 4.18. Substrate concentration profile and mass balance for varying Iron(III) initial conditions.

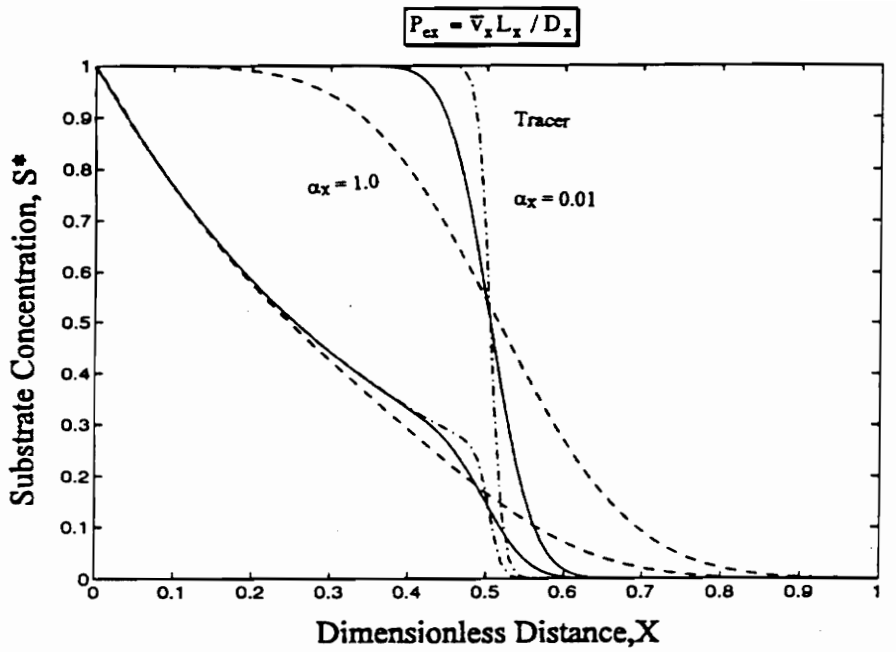

(a)

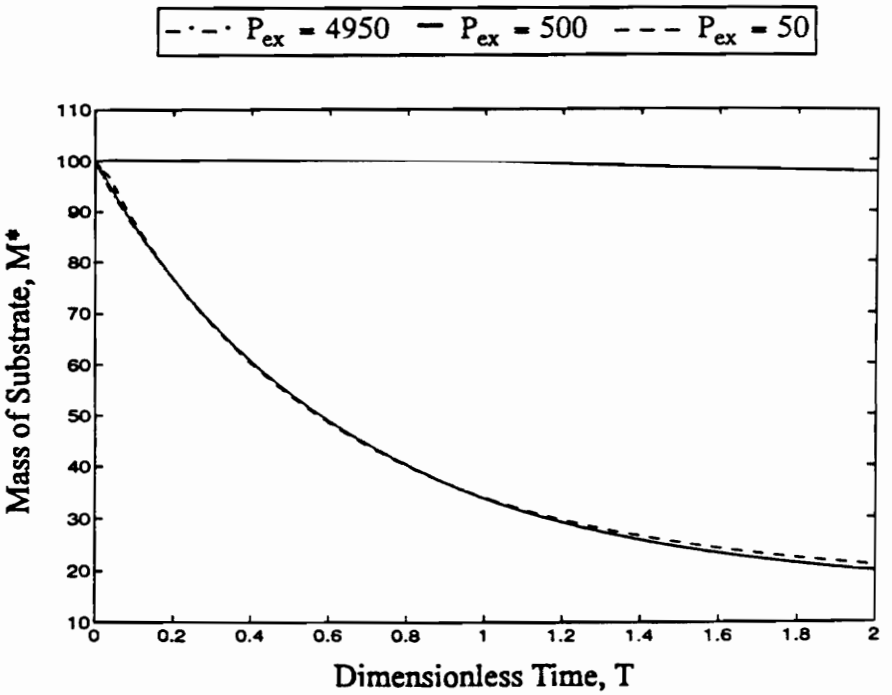

(b)

Figure 4.19. Substrate concentration profile and mass balance for varying Peclet number.

4.3.4 The D_k Number

As with the aqueous phase electron acceptor, Figures 4.20a and 4.20b indicate that changes in $D_{k,ana}$ have little impact on biodegradation, with increases in $D_{k,ana}$ producing a relatively small decrease in biodegradation.

4.3.5 The D^{II} Number

The D^{II}_{sf} dimensionless grouping can be individually varied by the yield coefficient, which varies directly with D^{II}_{sf}. As with the aqueous phase electron acceptors, increasing D^{II}_{sf} increases biodegradation by increasing substrate utilization efficiency. Figures 4.21a and 4.21b demonstrate that increases in D^{II}_{sf} produce increases in biodegradation under solid phase electron acceptor conditions.

4.3.6 The D^{IV} Number

The D^{IV}_{f} dimensionless grouping is unique to solid phase electron acceptors and may be individually varied by the use coefficient, γ, as shown schematically in Figure 4.4. Figures 4.22a and 4.22b indicate that changes in this dimensionless grouping have no effect on substrate biodegradation, unlike the corresponding aqueous phase electron acceptor simulations where decreases in the use coefficient (i.e. increases in D^{II}_{o}) produce increases in biodegradation. The difference between these results is explained by examining the utilization kinetics equations used for the various electron acceptors. As shown in Equation (3.3), the aqueous phase electron acceptor oxygen is modeled by modified Monod kinetics while the utilization kinetics for the solid phase electron acceptor, Iron(III) do not have the electron acceptor concentration term (see Equation 3.10). In the aqueous phase electron acceptor simulations presented earlier, oxygen is shown to be limiting, thus reducing the rate of substrate utilization, whereas iron(III) has no limiting effect on the reaction kinetics unless it is depleted beyond the accessible range (shown in Figure 4.22c). In either case, increases in the use coefficient indicate decreased

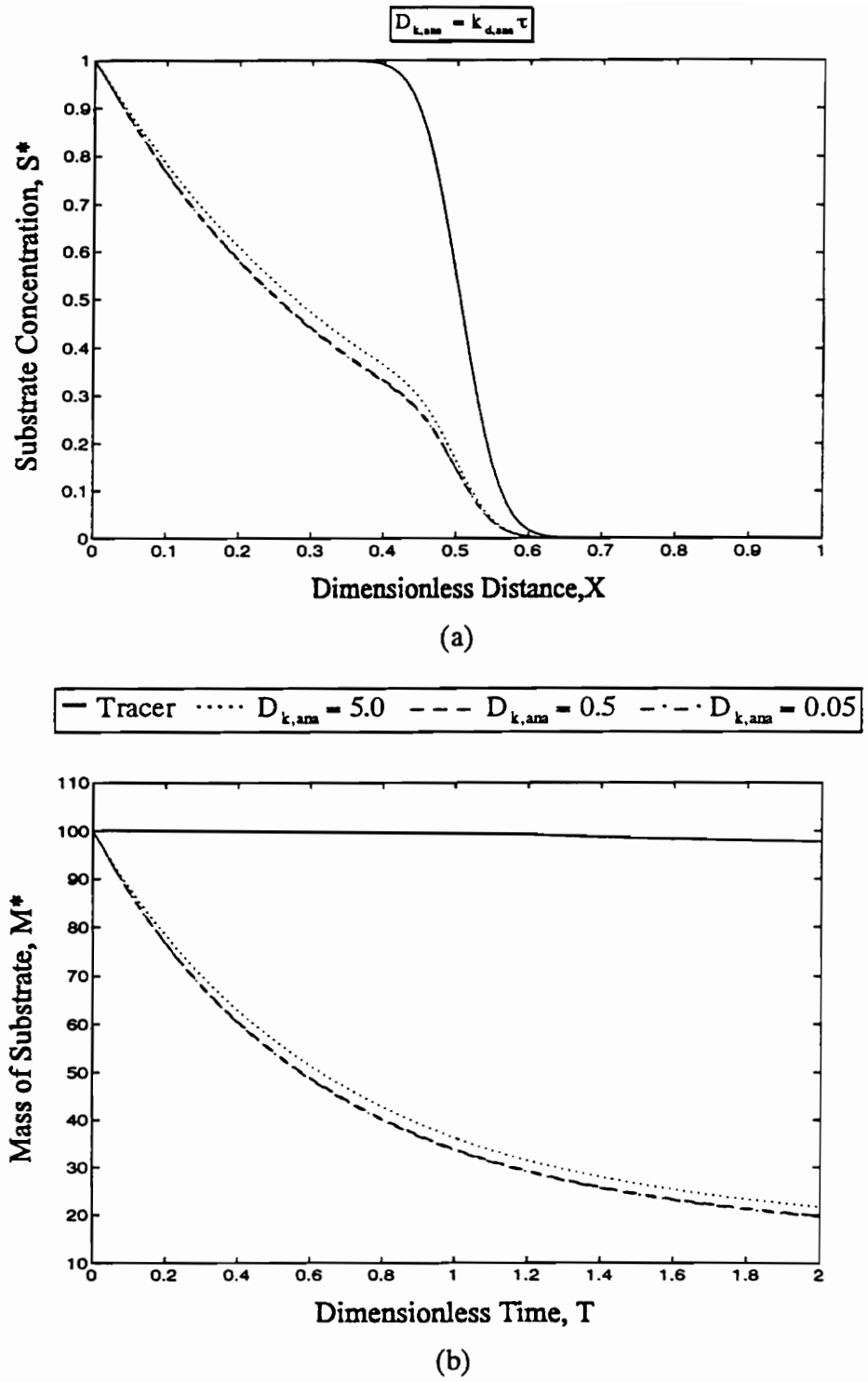

Figure 4.20. Substrate concentration profile and mass balance for varying $D_{k,ana}$.

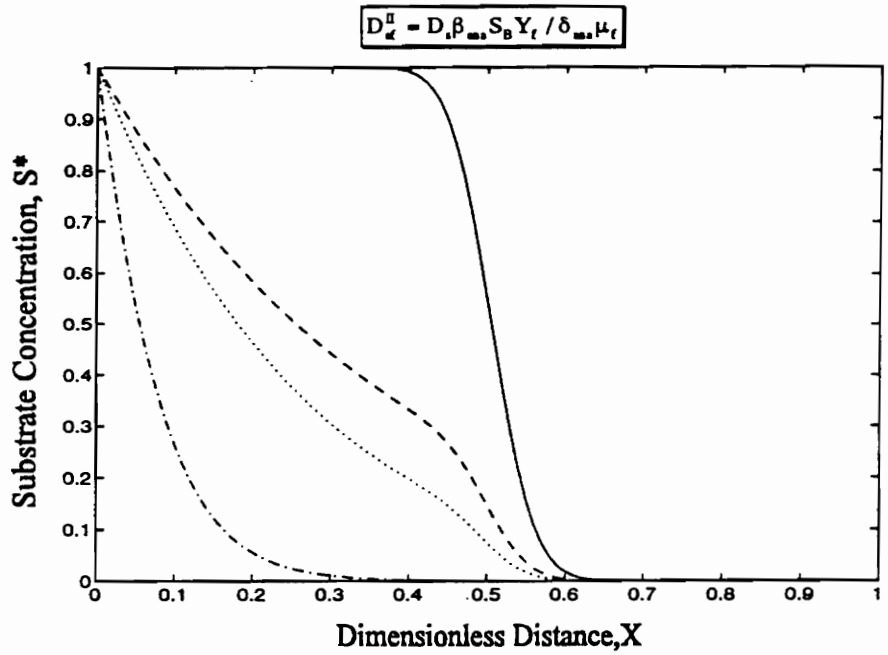

(a)

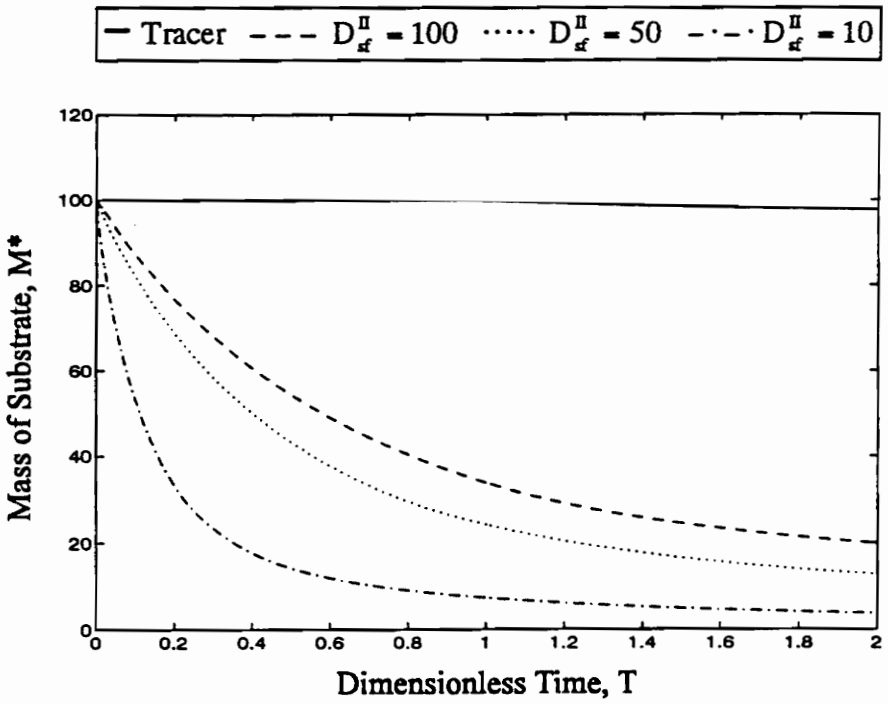

(b)

Figure 4.21. Substrate concentration profile and mass balance for varying D_{sf}^{II}.

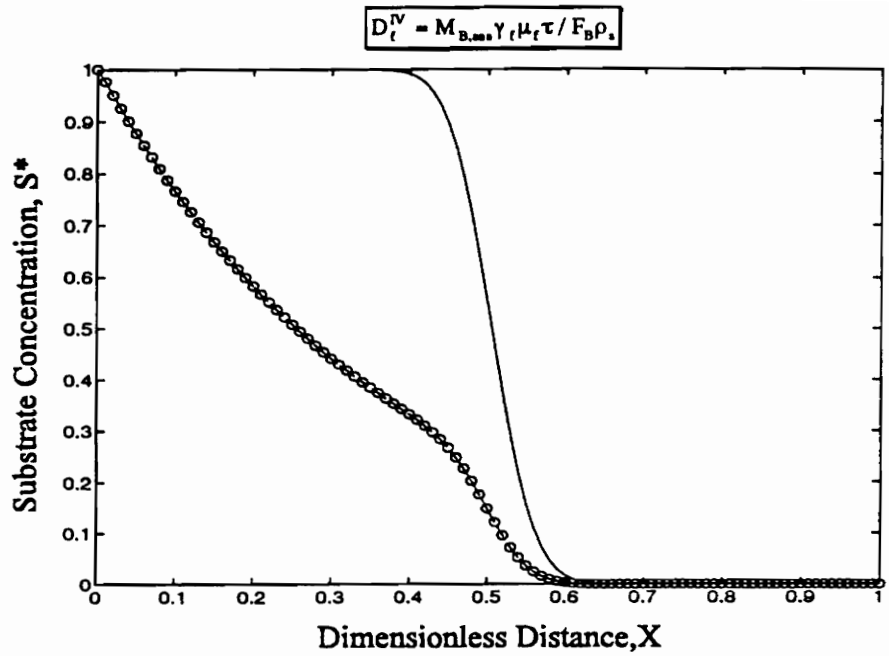

(a)

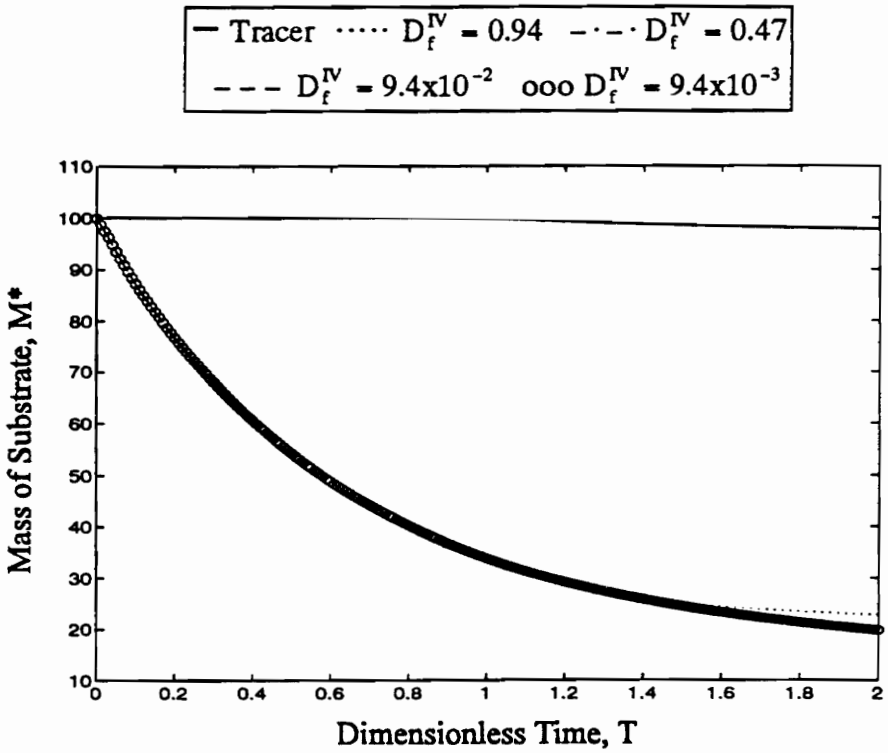

(b)

Figure 4.22. Substrate concentration profile and mass balance for varying D_f^{IV}.

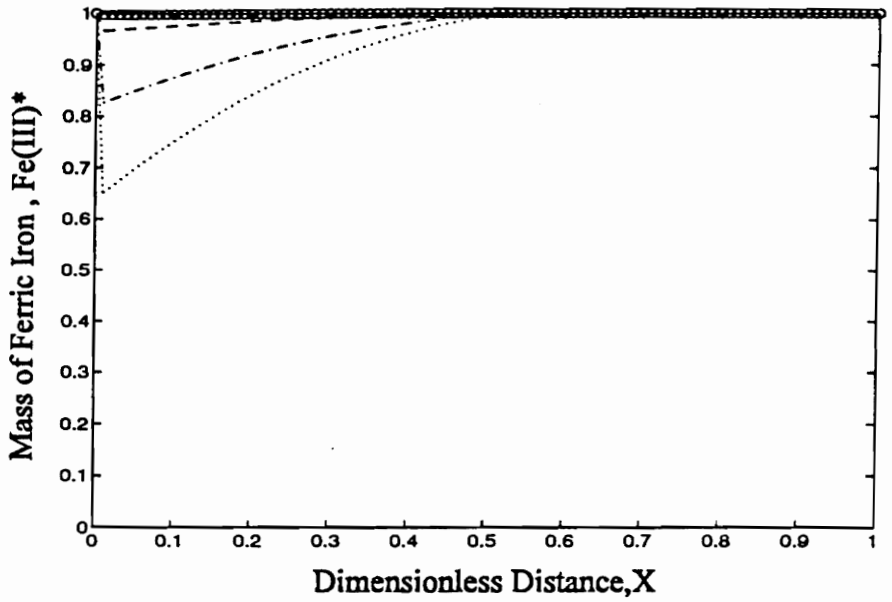

(c)

— Tracer ····· $D_f^{IV} = 0.94$ –·–· $D_f^{IV} = 0.47$
– – – $D_f^{IV} = 9.4x10^{-2}$ ooo $D_f^{IV} = 9.4x10^{-3}$

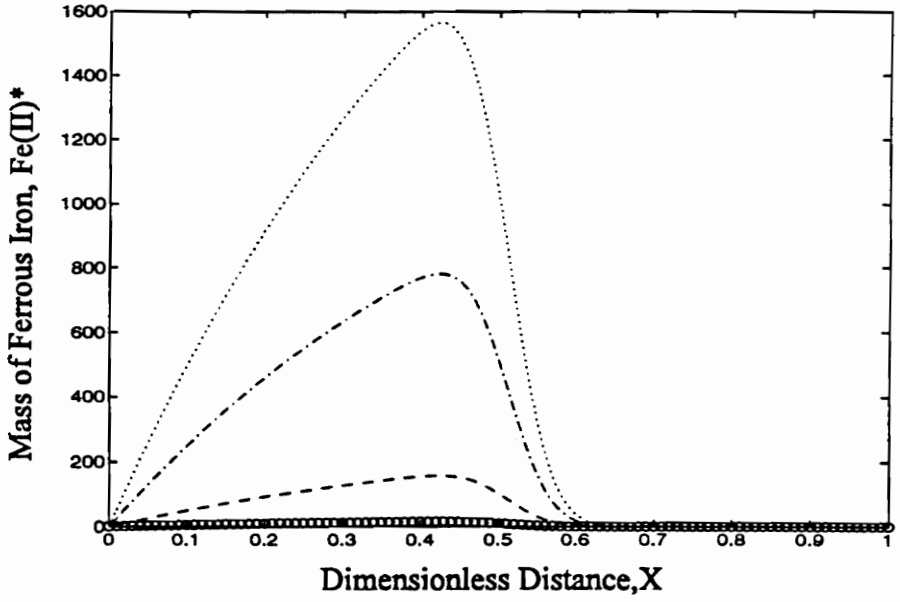

(d)

Figure 4.22. Iron(III) and Iron(II) profiles for varying D_f^{IV}.

electron acceptor utilization efficiency and are expected to produce increases in the amount of electron acceptor consumed. Figures 4.22c and 4.22d confirm this hypothesis for the solid phase electron acceptor and illustrate increased iron(III) consumption and iron(II) production with increases in D_f^{IV}.

4.3.7 The K^* Number

As indicated in the previous section on aqueous phase electron accepting conditions, increases in the K^* dimensionless parameters indicate that the biodegradation reaction kinetics are approaching first order (i.e. substrate or electron acceptor limited conditions) and are expected to reduce biodegradation. For an aqueous phase electron acceptor, biodegradation is shown to increase for decreasing K^* unless the available electron acceptor is consumed (see Figures 4.13b and 4.13e). Figures 4.23a and 4.23b indicate that, for the solid electron acceptor, iron(III), biodegradation decreases for increases in K_{sf}^*.

4.3.8 Biomass Population and the D^{III} and D^{IV} Numbers

Both the D_{ana}^{III} and the D_f^{IV} dimensionless groupings increase with increases in the initial biomass population. Increases in the biomass population are expected to produce increases in biodegradation, especially if the electron acceptor is non-limiting. Figures 4.24a and 4.24b show that increases in D_{ana}^{III} and D_f^{IV} produce increases in biodegradation. Figures 4.24c and 4.24d indicates that increases in D_{ana}^{III} and D_f^{IV} also produce increases in iron(III) consumption an iron(II) production. Figure 4.24c also indicates that the solid phase electron acceptor (iron(III)) is not limiting at T = 0.5, even for larger microbial populations (i.e. larger D_{ana}^{III} and D_f^{IV}).

4.3.9 Biofilm Parameters β and δ

The β/δ ratio used to describe the microbial populations ability to diffuse substrate

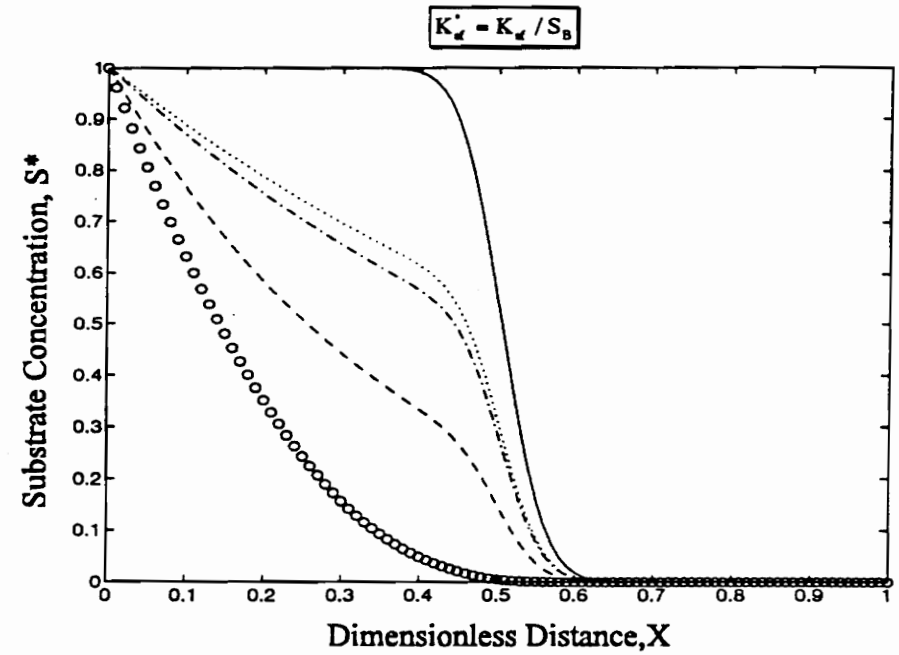

(a)

— Tracer ····· $K^*_{sf} = 100$ –·–· $K^*_{sf} = 10$ – – – $K^*_{sf} = 1.0$ ooo $K^*_{sf} = 0.1$

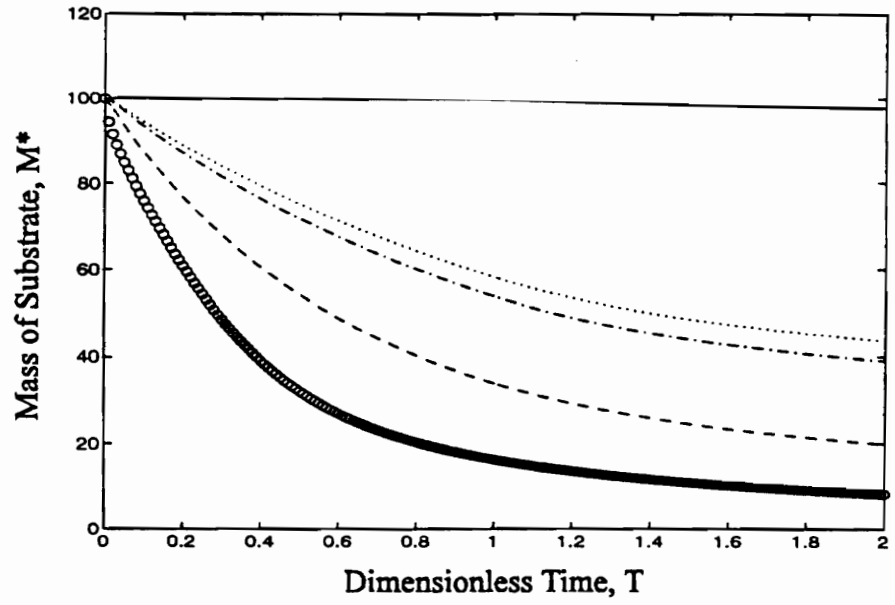

(b)

Figure 4.23. Substrate concentration profile and mass balance for varying K^*_{sf}.

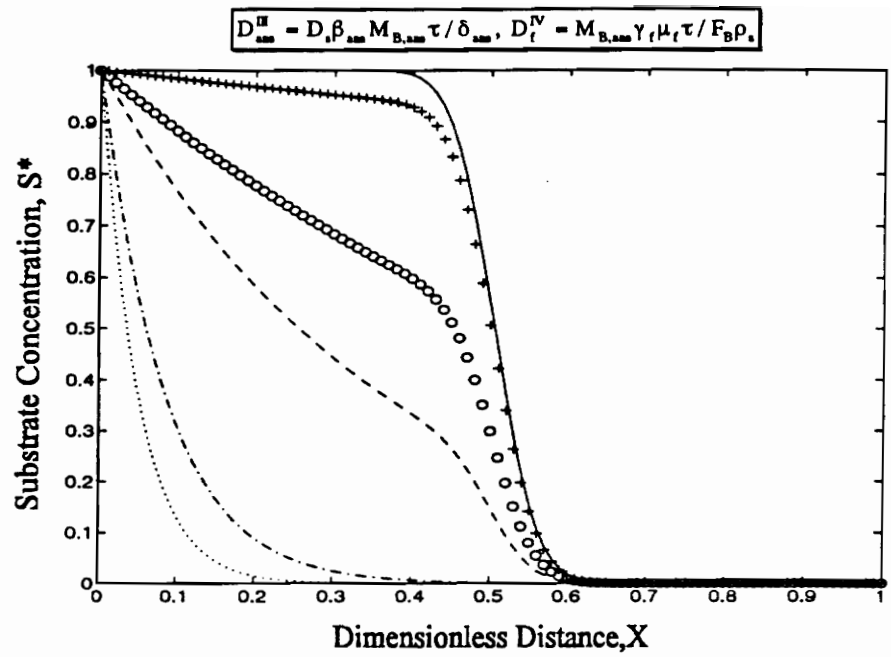

(a)

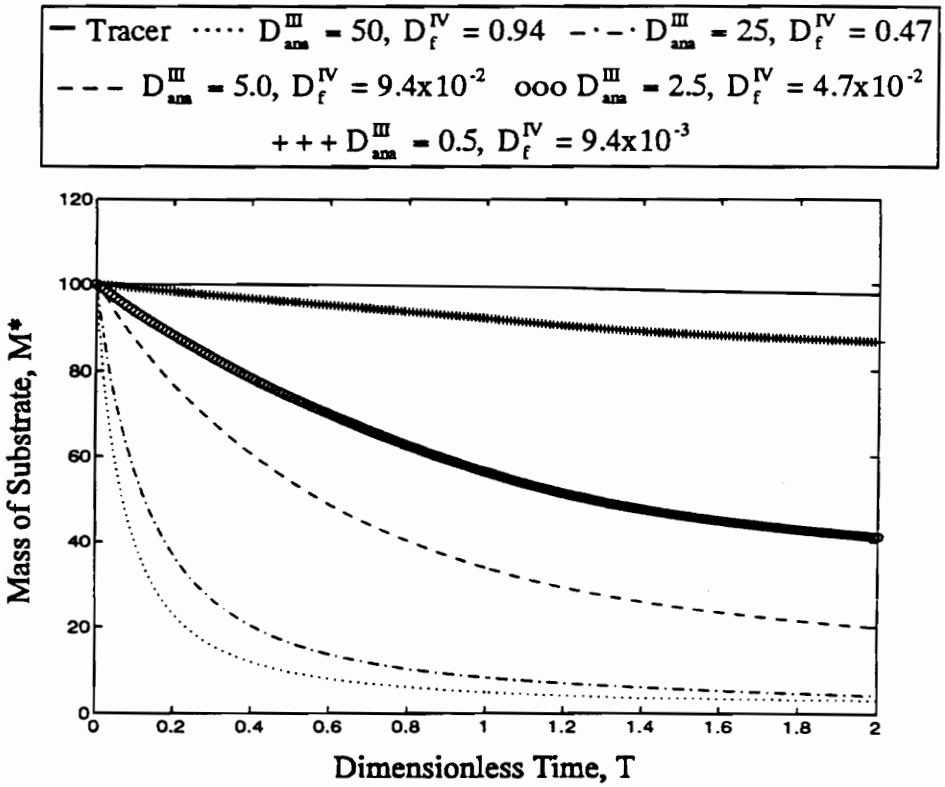

(b)

Figure 4.24. Substrate concentration profile and mass balance for varying $M_{B,ana}$.

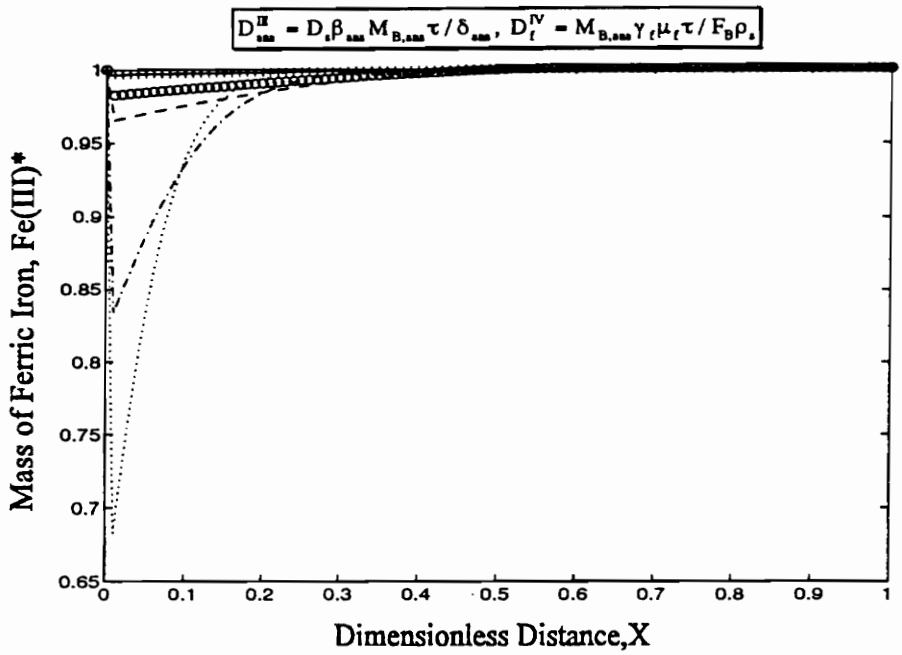

(c)

— Tracer ····· $D^{III}_{ana} = 50$, $D^{IV}_f = 0.94$ –·–· $D^{III}_{ana} = 25$, $D^{IV}_f = 0.47$
– – – $D^{III}_{ana} = 5.0$, $D^{IV}_f = 9.4\text{x}10^{-2}$ ooo $D^{III}_{ana} = 2.5$, $D^{IV}_f = 4.7\text{x}10^{-2}$
+ + + $D^{III}_{ana} = 0.5$, $D^{IV}_f = 9.4\text{x}10^{-3}$

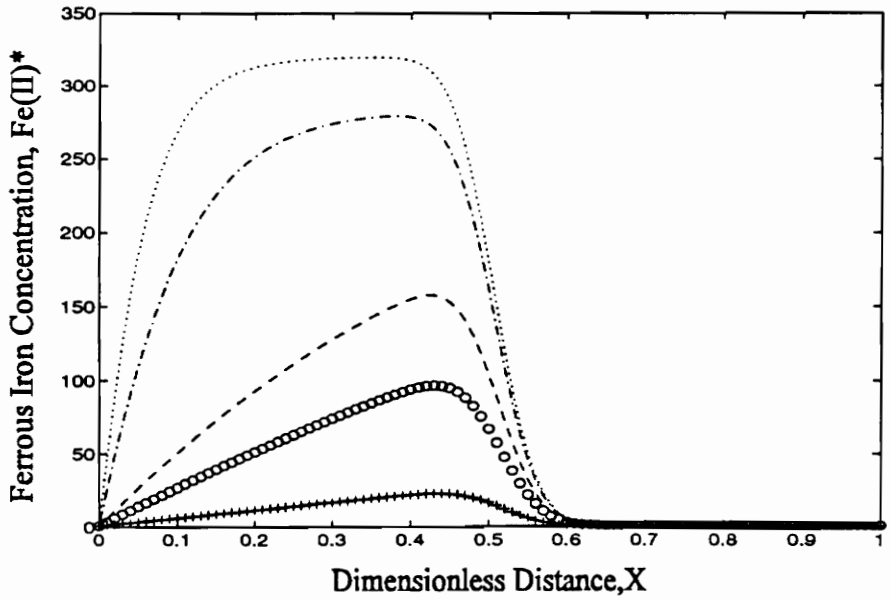

(d)

Figure 4.24. Iron(III) and Iron(II) concentration profiles for varying $M_{B,ana}$.

into the microbial phase varies directly with both D_{sf}^{II} and D_{ana}^{III}. Increases in this ratio imply that more area is available for diffusion or a that the diffusion layer is thinner, either of which result in increased interphase transport. As indicated in Figures 4.25a and 4.25b, increases in D_{sf}^{II} and D_{ana}^{III} produce increases in biodegradation.

4.3.10 The D^{I} Number and μ_f

For solid phase electron acceptors, the maximum specific growth rate, μ_f, varies directly with the D_f^{I} and D_f^{IV} dimensionless groupings, while varying inversely with the D_{sf}^{II} dimensionless number for substrate. Figures 4.26a and 4.26b indicate that an increase in μ_f produces an increase in substrate biodegradation.

4.4 Results for Sequential Electron Acceptor Simulations

4.4.1 Effects of Sequential Electron Acceptors

Figures 4.27a and 4.27b show that sequential electron acceptor conditions can significantly increase biodegradation when compared to single electron acceptor conditions. The parameters listed in Table 4.3 cause the aqueous phase electron acceptor to be utilized more rapidly than the solid phase electron acceptor, producing the rapid substrate mass reduction shown at early time in Figure 4.27b. Once the majority of the aqueous phase electron acceptor has been consumed, biodegradation slows, allowing solid phase electron acceptor based biodegradation to first approach and eventually surpass the total mass of biodegraded substrate when compared to the aqueous phase electron acceptor simulations. Figures 4.27a and 4.27b also indicate that the sequential electron acceptor conditions of a primary aqueous phase electron acceptor and a terminal solid phase electron acceptor produce nearly double the biodegradation as either of the electron acceptors being consumed individually.

4.4.2 The K_c^* Number

The K_c^* dimensionless grouping relates terminal electron acceptor inhibition by the

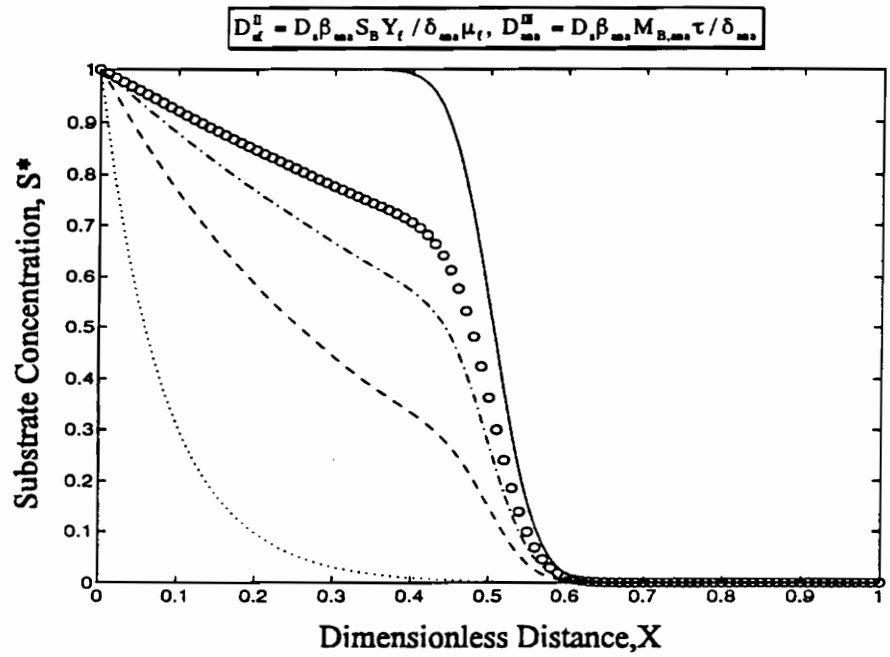

(a)

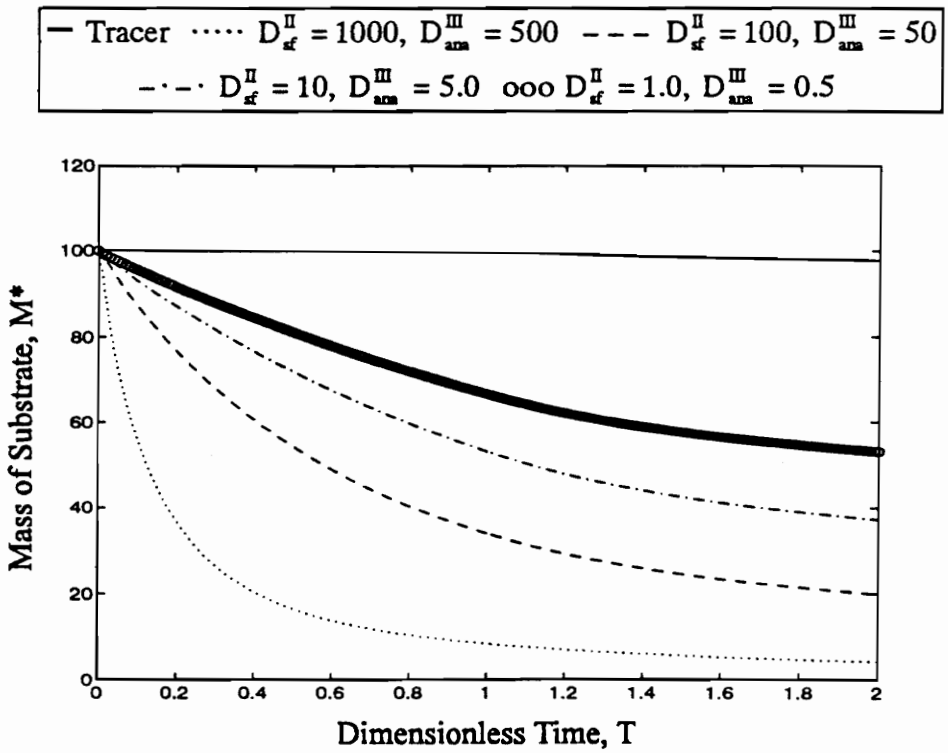

(b)

Figure 4.25. Substrate concentration profile and mass balance for varying β_{ana}/δ_{ana}.

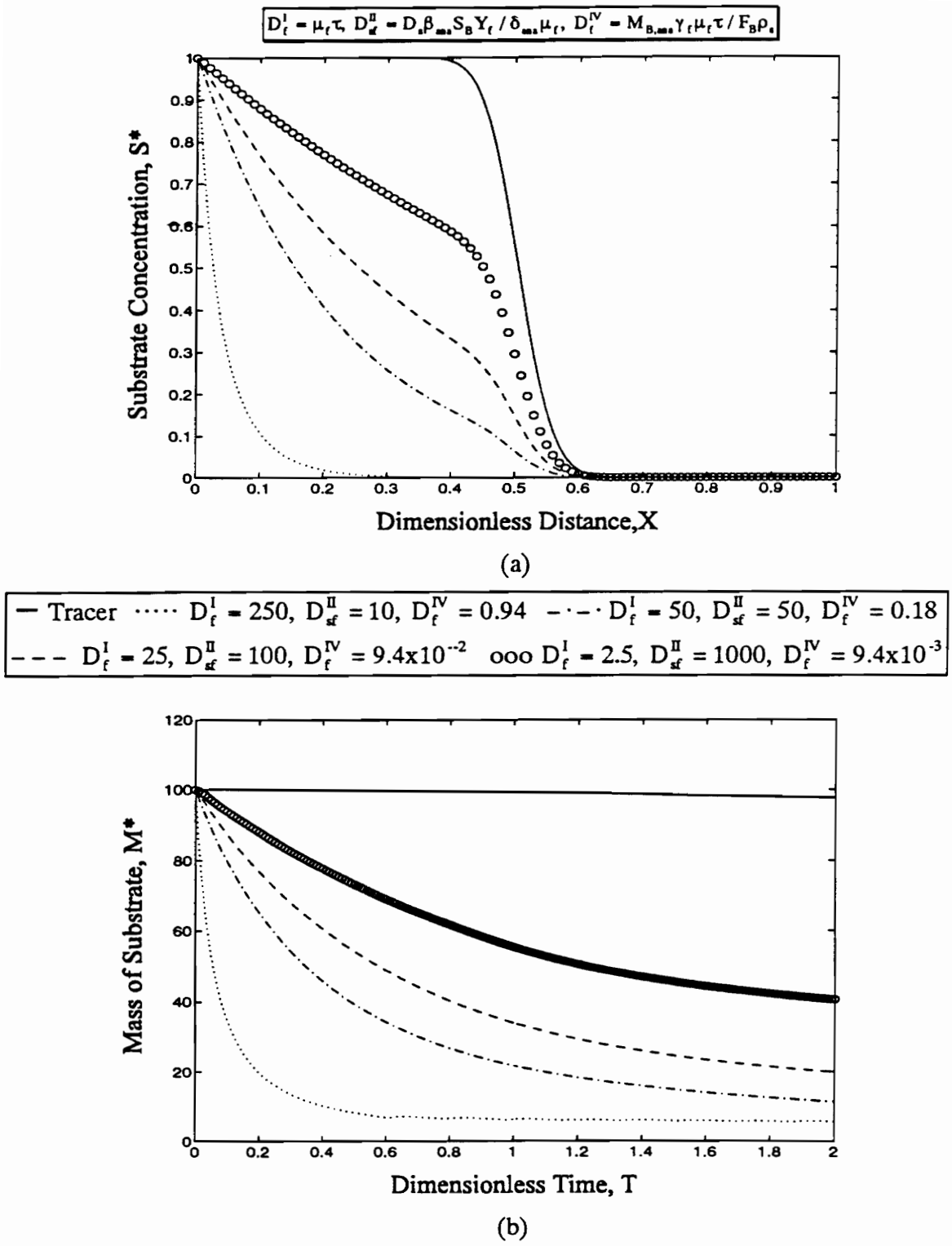

Figure 4.26. Substrate concentration profile and mass balance for varying μ_f.

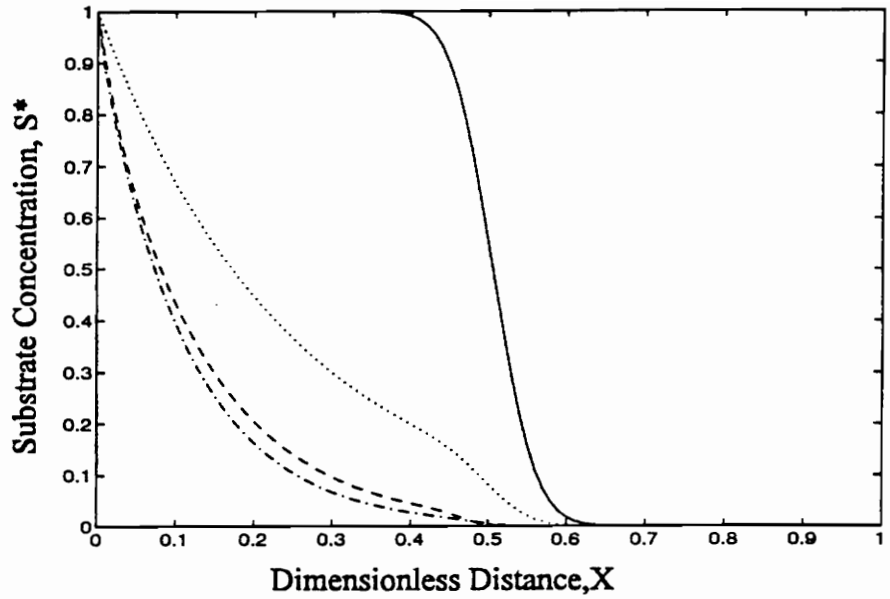

(a)

— Tracer - - - O_2 only ····· Iron(III) only -·-· O_2 and Iron(III)

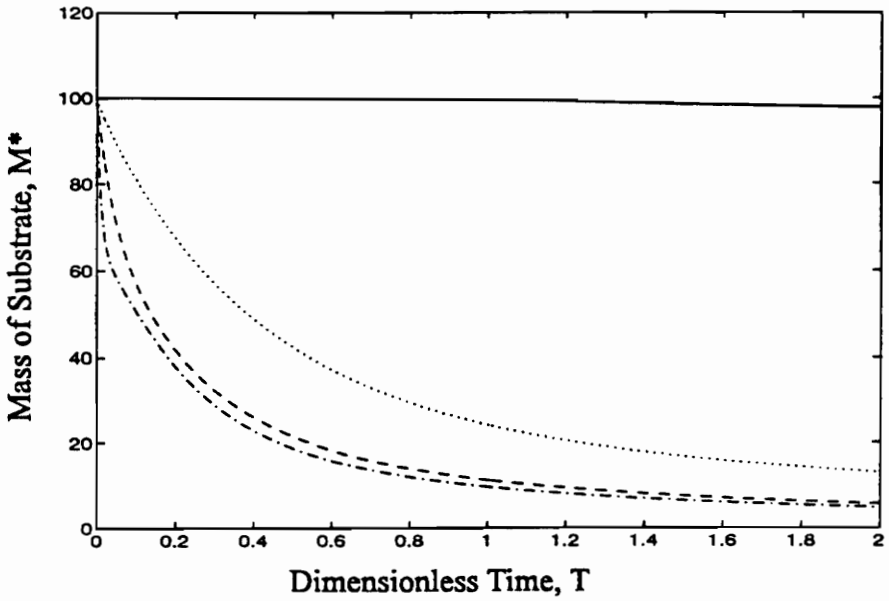

(b)

Figure 4.27. Substrate concentration profile and mass balance for varying electron acceptor conditions.

presence of a primary electron acceptor to the initial concentration of the primary electron acceptor, with increases in this dimensionless grouping implying that less inhibition is occurring. For the parameters indicated in Table 4.3, changes in K_c^* do not produce significant change in biodegradation, as shown in Figures 4.28a and 4.28b. Figures 4.28d and 4.28e do indicate that variation of this dimensionless grouping has a more significant impact on terminal electron acceptor consumption, with increases in K_c^* producing increases in terminal electron acceptor (i.e. iron(III)) consumption and end product (i.e. iron(II)) production. Further investigation of inhibition effects is accomplished by varying the influent boundary concentrations of substrate and/or the aqueous phase electron acceptor. Results of these simulations indicate that changes in K_c^* do not affect substrate biodegradation but do have an impact on the electron acceptor concentrations similar to the effects noted above.

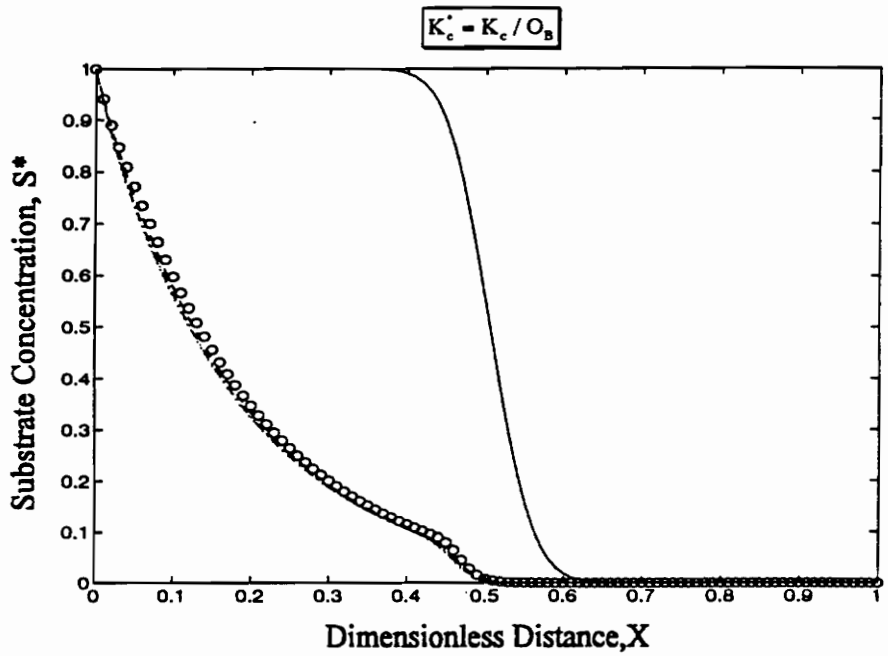

(a)

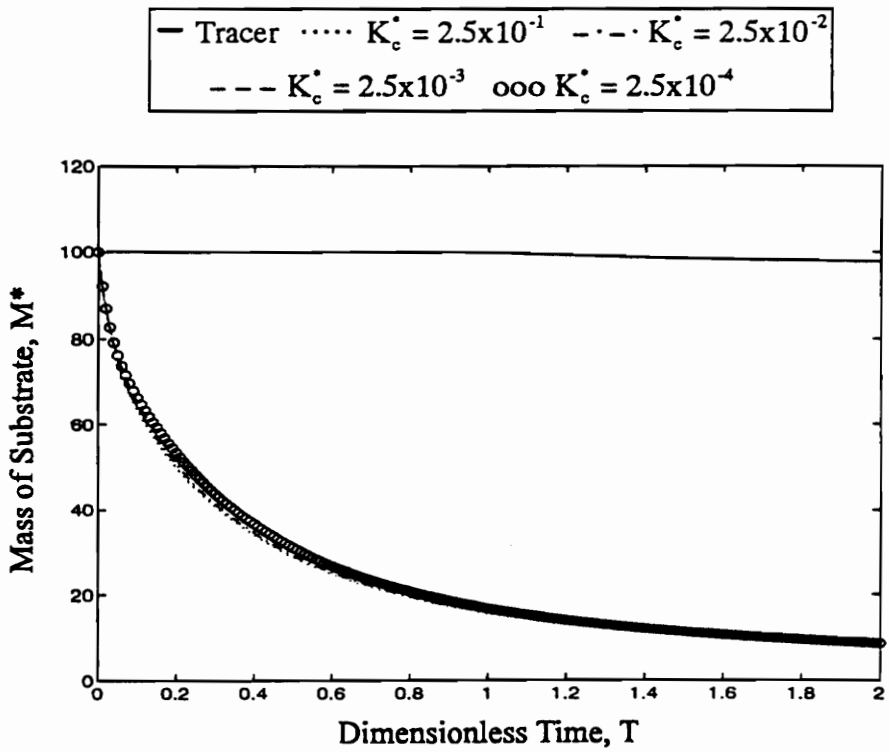

(b)

Figure 4.28. Substrate concentration profile and mass balance for varying K_c^*.

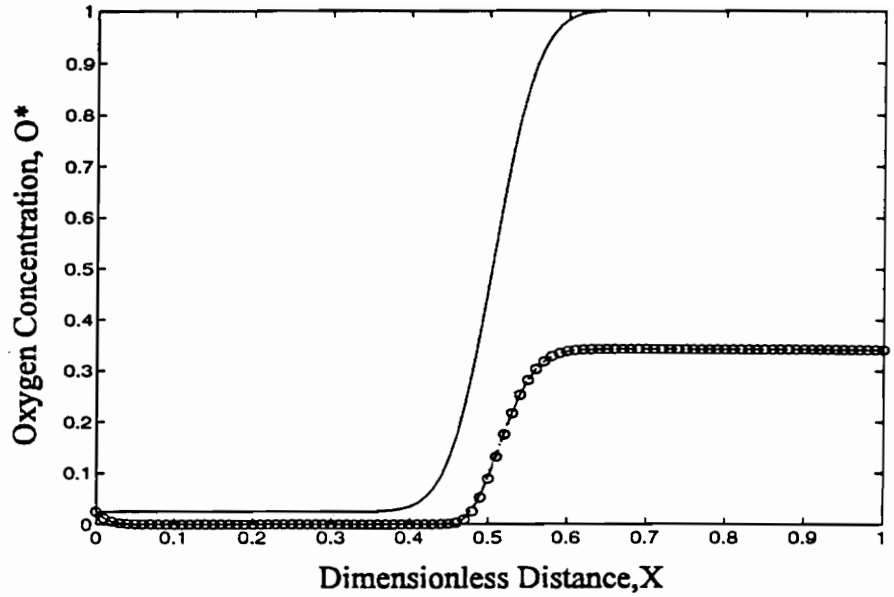

(c)

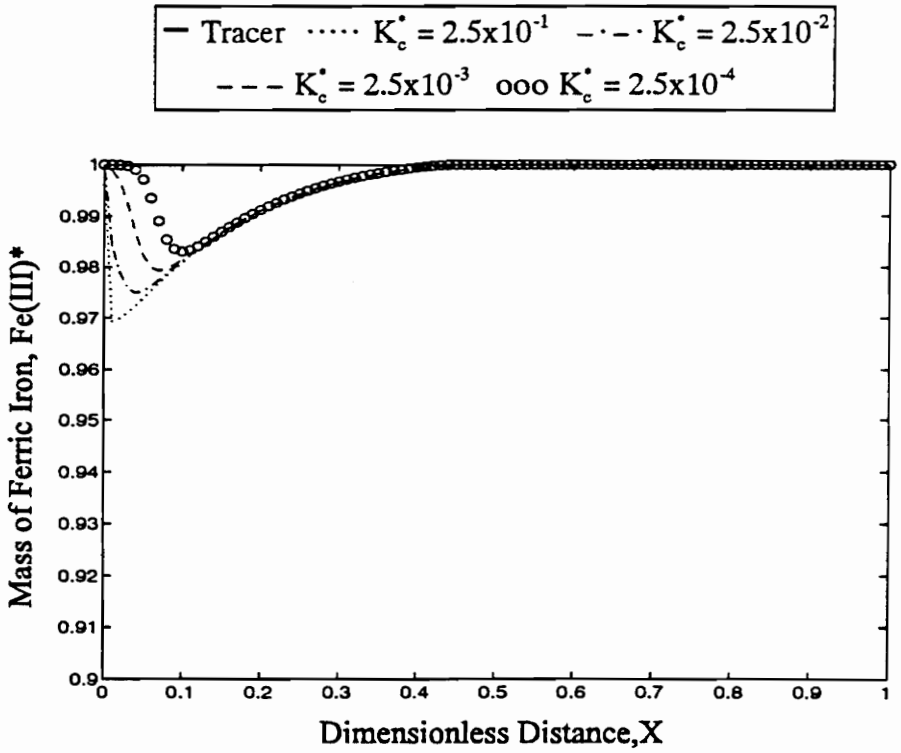

(d)

Figure 4.28. Oxygen concentration and Iron(III) profile for varying K_c^*.

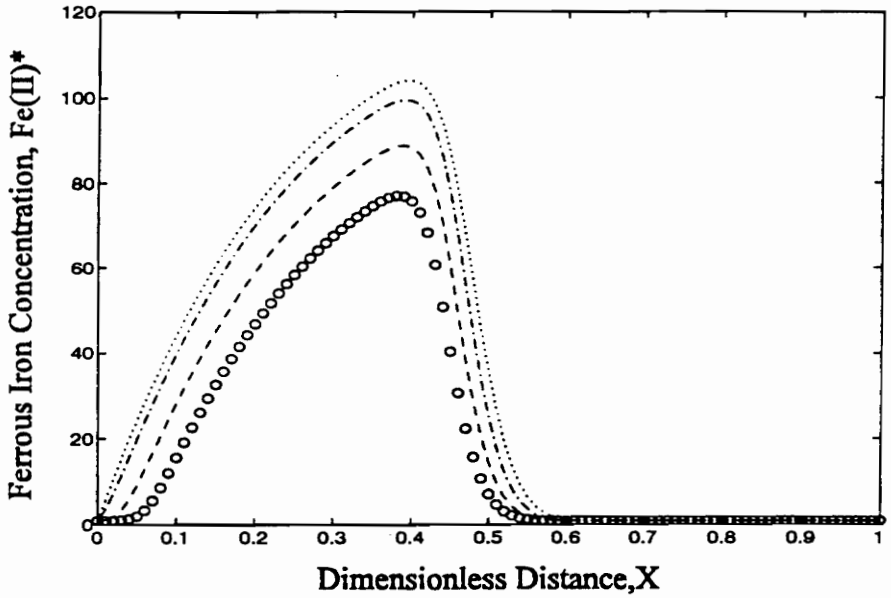

(e)

— Tracer ····· $K_c^* = 2.5x10^{-1}$ –·–· $K_c^* = 2.5x10^{-2}$
– – – $K_c^* = 2.5x10^{-3}$ ooo $K_c^* = 2.5x10^{-4}$

Figure 4.28. Iron(II) concentration profile for varying K_c^*.

CHAPTER 5. Site Application of the SEAM2D Model

5.1 Introduction

To further illustrate the capabilities of the SEAM2D model, a site application is provided, simulating the transport and biodegradation of the aromatic hydrocarbon, toluene. Model results are presented as a combination of one-dimensional concentration profiles and two-dimensional contour maps. The goal of these simulations is to first replicate trends observed for a limited data set collected for a contaminant plume undergoing sequential oxygen-iron(III) based biodegradation and then simulate future plume migration under natural conditions. The fate and transport of toluene is modeled specifically, as this compound has been shown to degrade under both aerobic (Raymond et al., 1976) and iron(III) based (Lovely and Lonergan, 1990) conditions. The model's basic input parameters are determined by direct field measurements, when available, or literature values, adjusted to produce the trends observed in the existing data set. The SEAM2D model is then used to predict future trends of plume migration under both sequential and oxygen only electron acceptor conditions.

5.2 Site Application

5.2.1 Laurel Bay Exchange, SC

The model simulations presented here are based on conditions observed at a USGS study site at the Marine Corps Air Station located at Laurel Bay Exchange, Beaufort, South Carolina (see location map, Figure 5.1). The initial site investigation indicated that the contaminant plume consists of multiple contaminants inlcuding the BTEX compounds and the gasoline additive, MTBE, and is located in an unconfined, coastal aquifer composed mostly of fine sand (ABB Environmental Services, Inc. 1993). The contaminant leak is believed to have begun in September 1991 and to have continued up until source removal via tank excavation in early 1994 (Landmeyer et al, 1994). Monitoring wells were installed to determine the extent of the contaminant plume and

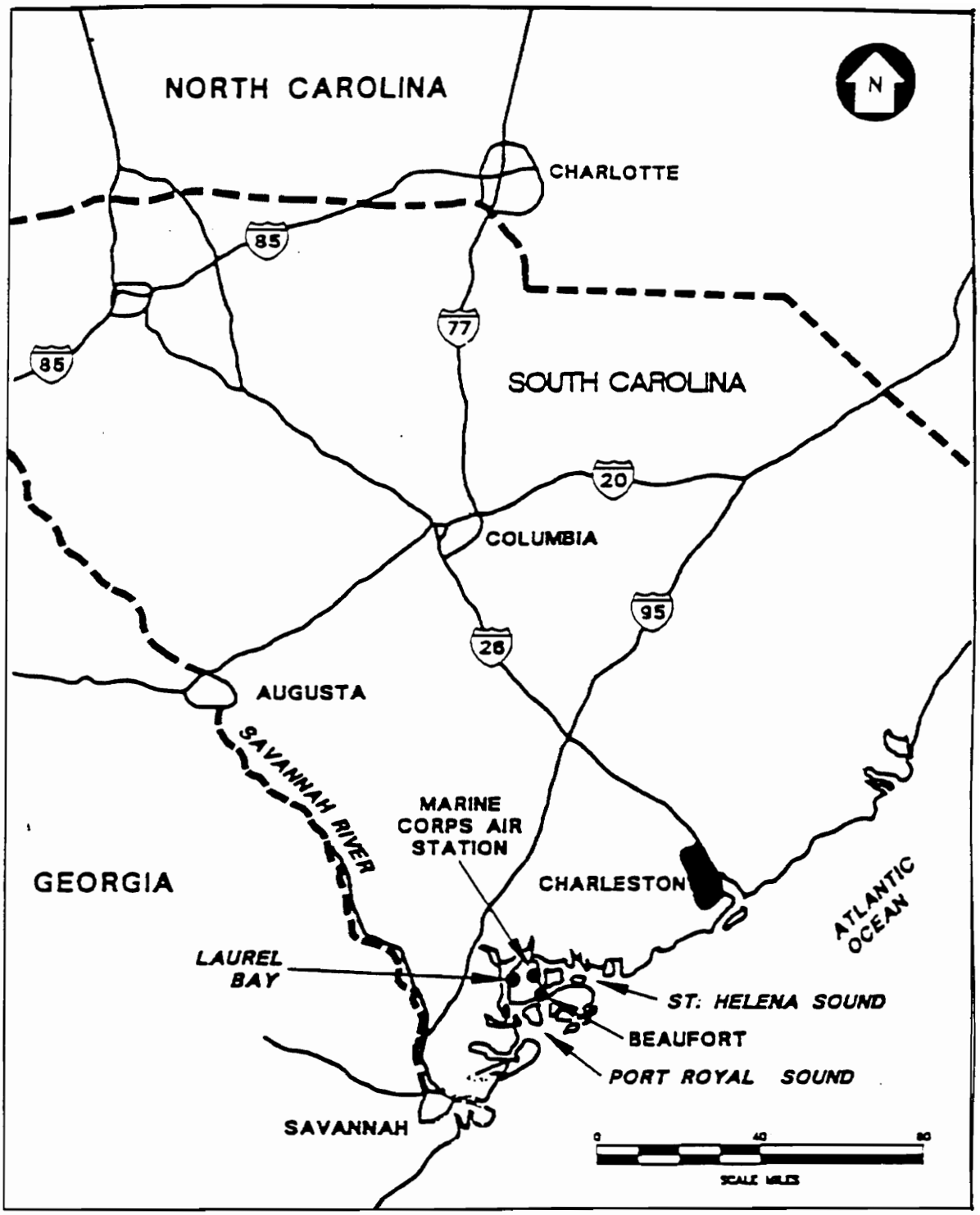

Figure 5.1. Laurel Bay Exchange site location map. (from ABB Environmental Services, Inc., 1993)

show that, as of March 1994, the toluene plume has migrated with groundwater transport, and that the plume has extended approximately 85 meters in the longitudinal direction and 37.5 meters in the transverse direction. Figure 5.2 displays the monitoring well locations and toluene plume delineation for concentration levels of 20 mg/liter and 0.1 mg/liter, while Table 5.1 lists the concentrations of various groundwater constituents for the monitoring wells.

Both aerobic and anaerobic biodegradation conditions are believed to exist at the Laurel Bay site (Landmeyer et al., 1994). Table 5.1 indicates that monitoring wells located outside of the contaminant plume exhibit a background dissolved oxygen (DO) concentration of approximately 5 mg/liter. Aerobic biodegradation is demonstrated by the depletion of DO at wells where BTEX contaminants are present. Existence of iron(III)-based anaerobic biodegradation is supported by the presence of ferrous iron (Fe(II)), an end product of iron(III) based oxidation of toluene (for stoichiometric reaction, see Table 2.3). Oxygen based inhibition of iron(III) biodegradation is demonstrated by the trend shown in Figure 5.3, where iron(II) production is noted only when DO is severely or completely depleted. This field data supports the hypothesis that iron(III) reduction occurs predominately in groundwater in a highly reduced condition.

5.2.2 Model Grid and Orientation

Size and orientation of the SEAM2D grid is selected by considering both the direction and magnitude of groundwater flow. Field measurements indicate that the average groundwater velocity is between 18.2 and 21.2 meters/year and flowing nearly due south as indicated in Figure 5.4. Figure 5.4 also displays field data indicating that groundwater flow is nearly uni-directional near and down-gradient of the source area. By orienting the SEAM2D grid along the direction of flow with the line-boundary source centered in the grid, the contaminant plume can then be modeled as two symmetrical halves, with the centerline of the plume corresponding to a hydraulic no-flow boundary (streamline). Considering the ambient groundwater velocity, a ten year tracer simulation

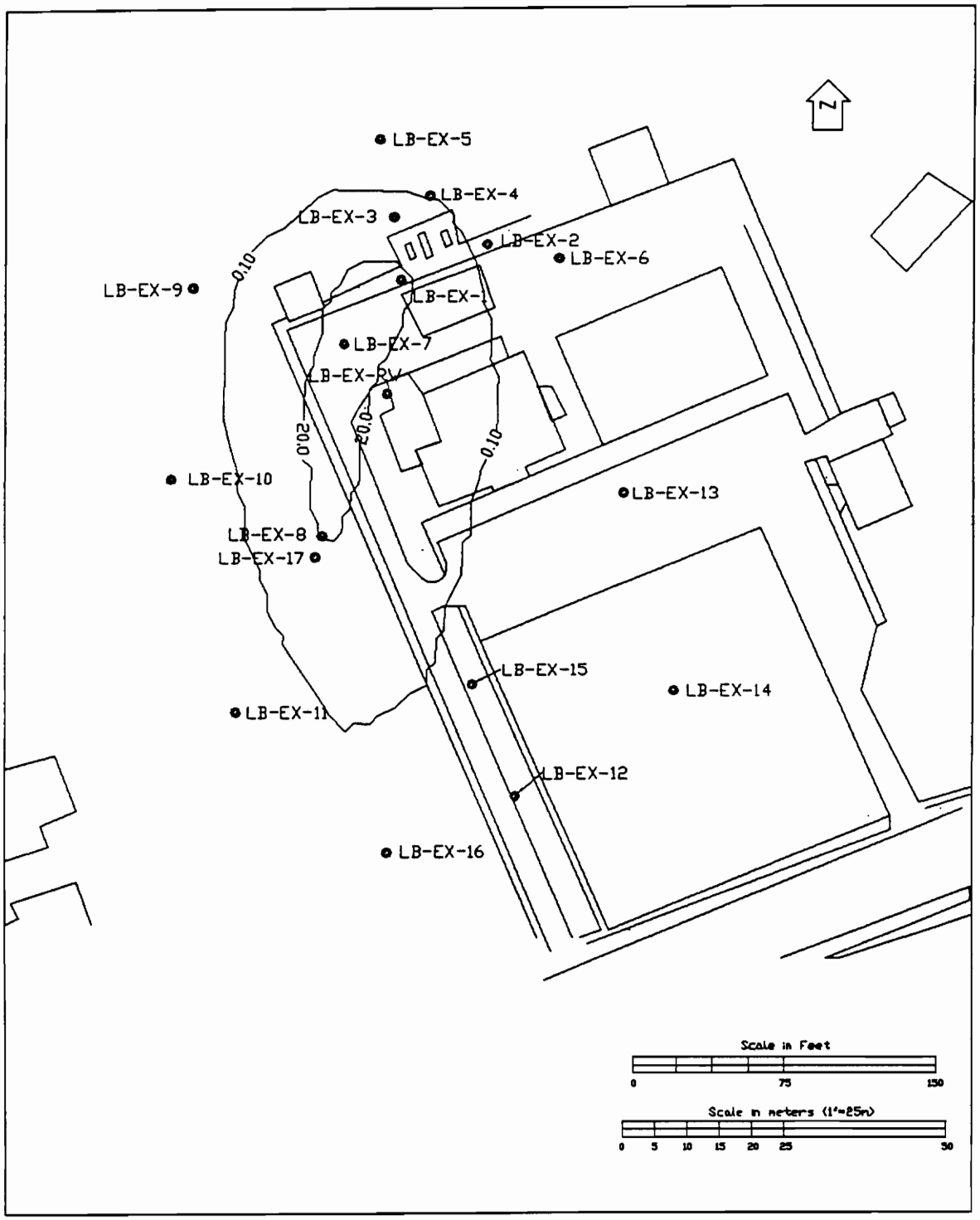

Figure 5.2. Laurel Bay Exchange monitoring well locations and toluene plume delineation. (from ABB Environmental Services, Inc., 1993)

Table 5.1. Solute concentration levels for selected groundwater constituents at the Marine Corps Air Station, Laurel Bay, Beaufort, SC, March 11,1994. (from Landmeyer et al., 1994)

Monitoring Well Number	Benzene (mg/liter)	Toluene (mg/liter)	Dissolved Oxygen (mg/liter)	Iron (II) (mg/liter)
LB-EX-1	8.450	20.600	0.00	19.8
LB-EX-3	0.0061	0.0222	2.18	0.7
LB-EX-4	BD	BD	5.34	0.6
LB-EX-5	BD	BD	5.07	BD
LB-EX-7	9.450	22.300	0.00	20.0
LB-EX-8	9.180	22.500	0.00	6.8
LB-EX-9	0.036	0.132	4.11	BD
LB-EX-10	BD	BD	2.93	BD
LB-EX-11	BD	BD	4.66	BD
LB-EX-12	BD	BD	4.43	BD
LB-EX-13	BD	BD	5.91	ND
LB-EX-14	BD	BD	5.30	ND
LB-EX-15	0.0067	0.0061	0.90	2.8
LB-EX-16	0.0065	BD	4.92	BD
LB-EX-RW	8.650	16.100	0.00	9.8

BD = Below detection; ND = No data collected

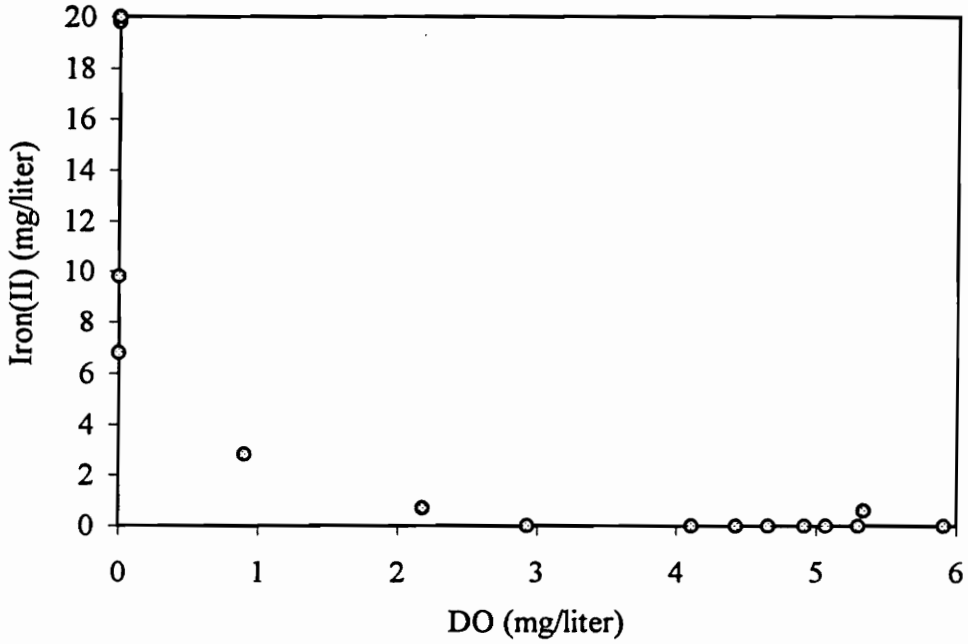

Figure 5.3. Graph depicting relationship between dissolved oxygen (DO) and Iron(II) using data collected from monitoring wells at the Marine Corps Air Station, Laurel Bay, Beaufort, SC, March 11, 1994. (Landmeyer et al., 1994)

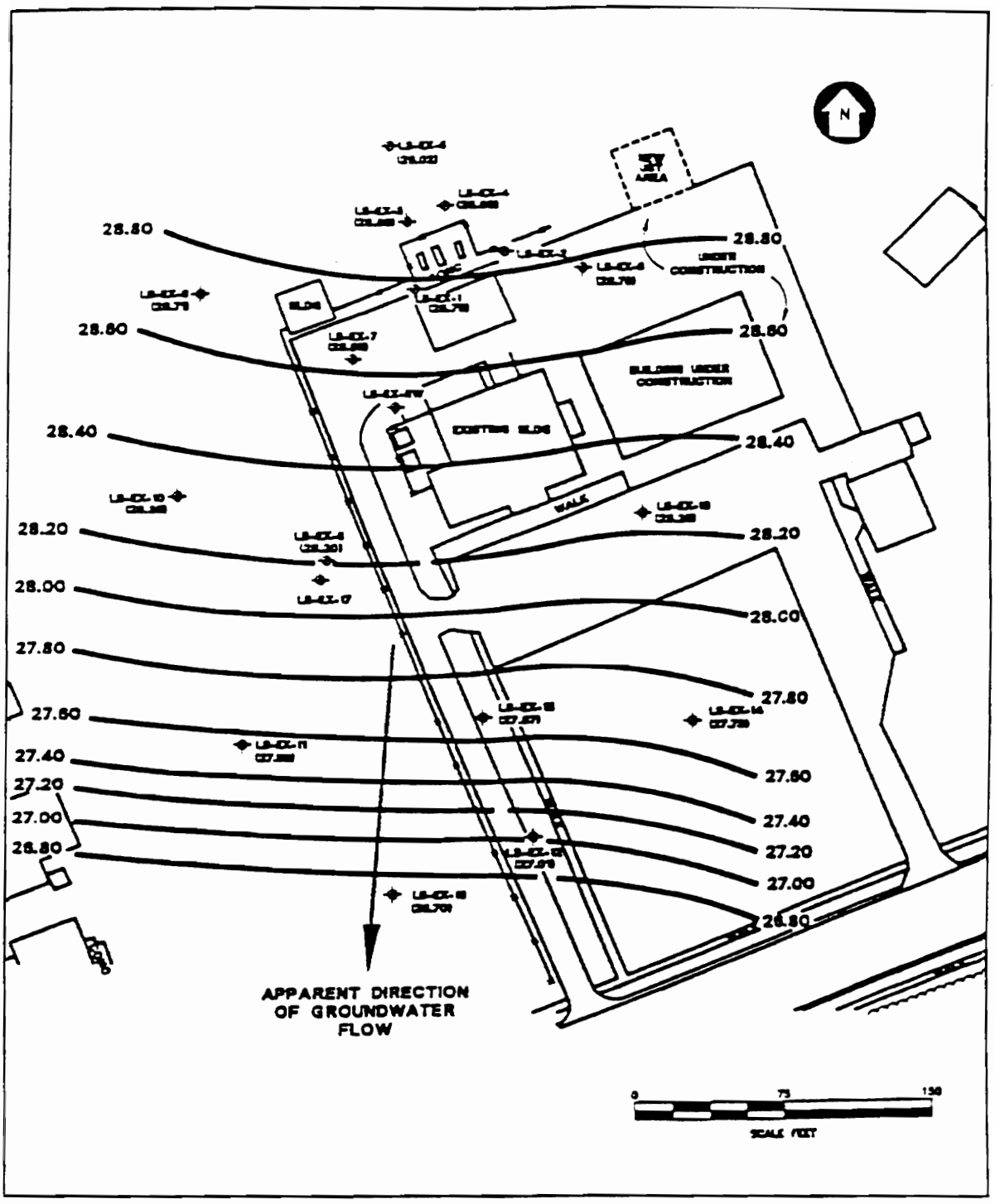

Figure 5.4. Field measurements indicating the direction of groundwater flow. (from ABB Environmental Services, Inc.)

would produce solute transport of approximately 250 meters, thus providing an upper limit for grid length. As indicated above, the plume is approximately 37.5 meters wide and a grid width of 40 meters is selected. Recalling that the plume is modeled as two halves with respect to the transverse direction, a 40 meter domain width can effectively model a transverse width of 80 meters. Figure 5.5 shows grid placement and orientation for the Laurel Bay site.

5.2.3 Model Boundary and Initial Conditions

Boundary conditions at the source are based on field data from prior site characterization studies. Data collected by ABB Environmental Services in April, 1993 indicates that the toluene source concentration in monitoring wells close to the source area (e.g. LB-EX-1, LB-EX-7) ranges between 30 and 40 mg/liter. For the simulations conducted here, the influent toluene concentration is varied to simulate the effects of the source removal in early 1994. For the first two and a half years (corresponding to the time when the leak allegedly occurred) of the SEAM2D simulations, the source concentration is designated a constant concentration of 35 mg/liter. At time = 2.5 years (925 days), the simulated influent source concentration is reduced exponentially, corresponding to the effects of tank extraction in early 1994, such that the influent concentration is approximately zero by middle of 1996 (Time $\approx$ 3.75 years). Figure 5.6 shows the temporal variation of substrate influent concentration used for the SEAM2D simulations.

Landmeyer et al. (1994) collect field data on background DO and ferrous iron concentrations and report DO concentrations of approximately 5 mg/liter and iron(II) concentrations below detection limits for monitoring wells located outside the contaminant plume. Uniform initial conditions are therefore assumed in the model domain with low background substrate and ferrous iron concentrations and a DO background concentration of 5 mg/liter. The influent oxygen concentration is set at 3.0 mg/liter, simulating the effects of DO utilization occurring up-gradient of the model domain and oxygen

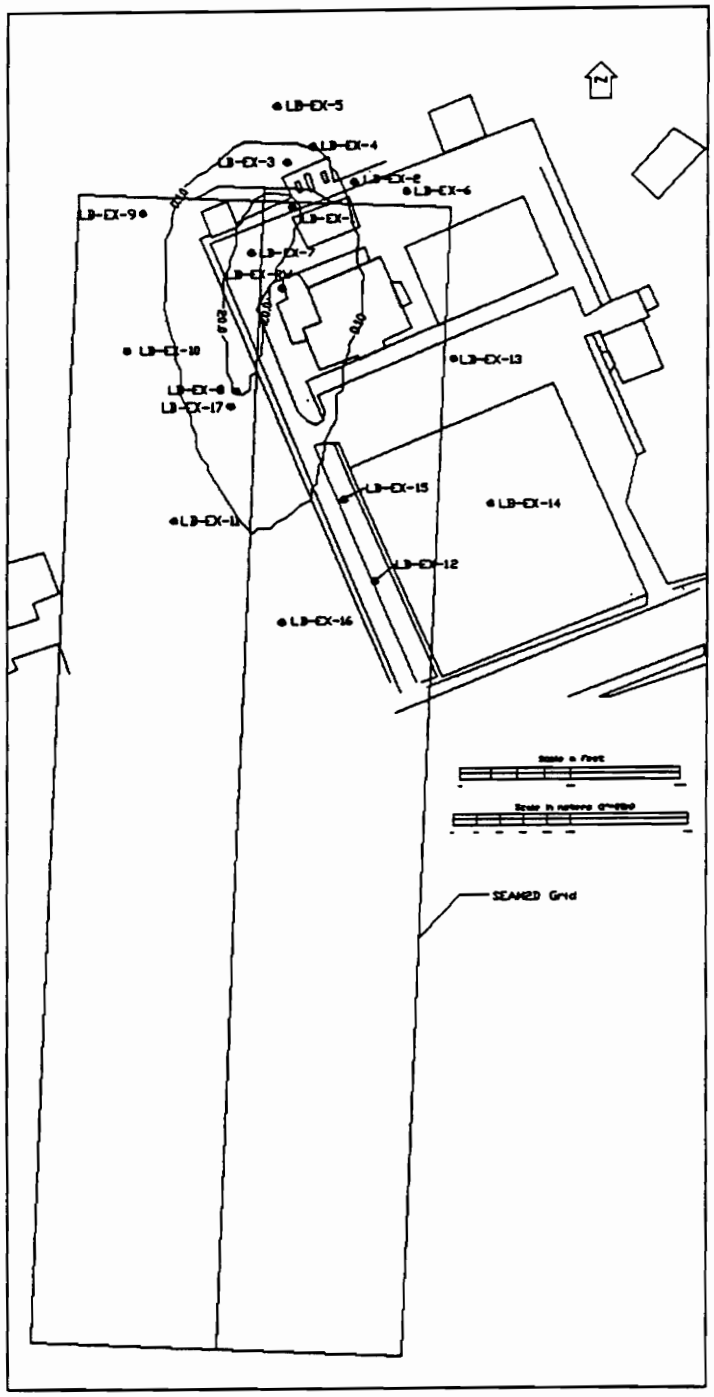

Figure 5.5. SEAM2D grid orientation for the Laurel Bay Exchange site. (from ABB Environmental Services, Inc., 1993)

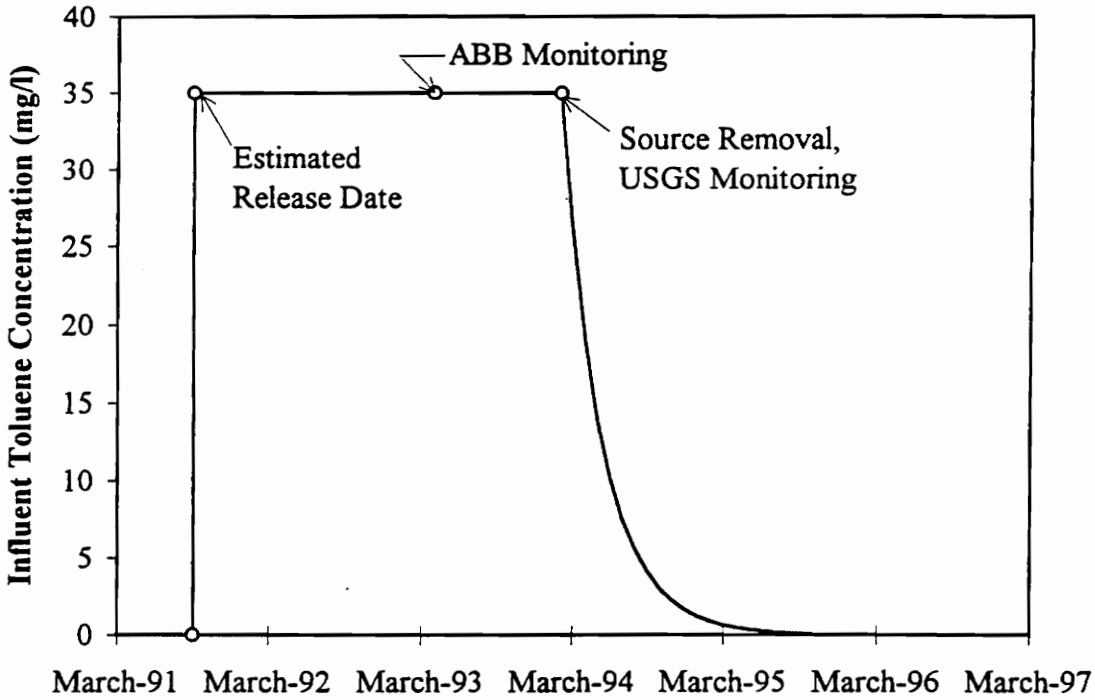

Figure 5.6. Temporal variation in influent substrate concentration.

consumption due to the presence of other groundwater contaminants.

5.2.4 Input Parameters

Selection of input parameters for the Laurel Bay simulations is based on a combination of field measurements and estimates taken from the literature and are listed in Table 5.2. The groundwater velocity is set at 0.0535 meters/day (19.5 meters/year), based on average measurements reported by ABB Environmental, Inc. (1993) and Landmeyer et al. (1994). The remaining hydrodynamic parameters (i.e. dispersivities and diffusion coefficients) are selected based on typical values from the literature. Contaminant adsorption is considered negligible, as Landmeyer et al. (1994) indicate that the sandy aquifer material has relatively low sorption capabilities. Landmeyer et al. (1994) also note that anaerobic biodegradation occurs much slower than aerobic biodegradation, estimating that iron-reducers exhibit first order rate constants two orders of magnitude smaller than the oxygen-reducers. Although the microbial parameters employed in these model simulations are primarily based on literature values, an effort is made to account this observed difference in degradation rates.

5.3 Model Results

5.3.1 Concentration Profiles

By plotting measured concentration data for toluene, dissolved oxygen and iron(II) from monitoring wells located along the plume's central axis, biodegradation trends can be observed as one-dimensional concentration profiles. The data, plotted as Figure 5.7a, indicates a fairly consistent concentration of both groundwater contaminants and dissolved oxygen over the initial 45 meters of the contaminant plume. After this point, toluene and benzene levels decrease significantly and oxygen begins to return to background levels, with each solute reaching background concentrations by approximately 75 meters. The iron(III)-reduction end product, iron(II), is also present at significant levels in the early portion of the plume, with a sharp decrease at monitoring well LB-EX-RW (i.e. $\approx$ 20

Table 5.2. Input parameters base values for Laurel Bay simulations.

Parameter	Primary Electron Acceptor (Oxygen)	Terminal Electron Acceptor (Iron(III))
Microbial Parameters		
K_c (mg_{O2}/L)	n/a	0.10
k_d (d^{-1})	0.01	0.01
K_s (mg/L)	10.0	50.0
F_B ($\mu g_{Fe(III)}/g$)	n/a	100.0
O_B (mg_S/L)	5.0	n/a
M_B (g_{bio}/m^3)	0.1	0.005
S_B (mg_S/L)	35.0	35.0
Y(mg_S/mg_{bio})	0.25	0.50
β (m^2/g_{bio})	1.0	1.0
δ (m)	10^{-4}	10^{-4}
γ (mg_o/mg_S)	10.0	150.0
μ_{max} (d^{-1})	0.20	0.10
ζ($mg_{Fe(II)}/mg_{Fe(III)}$)	n/a	0.60
Hydrodynamic Parameters		
D_o (m^2/d)	10^{-4}	n/a
D_s (m^2/d)	10^{-4}	10^{-4}
$\overline{v}_x$ (m/d)	0.0535	0.0535
α_L (m)	0.1	0.1
α_T (m)	0.01	0.01

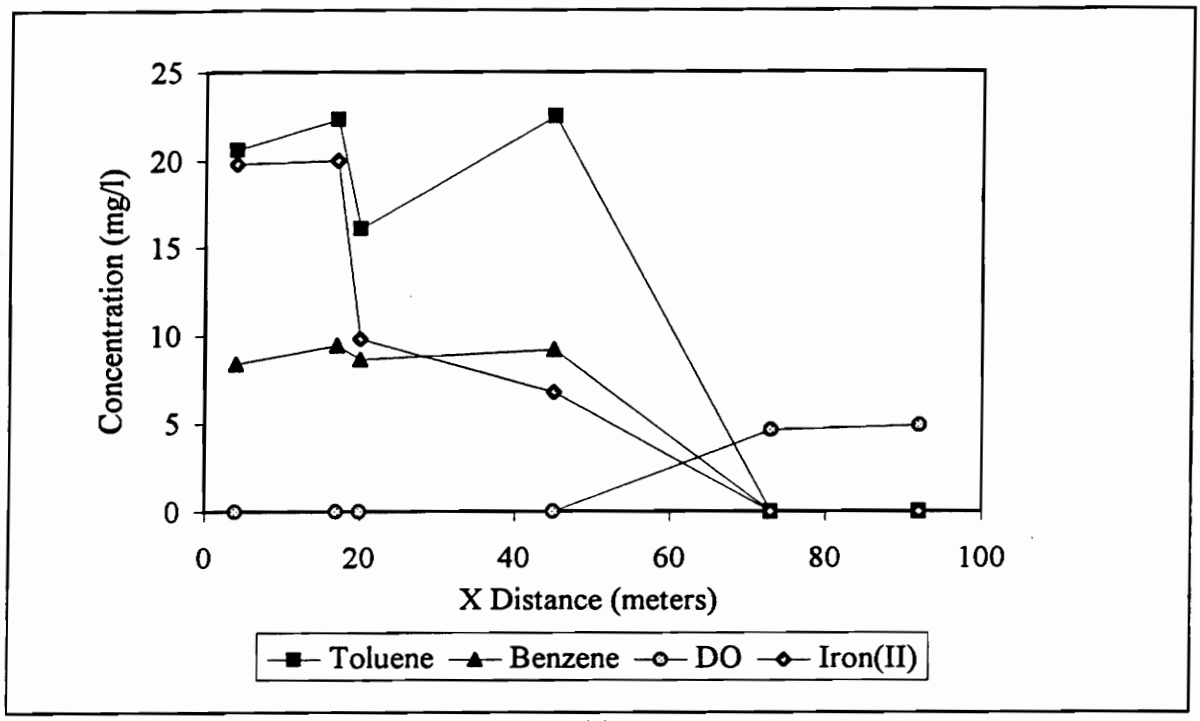

(a)

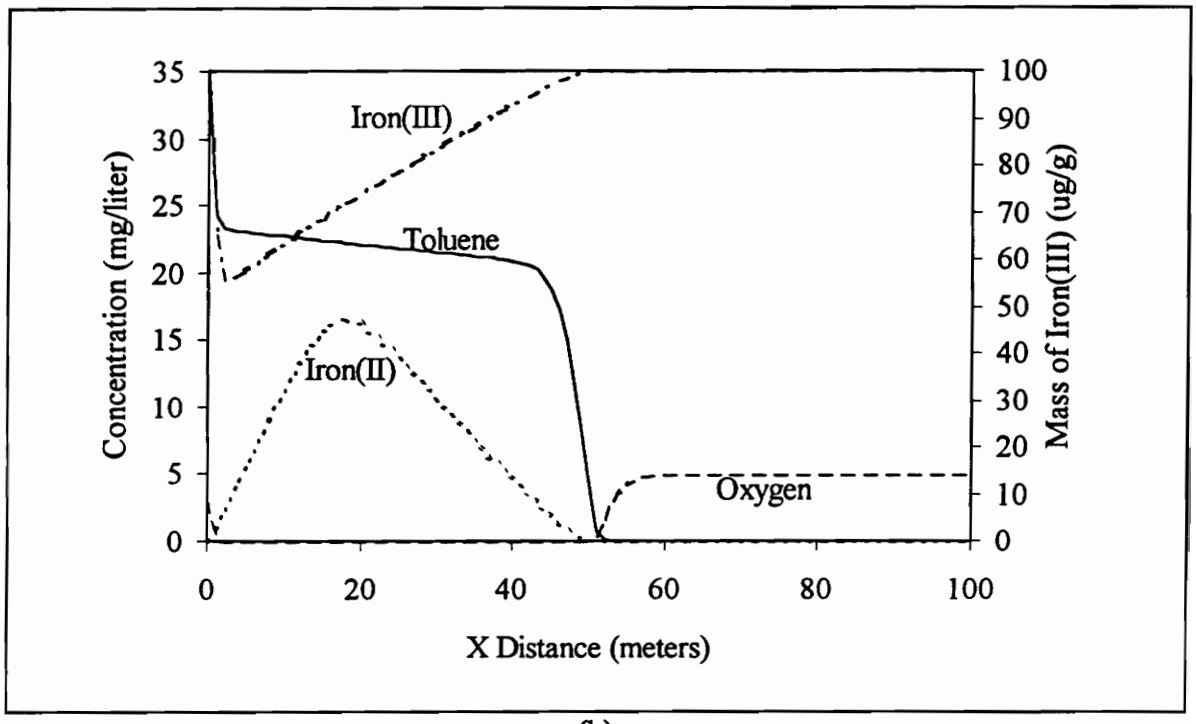

(b)

Figure 5.7. Longitudinal concentration profiles for (a) field data and (b) SEAM2D simulation results.

meters down-gradient of the source) followed by a gradual decrease to background levels between 45 and 75 meters from the contaminant source. This concentration data thus indicates that the contaminant plume edge lies somewhere in the 45 to 75 meter range, providing a target area for the SEAM2D simulations. Using the input parameters and source designations discussed in the previous section, the toluene, dissolved oxygen and iron(II) levels depicted in Figure 5.7b are realized at time = 925 days. This time corresponds to the data collection date of March 1994 at approximately two and a half years after the origination of the contaminant leak. Figure 5.7b illustrates that the SEAM2D model is capable of reproducing the trends observed at the Laurel Bay site, with the contaminant plume edge falling in the desired 45 to 75 meter range, iron(II) production occurring in the absence of oxygen, and complete oxygen depletion within the plume. Simulation results predict that solute concentrations return to ambient conditions ahead of the contaminant plume. Finally, iron(III) depletion is reported on Figure 5.7b, indicating that a significant portion of this electron acceptor is consumed while also indicating that, by time = 2.5 years, this electron acceptor has not fallen below the minimum value associated with iron(III) accessibility and has not become limiting.

5.3.2 Future Predictions and Two-Dimensional Contour Plots

Future predictions for the fate and transport of toluene under sequential oxygen-iron(III) biodegradation conditions are presented here in the form of two-dimensional contour plots. Using the input parameters and influent concentration conditions presented above, future conditions are predicted here for model input parameters used to produce the simulation results shown in Figure 5.7b. To evaluate the effects of biodegradation, a tracer simulation is first conducted, shown here as Figure 5.8, and illustrates that the a conservative substance would migrate through the entire domain, breaking through the edge of the domain approximately 12.5 years after the onset of the leak (i.e. 10 years after source removal. The effects of biodegradation can now be observed by comparing the results of the tracer simulation to simulation results for varying biodegradation conditions.

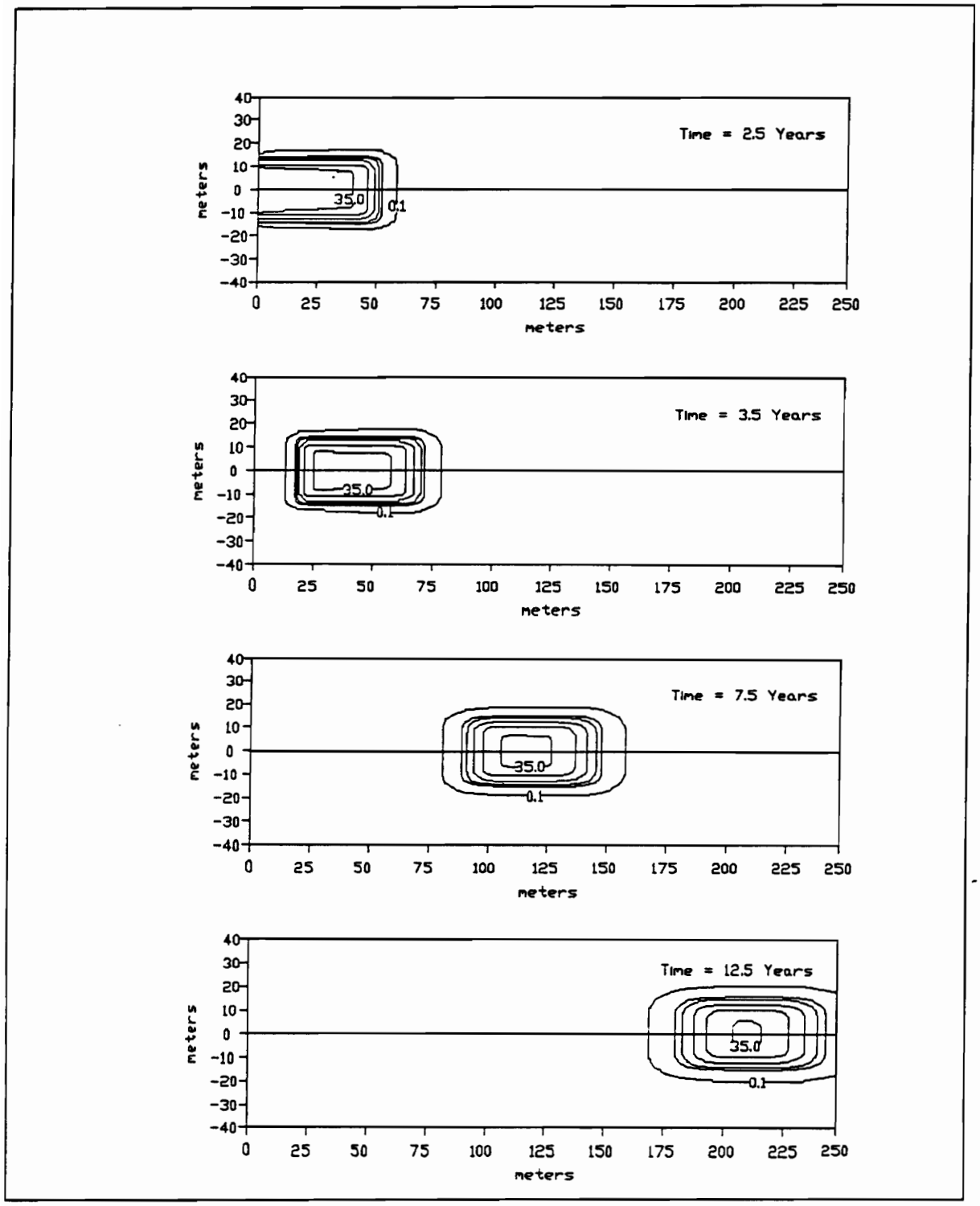

Figure 5.8. SEAM2D simulation results for substrate concentration (mg/liter) of a conservative tracer.

For the sequential biodegradation parameters listed in Table 5.2, SEAM2D results indicate that contaminant levels are reduced to levels below the background concentration of 1 μg/liter before the plume reaches the end of the model domain. Figure 5.9 displays the fate and transport of toluene, indicating that contaminant levels have fallen below 1μg/liter by time = 12.5 years. Figures 5.10 and 5.11 indicate that both oxygen and iron(III) biodegradation is occurring in the simulations, with Figure 5.10 indicating DO depletion in the heart of the contaminant plume and Figure 5.11 indicating iron(II) production in the absence of oxygen. The positive charge associated with iron(II) produces an attraction between iron(II) and the negatively-charged aquifer sediments, justifying the application of a retardation factor for this solute, and accounting for the retarded movement simulated for iron(II).

To more fully investigate the effects of the oxygen-iron(III) sequential electron accepting conditions, two additional series of simulations are provided. In the first series, the influent oxygen concentration is reduced to 0.1 mg/liter, causing aerobic biodegradation to decrease and placing more significance on the terminal electron accepting processes (i.e. iron(III) reduction). As shown in Figure 5.12, substrate concentrations increase within the plume under these conditions, especially for early time. By time = 12.5 years, however, contaminant concentrations have once again been reduced to levels below the background condition of 1 μg/liter. Figure 5.13 indicates that the oxygen depleted zone (DO less than 0.1 mg/liter) is significantly larger for these simulations, allowing increased iron(III) based biodegradation and increased iron(II) production, as is shown in Figure 5.14. The second series of simulations evaluates the effects of a single terminal electron acceptor (oxygen), providing a comparison for the sequential electron acceptor conditions examined above. As indicated in Figures 5.15 and 5.16, oxygen-only biodegradation produces substrate and oxygen concentrations similar to those simulated in the base scenario presented above, although the contaminant plumes in the oxygen-only simulations tend to be slightly larger than the basic sequential simulations. Figure 5.17a depicts the longitudinal concentration profiles for each simulation at time

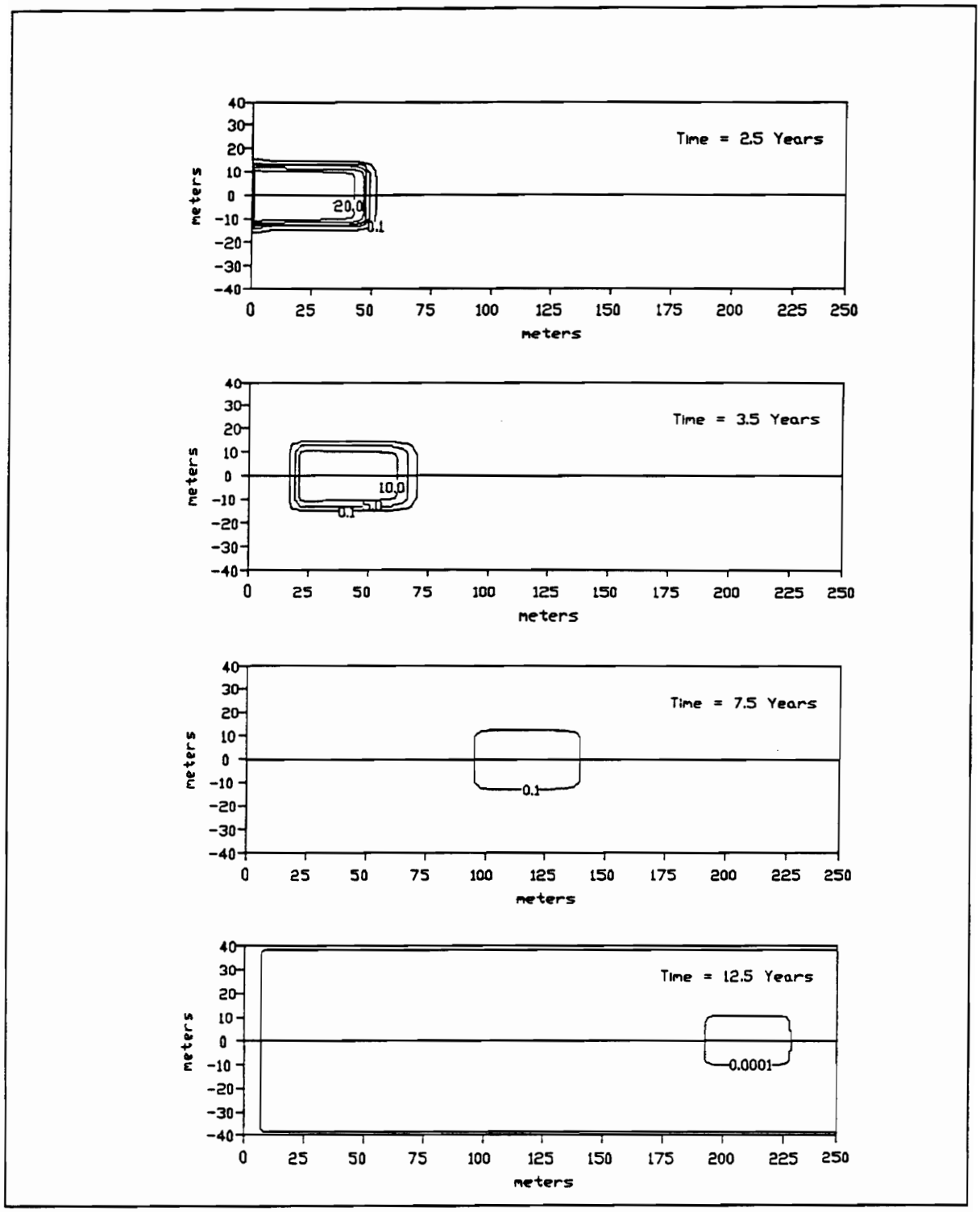

Figure 5.9. SEAM2D simulation results for substrate concentration (mg/liter) using base parameters values.

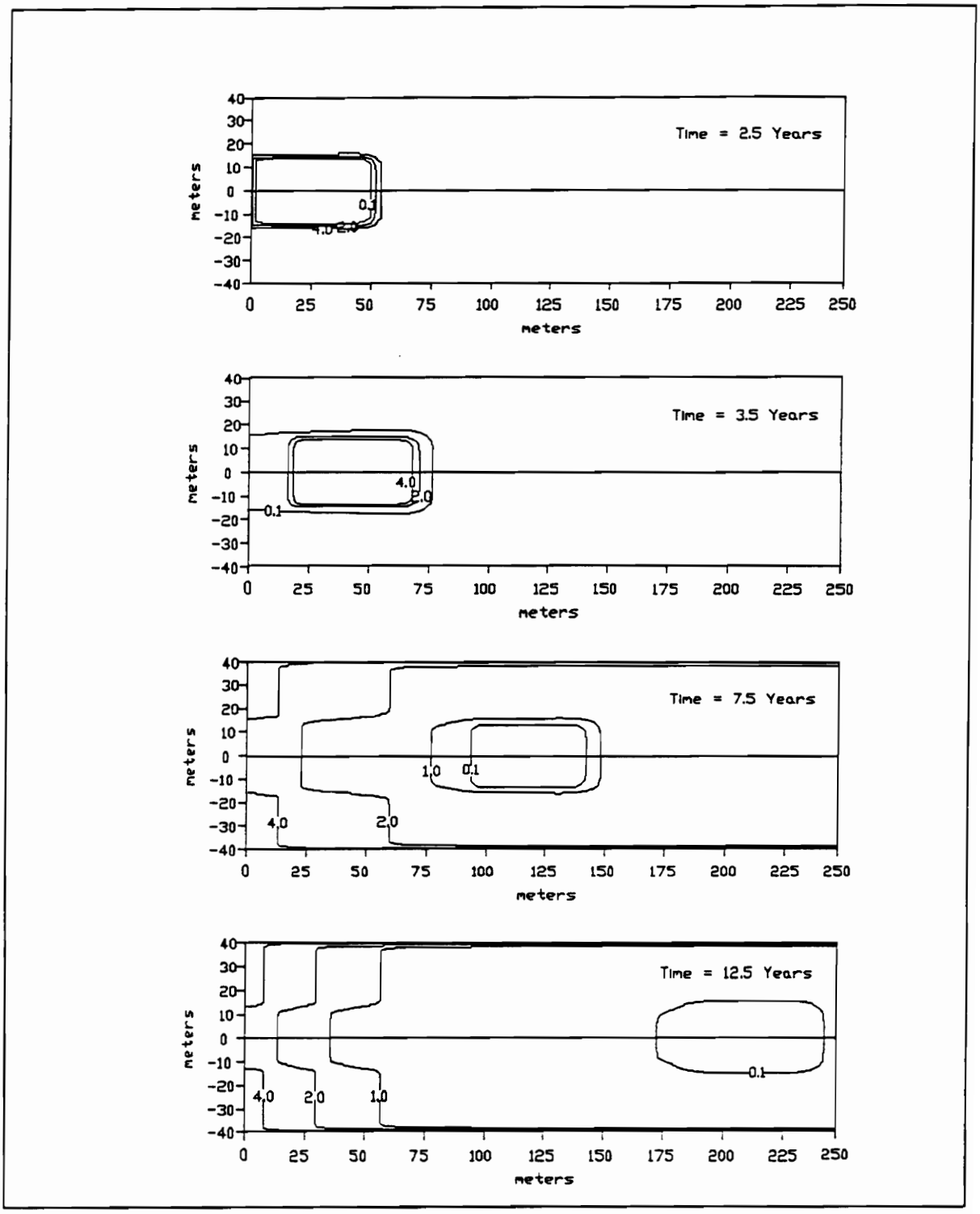

Figure 5.10. SEAM2D simulation results for oxygen concentration (mg/liter) using base parameters values.

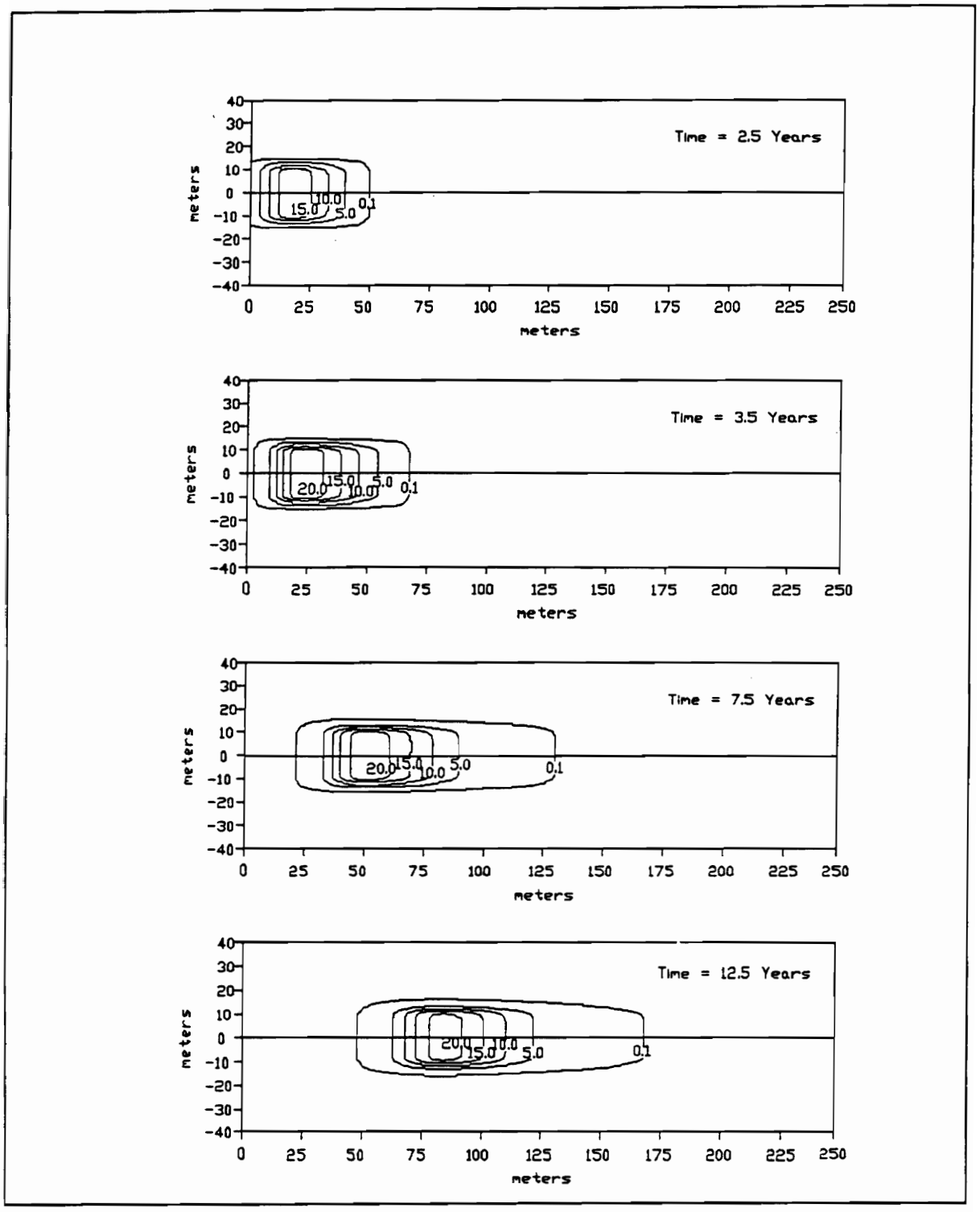

Figure 5.11. SEAM2D simulation results for iron(II) concentration (mg/liter) using base parameters values.

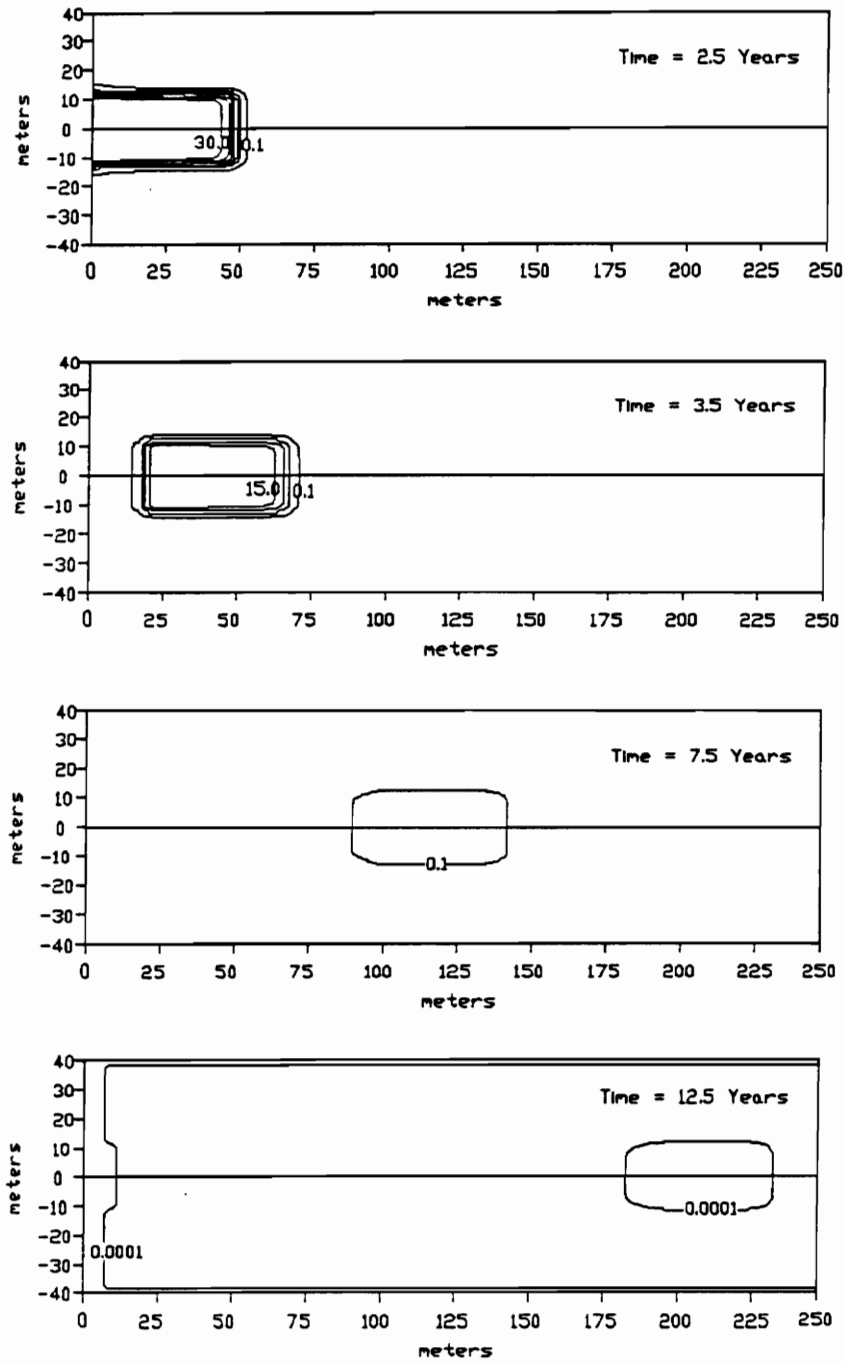

Figure 5.12. SEAM2D simulation results for substrate concentration (mg/liter) using a reduced oxygen influent concentration.

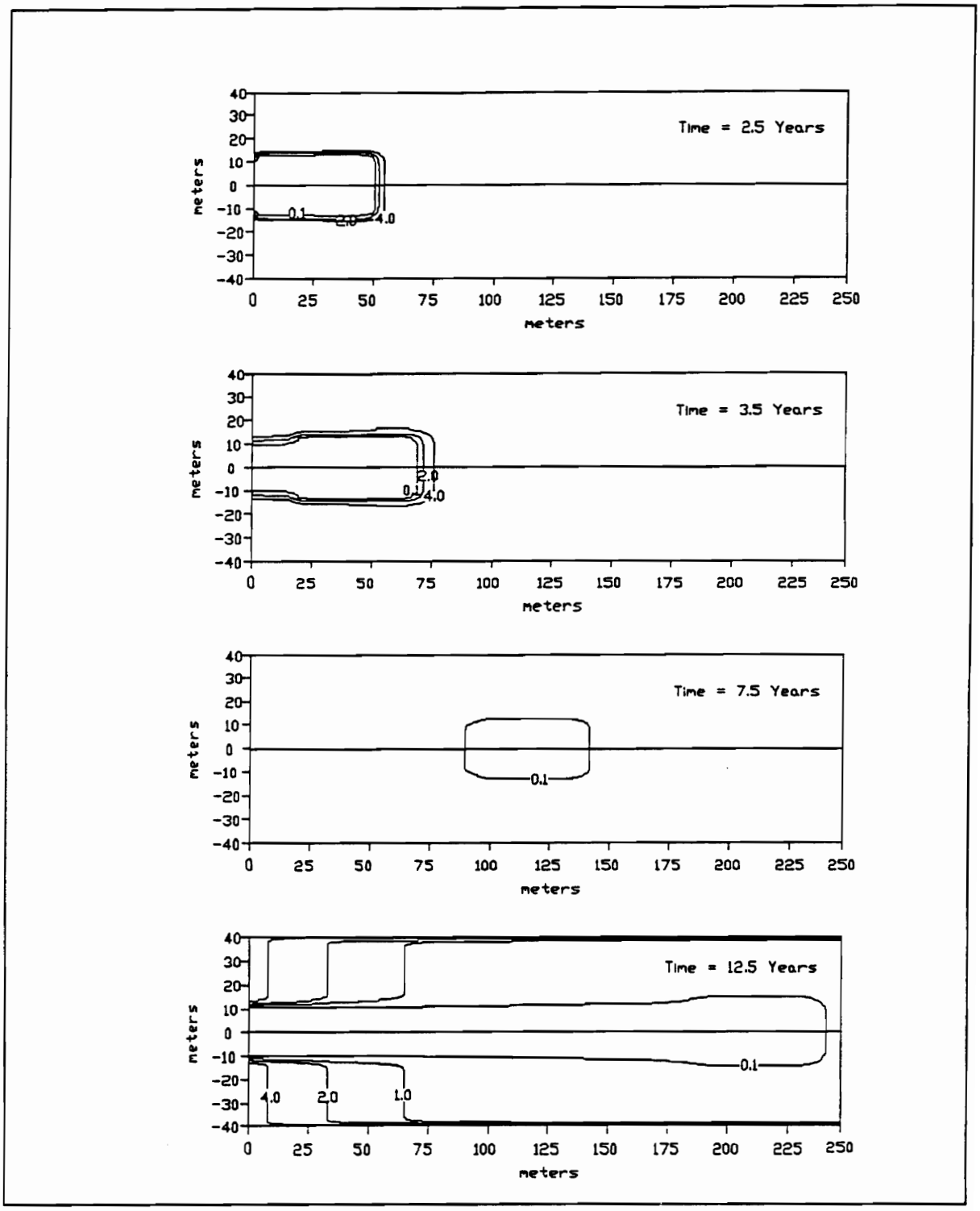

Figure 5.13. SEAM2D simulation results for oxygen concentration (mg/liter) using a reduced oxygen influent concentration.

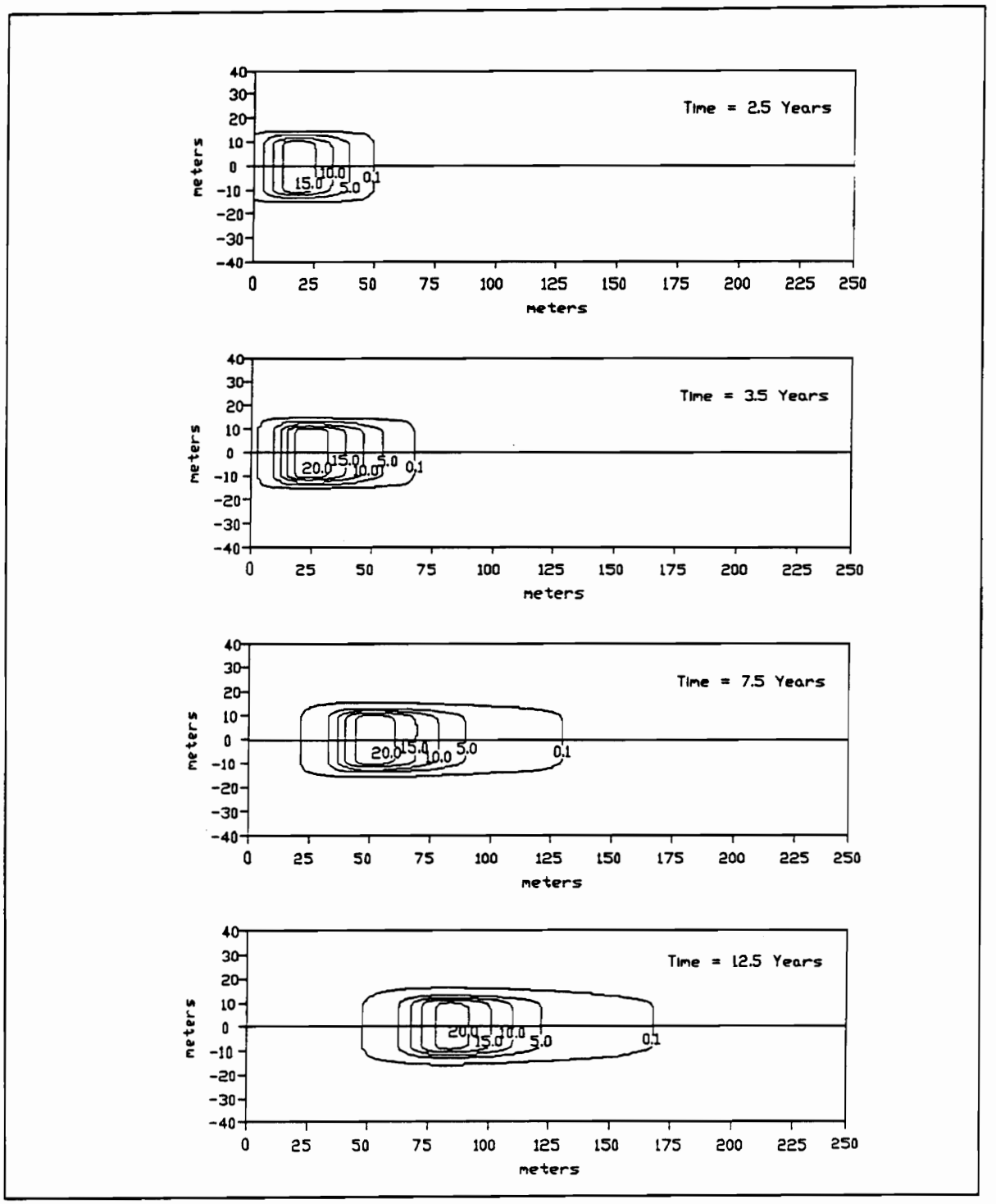

Figure 5.14. SEAM2D simulation results for iron(II) concentration (mg/liter) using a reduced oxygen influent concentration.

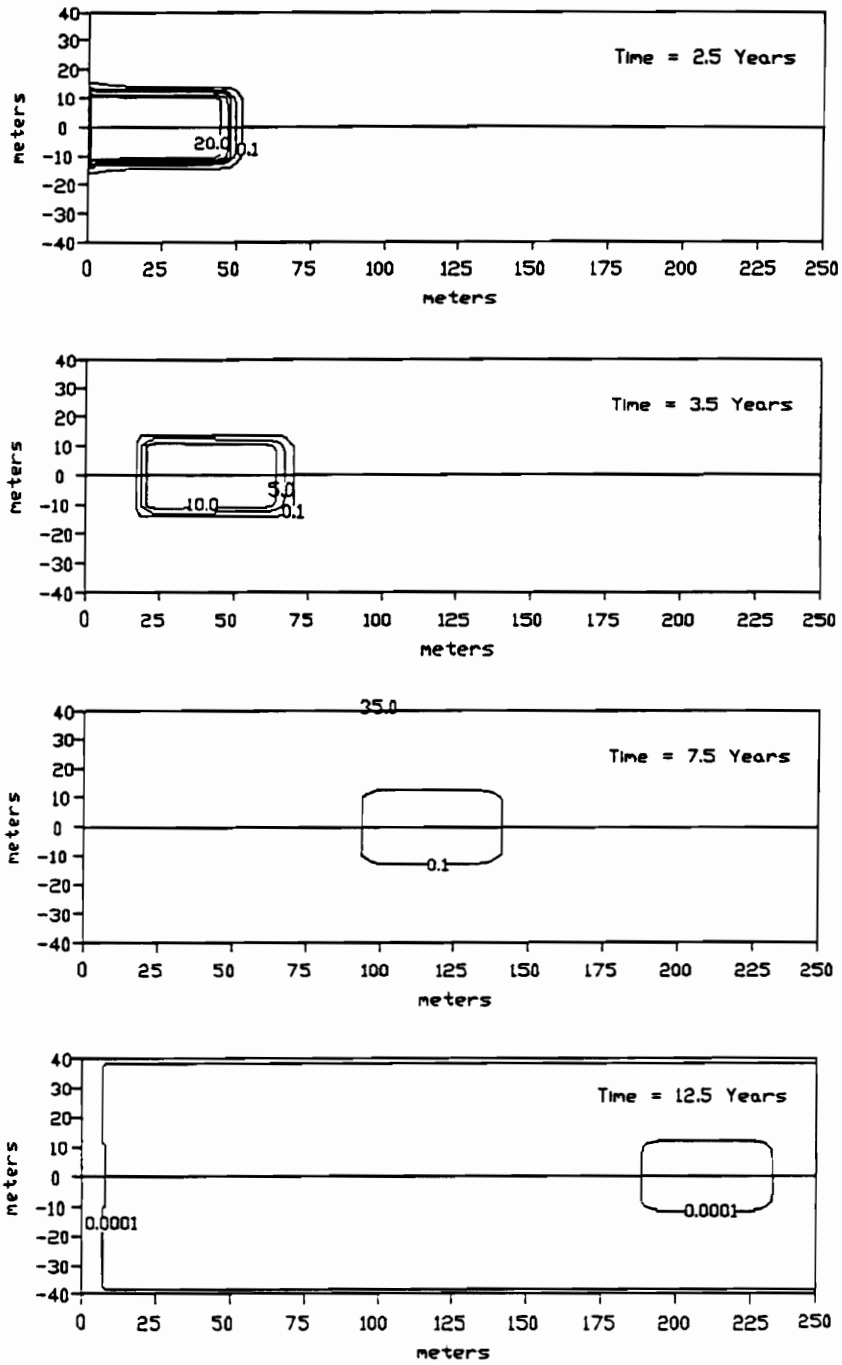

Figure 5.15. SEAM2D simulation results for substrate concentration (mg/liter) under single electron acceptor (oxygen) conditions.

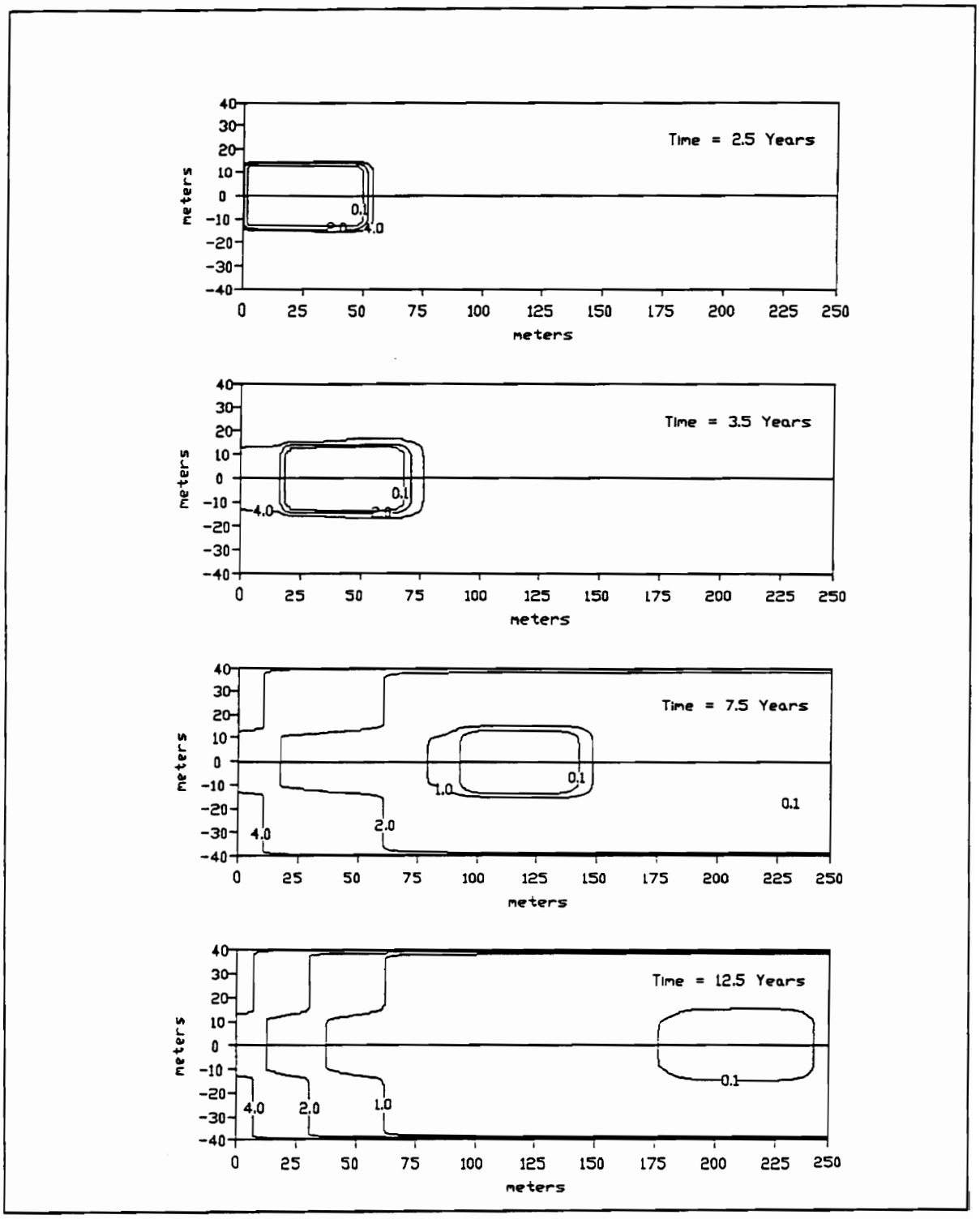

Figure 5.16. SEAM2D simulation results for oxygen concentration (mg/liter) under single electron acceptor (oxygen) conditions.

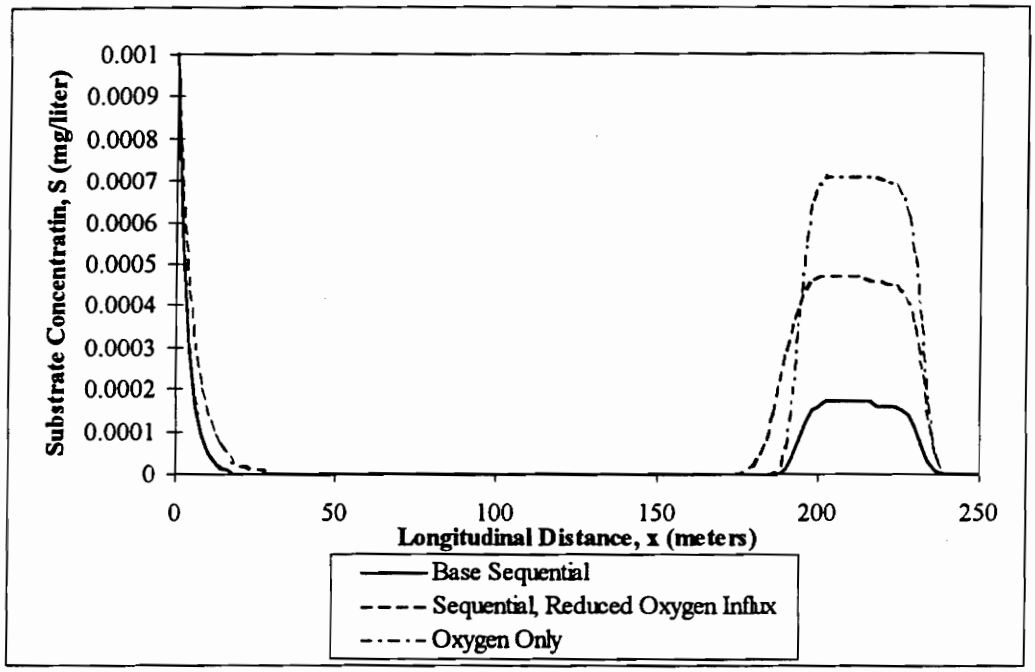

(a)

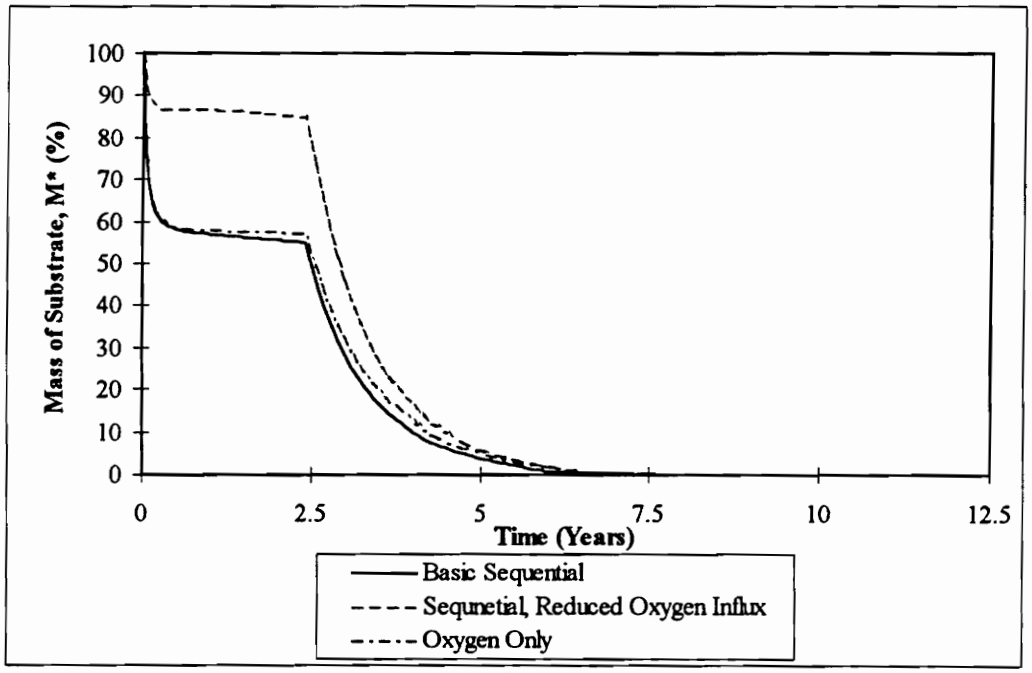

(b)

Figure 5.17. SEAM2D simulation results for varying electron acceptor conditions plotted as (a) longitudinal concetration profiles and (b) substrate mass balance.

12.5 years, showing that the presence of the additional electron acceptor, iron(III) does reduce substrate concentrations within the plume. Figure 5.18b shows the variation in substrate mass with time and indicates that the influent oxygen concentration impacts biodegradation results most significantly when the toluene source is present (i.e. from time 0 to 2.5 years). Figure 5.18b also indicates that each of the simulations provided predicts significant toluene removal.

CHAPTER 6. Conclusions

6.1 Summary of Findings

This research is designed to evaluate the effects of the solid phase, iron(III)-based biodegradation of petroleum hydrocarbons. By modifying an existing sequential electron accepting model (SEAM2D) to incorporate a solid phase electron acceptor, iron(III), natural *in situ* biodegradation can be more realistically simulated. The development of a sequential biodegradation model for both aqueous and solid phase electron acceptors allows a more accurate simulation of the sequential biodegradation processes observed during field investigations. Iron(III)-based oxidation of petroleum hydrocarbons is simulated using the standard Monod kinetics equation, with the assumption that reaction kinetics are zero order with respect to iron(III) and first order with respect to a petroleum hydrocarbon substrate. Model results indicate that iron(III)-based biodegradation does reduce substrate concentration and total mass, but, for conditions similar to those of the site application simulations presented in this research, iron(III)-based biodegradation is shown to occur at a significantly slower rate than aerobic biodegradation.

Both a sensitivity investigation and a site application of iron(III)-based biodegradation are provided. For comparison, biodegradation results for the aqueous phase electron acceptor oxygen are also presented. Model results from the sensitivity investigation indicate that the dimensionless parameters pertaining to utilization have, in general, the most influence on model output. Specifically, variations in the parameters describing the individual microbial populations (i.e. the D^{II} and D^{III} numbers for oxygen and the D^{II} and D^{IV} number for iron(III)) are observed to most significantly impact model results. Iron(III) is also shown to be sensitive to the Monod kinetics parameters. The differences in results noted for the aqueous phase electron acceptor, oxygen, and the solid phase electron acceptor, iron(III), are explained by examining the kinetics equations, which indicate that aqueous phase electron acceptors follow modified Monod kinetics (i.e. substrate and/or electron acceptor limited) while solid phase electron acceptor kinetics are

limited solely by substrate when iron(III) is available. Iron(III)-based biodegradation effects, as evaluated on the basis of site application, are also provided. Results for the SEAM2D simulations indicate that the model is capable of predicting trends observed in field data collected for oxygen-iron(III) sequential biodegradation of the aromatic hydrocarbon, toluene. Site application simulations demonstrate that, for the selected aquifer conditions, oxygen-based biodegradation has a major impact on toluene removal while iron(III)-based biodegradation has a noticeable, but less significant impact. Although the site application presented reproduces the observed trends at one site, additional simulations need to be conducted for alternate sites and at this site as data sets at later times becomes available. This additional data will allow a more complete calibration of the model to the site and a more thorough evaluation of iron(III)-based biodegradation modeling.

6.2 Future Research

This research concentrates on a dual electron acceptor model for an electron acceptor sequence of oxygen as the primary electron acceptor and iron(III) as the terminal electron acceptor. Although this research marks an improvement in natural, intrinsic bioremediation modeling, the need exists for continued research and development of biodegradation models. Future research is recommended into expanding the dual electron acceptor model presented here (i.e. oxygen and iron(III)) to incorporate multiple electron acceptors, specifically including nitrate-based, sulfate-based, and methanogenic biodegradation processes. Simulations presented here are confined to a single substrate under sequential biodegradation and additional investigation into multiple substrates and competitive inhibition kinetics is merited. Further research is also needed to evaluate the effects of various source terms (e.g. point sources) and non-uniform flow fields on model results. Finally, additional research into field data collection and subsequent model calibration for sequential electron acceptor biodegradation conditions is recommended.

References

ABB Environmental Services, Inc. 1993. Contaminant assessment report - Marine Corps Air Station, Laurel Bay. GWPD#A-07-AA-13575.

Anderson, M.P. and W.W.Woesner. 1992. *Applied Groundwater Modeling: Simulation of Flow and Advective Transport*. Academic Press, San Diego, CA

Arcangeli, J.P. and E. Arvin. 1992. Modeling of toluene biodegradation and biofilm growth in a fixed film reactor. *Water Sci. Technol.* 26(3-4):617-626.

Arcangeli, J.P. and E. Arvin. 1994. Biodegradation of BTEX compounds in a biofilm system under nitrate reducing conditions. In R.E. Hinchee, B.C. Alleman, R.E. Hoeppel, and R.N. Miller, eds., *Hydrocarbon Bioremediation.* Lewis Publishers, Boca Raton, FL. pp. 374-382.

Bailey, J.E. and D.F. Ollis. 1977. *Biochemical Engineering Fundamentals*. McGraw-Hill, New York.

Baker, K.H. and D.S. Herson. 1994. *Bioremediation.* McGraw-Hill, Inc., New York.

Baveye, P. and A. Valocchi. 1989. An evaluation of mathematical models of the transport of biologically reacting solutes in saturated soils and aquifers. *Water Resour. Res.* 25(6):1413-1421

Barbaro, J.R., J.F. Barker, L.A. Lemon and C.I. Mayfield. 1992. Biotransformation of BTEX under anaerobic, denitrifying conditions: Field and laboratory observations. *J. Contamin. Hydrol.* 11:245-272.

Barcelona, M.J. and T.R. Holm. 1991. Oxidation-reduction capacities of aquifer solids. *Environ. Sci. Technol.* 25(9):1565-1572.

Barker, J.F., G.C. Patrick, and D. Major. 1987. Natural attenuation of aromatic hydrocarbons in a shallow sand aquifer. *Ground Water Monit. Rev.* 7:64-71.

Bear,J. 1972. *Dynamics of Fluids in Porous Media*. American Elsevier, New York

Bedient, P.B., H.S. Rifai, and C.J. Newell. 1994. *Ground Water Contamination: Transport and Remediation.* PTR Prentice-Hall, Inc., Englewood Cliffs, NJ.

Borden, R.C. and P.B. Bedient. 1986. Transport of dissolved hydrocarbons influenced by oxygen-limited biodegradation: 1. Theoretical development. *Water Resour. Res.* 13:1973-1982.

Borden, R.C., P.B. Bedient, M.D. Lee, C.H. Ward, and J.T. Wilson. 1986. Transport of dissolved hydrocarbons influenced by oxygen-limited biodegradation: 2. Field Application. *Water Resour. Res.* 13:1983-1990.

Button, D.K. 1985. Kinetics of nutrient-limited transport and microbial growth. *Microbiological Rev.* 49(3):270-297.

Celia, M.A., J.S. Kindred, and I. Herrera. 1989. Contaminant transport and biodegradation: 1. A numerical model for reactive transport in porous media. *Water Resour. Res.* 25(6):1141-1148.

Chang M-K, T.C. Voice, and C.S. Criddle. 1993. Kinetics of competitive inhibition and cometabolism in the biodegradation of benzene, toluene, and p-xylene by two Pseudomonas isolates. *Biotechnol. Bioeng.* 41(11):1057-1065.

Chapelle, F.H. 1995. Factors affecting the efficiency of intrinsic bioremediation under anaerobic conditions. In *Platform Abstracts, In Situ and On-Site Bioreclamation, The Third Int'l Symp.*, April 24-27, 1995, San Diego, CA.

Chapelle, F.H. and D.R. Lovley. 1992. Competitive exclusion of sulfate reduction by Fe(III)-reducing bacteria: A mechanism for producing discrete zones of high-iron ground water. *Ground Water.* 30(1):29-36.

Chiang, C.Y., J.P. Salanitro, E.Y. Chai, J.D. Colthart, and J.D. Klein. 1989. Aerobic biodegradation of benzene, toluene, and xylene in a sandy aquifer - Data analysis and computer modeling. *Ground Water.* 6:823-834.

Connor, J.A. 1994. Hydrogeologic site invesitgations. In *Ground Water Contamination: Transport and Remediation*, by P.B. Bedient, H.S. Rifai, and C.J. Newell. PTR Prentice-Hall, Inc., Englewood Cliffs, NJ.

Dean, B.J. 1985. Recent findings on the genetic toxicology of benzene, toluene, xylenes, and phenols. *Mutat. Res.* 145:153-181.

Domenico, P.A. 1987. An analytical model for multidimensional transport of a decaying contaminant species. *J. Hydrol.* 91:49-58.

Domenico, P.A. and F.W. Schwartz. 1990. *Physical and Chemical Hydrogeology*. John Wiley & Sons, New York.

Edwards, E.A. and D. Grbic-Galic, 1992. Complete mineralization of benzene by aquifer microorganisms under strictly anaerobic conditions. *Appl. Environ. Microbiol.* 58(8):2663-2666.

Firestone, M.K. 1982. Biological denitrification. In F.J. Stevenson, ed., *Nitrogen in Agriculture Soils.* American Society of Agronomy, Madison, WI. pp. 289-326.

Freeze, R.A. and J.A. Cherry. 1979. *Groundwater*. Prentice-Hall, Inc., Englewood Cliffs, NJ.

Gelhar, L.W. A. Mantoglou, C. Welty, and K.R. Rehfeldt. 1985. A review of field-scale physical solute transport processes in saturated and unsaturated porous media: Electric Power Research Institute EPRI EA-4190, Project 2485-5.

Ghiorse, W.C. and D.L. Balkwill. 1983. Enumeration and morphological characterization of bacteria indigenous to subsurface environments. *Dev. Ind. Microbiol.* 24:213-225.

Grbic-Galic, D. and T.M. Vogel. 1987. Transformation of toluene and benzene by mixed methanogenic cultures. *Appl. Environ. Microbiol.* 53(2):254-260.

Haag, F.M., M. Reinhard, and P.L. McCarty. 1991. Degradation of toluene and p-xylene in anaerobic microcosms: Evidence for sulfate as a terminal electron acceptor. *Environ. Toxicol. Chem.* 10:1379-1390.

Harris, N.P. and G.S. Hanford. 1976. A study of substrate removal in a microbial film reactor. *Water Res.* 10:935-943.

Hartley, W.R. and A.J. Englande, Jr. 1992. Health risk assessment of the migration of unleaded gasoline - a model for petroleum products. *Water Sci. Technol.* 25(3):65-72.

Harvey, R.W., R.L. Smith, and L. George. 1984. Microbial distribution and heterotrophic uptake in a sewage plume. Movement and fate of solutes in a plume of sewage-contaminated ground water: Cape Cod, Mass., USGS Open-File Report. 84-475. p139-152.

Harvey, R.W. and M.A. Widdowson. 1992. Microbial distributions, activities, and movement in the terrestrial subsurface: Experimental and theoretical studies. In R.J. Wagenet, P. Baveye, and B.A. Stewart, eds., *Interacting Processes in Soil Science*. Lewis Publishers, Boca Raton, FL. pp. 185-225.

Herbert, D. 1958. Some principles of continuous culture. In G. Tunevall, ed., *Recent Progress in Microbiology*. Blackwell Scientific, Oxford, England. pp. 381-396.

Heron, G., T.H. Christensen, and J.C. Tjell. 1994. Oxidation capacity of aquifer sediments. *Environ. Sci. Technol.* 28(1):153-158.

Hutchins, S.R. 1991a. Biodegradation of monoaromatic hydrocarbons by aquifer microorganisms using oxygen, nitrate, or nitrous oxide as the terminal electron acceptor. *Appl. Environ. Microbiol.* 57(8):2403-2407.

Hutchins, S.R. 1991b. Optimizing BTEX biodegradation under denitrifying conditions. *Environ. Toxicol. Chem.* 10:1437-1448.

Jamison, V.M., R.L. Raymond, and J.O. Hudson. 1975. Biodegradation of high-octane gasoline in ground water. *Dev. Ind. Microbiol.* 16:305-312.

Jørgensen, B.B. 1989. Biochemistry of Chemoautotrophic Bacteria. In H.G. Schlegel and B. Bowien, eds., *Autotrophic Bacteria.* Science Tech Publishers, Madison, WI. pp. 117-146.

Kissel, J.C., P.L. McCarty, and R.L. Street. 1984. Numerical simulation of mixed-culture biofilm. *J. Environ. Engineering.* 110(2):393-411.

Klecka, G.M., J.W. Davis, D.R. Gray, and S.S. Madsen. 1990. Natural bioremediation of organic contaminants in ground water: Cliffs-Dow Superfund site. *Ground Water.* 4:534-543.

Landmeyer, J.E, F.H. Chapelle, and P.M. Bradley. 1994. Evaluation of intrinsic bioremediation as an option to contain gasoline contamination, Laurel Bay Exchange, Marine Corps Air Station, Beaufort, South Carolina. *USGS Water-Resources Investigations Report 94-XXXX.*

Lee, M.D., V.W. Jamison, and R.L. Raymond. 1987. Applicability of in situ bioreclamation as a remedial action alternative. In *Proceed. of the Petroleum Hydrocarbons and Organic Chemicals in Ground Water: Prevention, Detection, and Restoration.* Houston, TX, National Water Well Association, Dublin, OH, pp. 167-185.

Lovley, D.R. and D.J. Lonergan. 1990. Anaerobic oxidation of toluene, phenol, and *p*-cresol by the dissimilatory iron-reducing organism, GS-15. *Appl. Environ. Microbiol.* 56(6):1858-1864.

Lovely, D.R., J.C. Woodward, and F.H. Chapelle. 1994. Stimulated anoxic biodegradation of aromatic hydrocarbons using Fe(III) ligands. *Nature.* 370:128-131.

Lyngkilde, J., T.H. Christensen, B. Skov, and A. Foverskov. 1991. Redox zones downgradient of a landfill and implications for biodegradation of organic compounds. In R.E. Hinchee and

R.F. Olfenbuttel, eds., *In Situ Bioreclamation: Applications for Hydrocarbon and Contaminated Site Remediation.* Butterworth-Heinemann, Boston. pp. 363-376.

McCarty, P.L., B.E. Rittman, and E.J. Bouwer. 1984. Microbiological processes affecting chemical transformations in groundwater. In G. Bitton and C.P. Gerba, eds., *Groundwater Pollution Microbiology.* J. Wiley & Sons, New York. pp. 89-115.

Molz, F.J., M.A. Widdowson, and L.D. Benefield. 1986. Simulation of microbial growth dynamics coupled to nutrient and oxygen transport in porous media. *Water Resour. Res.* 22(8):1207-1216.

Monod, J. 1942. *Recherche sur la croissance des cultures bacteriénnes.* Herman &Cie, Paris.

Nicholson, R.V., J.A. Cherry, and E.J. Reardon. 1983. Migration of contaminants in groundwater at a landfill: A case study. *J. Hydrol.* 63:131-176.

Ogata, A. 1970. Theory of dispersion in a granular medium. *U.S. Geological Survey Professional Paper 411-I.*

Oh, Y-S., Z. Shareefdeen, B.C. Baltzis, and R. Bartha. 1994. Interactions between benzene, toluene, and p-xylene (BTX) during their biodegradation. *Biotechnol. Bioeng.* 44(#):533-538.

Oremland, R.S. 1988. Biochemistry of Methanogenic Bacteria. In A.J.B. Zehnder, ed., *Biology of Anaerobic Microorganisms.* J. Wiley & Sons, New York. Chapter 12.

Pirt, S.J. 1975. *Principles of microbe and cell cultivation.* John Wiley & Sons, New York.

Raymond, R.L, V.W. Jamison, and J. O. Hudson, Jr. 1976. Beneficial stimulation of bacterial activity in ground waters containing petroleum products: I. Physical, chemical wastewater treatment. *AIChE Symp. Series.* 73:390-404.

Raymond, R.L., V.W. Jamison, J.O. Hudson, R.E. Mitchell, and V.E. Farmer. 1978. Field application of subsurface biodegradation of gasoline in sand formation. *Final Report submitted to American Petroleum Institute.* Washington, DC.

Rifai, H.S. and P.B. Bedient. 1990. Comparison of biodegradation kinetics with an instantaneous reaction model for groundwater. *Water Resourc. Res.* 26(4):637-645.

Rifai, H.S., P.B. Bedient, J.T. Wilson, K.M. Miller, and J.M. Armstrong. 1988. Biodegradation modeling at an aviation fuel spill site. *J. Environ. Engineering.* 114(5):1007-1029.

Rifai, H.S., C.J. Newell, R. Miller, S. Taffinder, and M. Roundsville. 1995. Simulating natural attenuation with multiple electron acceptors at a field site. In *Platform Abstracts, In Situ and On-Site Bioreclamation, The Third Int'l Symp.*, April 24-27, 1995, San Diego, CA.

Rittman, B.E., L. Crawford, C.K. Tuck, and E. Namkung. 1986. In situ determination of kinetic parameters for biofilms: Isolation and characterization of oligotrophic biofilms *Biotechnol. Bioeng.* 28(#):1753-1760.

Rittmann, B.E., P.L. McCarty, and P.V. Roberts. 1980. Trace-organics biodegradation in aquifer recharge. *Ground Water.* 18(3):236-243.

Stumm, W. and J.J. Morgan. 1981. *Aquatic Chemistry.* J. Wiley & Sons, New York. Chapter 7.

Sudicky, E.A. 1986. A natural gradient experiment on solute transport in a sand aquifer: Spatial variability of hydraulic conductivity and its role in the dispersion process. *Water Resour. Res.* 22(13):2069-2082.

Suflita, J.M. and G.W. Sewell. 1991. Anaerobic biotransformation of contaminants in the subsurface. EPA/600/90/024, Robert S. Kerr Research Laboratory, Ada, OK.

Tchobanoglous, G. and E.D. Schroeder. 1985. *Water Quality: Characteristics, Modeling, Modification.* Addison-Wessley, Reading, MA.

Tucker, W.A., C.T. Huang, J.M. Bral, R.E. Dickinson. 1986. Development and validation of the underground leak transport assessment model (ULTRA). *Proceedings of Petroleum Hydrocarbons and Organic Chemicals in Ground Water: Prevention, Detection, and Restoration,* Houston, TX, National Water Well Association, Dublin, OH, pp. 53-75.

Vogel, T.M. and D. Grbic-Galic. 1986. Incorporation of oxygen from water into toluene and benzene during anaerobic fermentative transformation. *Appl. Environ. Microbiol.* 52(1):200-202.

Voss, C.I. 1984. A finite-element simulation model for saturated-unsaturated, fluid-density-dependent ground-water flow with energy transport or chemically reactive single-species solute transport. *U.S. Geological Survey Investigations Report 84-4369.*

Widdowson, M.A. and C.M. Aelion. 1991. Application of a numerical model to the performance and analysis of an in situ bioremediation project. *In Situ and On Site Bioremediation.* Proc. of the Int'l Symp.

Widdowson, M.A., F.J. Molz, and L.D. Benefield. 1988. A numerical transport model for oxygen- and nitrate-based respiration linked to substrate and nutrient availability in porous media. *Water Resour. Res.* 24(9):1553-1565.

Widdowson, M.A. 1992. *Numerical simulation of in situ bioremediation using nitrate-based respiration*. Submitted to the USGS, Reston VA.

Wilson, B.H. and J.F. Rees. 1985. Biotransformation of gasoline hydrocarbons in methanogenic aquifer material. *Proceedings of the NWWA/API Conference on Petroleum Hydrocarbons and Organic Chemicals in Ground Water.* November 13-15, 1985, Houston, TX, National Water Well Association, Dublin, OH.

Wilson, J.T., L.E. Leach, M. Henson, and J.N. Jones. 1986. In situ biorestoration as a ground water remediation technique. *Ground Water Monit. Rev.* 6:56-64.

Zehnder, A.J.B. and W. Stumm. 1988. Geochemistry of Anaerobic Habitats. In A.J.B. Zehnder, ed., *Biology of Anaerobic Microorganisms*. J. Wiley & Sons, New York. Chapter 1.

Zeyer, J., E.P. Kuhn, and R.P. Schwarzenbach. 1986. Rapid microbial mineralization of toluene and 1,3-dimethylbenzene in the absence of molecular oxygen. *Appl. Environ. Microbiol.* 52(4):944-947

VITA

John Steven Brauner, son of John S. and Judith C. Brauner, was born May 25, 1971 in Harrisburg, Pennsylvania. After graduation from Hershey High School in 1989, Steve went on to pursue a Bachelor's Degree in Civil Engineering from Lehigh University in Bethlehem, Pennsylvania, graduating in May 1993. Steve then continued his education at Virginia Polytechnic Institute and State University where he completed his Master's Degree in Civil Engineering in September 1995. Steve is an active member of Water for People - Blacksburg Chapter and the Blacksburg Ultimate Frisbee Team.